DISSERTATION

INVESTIGATING MITOTIC VULNERABILITIES THAT ARISE UPON ONCOGENIC CELL TRANSFORMATION

Submitted by

Hazheen K. Shirnekhi

Department of Biochemistry and Molecular Biology

In partial fulfillment of the requirements

For the Degree of Doctor of Philosophy

Colorado State University

Fort Collins, Colorado

Spring 2020

Doctoral Committee:

Advisor: Jennifer G. DeLuca

Steven Markus
Erin Nishimura
Susan Bailey

ABSTRACT

INVESTIGATING MITOTIC VULNERABILITIES THAT ARISE UPON ONCOGENIC CELL TRANSFORMATION

During mitosis, cells must accurately divide their duplicated chromosomes into two new daughter cells. This process is highly regulated and much of this regulation is centered around kinetochores. Kinetochores are large proteinaceous structures built upon centromeric heterochromatin that must form stable, load-bearing attachments to microtubules (MTs) emanating from the spindle poles. Failure to undergo high-fidelity cell division can result in aneuploidy and even progress to continued mis-segregation in a phenomenon known as chromosome instability (CIN). As aneuploidy results from defective pathways in mitosis, it is important to characterize the changes cancer cells exhibit in their mitotic machinery, with the goal of identifying targets for therapeutic potential.

Here, we utilize a human papillomavirus cell culture model system to determine how expression of E6 or E7, two viral transforming proteins, influences mitosis. We find that E6-expressing cells exhibit a weakened spindle assembly checkpoint (SAC) and an increased incidence of pole-associated chromosomes. This combination of mitotic errors allows some of these cells to exit mitosis in the presence of improper kinetochore-MT attachments, leading to aneuploid daughter cells.

Defective mitotic processes in cancer cells provide a means of differentiating them from healthy cells, which may be important in developing new effective cancer

therapeutics. Through two independent cancer lethality screens, the mitotic proteins BuGZ and BubR1 were identified as essential for Glioblastoma Multiforme cancer cell survival but dispensable for healthy neural cell survival. We characterize the important chaperone-like role BuGZ plays in mitosis to examine its apparent dispensability in healthy cells. BuGZ aids in the kinetochore loading of Bub3, which in turn is needed for the kinetochore loading of proteins with important roles in kinetochore-MT attachment and in spindle assembly checkpoint signaling. BubR1's cancer lethality has also been previously described in Glioblastoma cells. BubR1 is needed to recruit the PP2A phosphatase to kinetochores, where it stabilizes kinetochore-microtubule attachments. We identify the HEC1 tail as a substrate for the BubR1-recruited population of PP2A, and we demonstrate that kinetochore-microtubule attachment defects in BubR1 depleted cells can be rescued with a phospho-null HEC1 mutant. This work identifies important changes in the mitotic machinery of transformed cells, providing potential pathways to target for therapeutics that may apply to many different cancers.

ACKNOWLEDGEMENTS

I cannot imagine a better place to have spent the last six years than at Colorado State University and in the department of Biochemistry and Molecular Biology, where everyone has been kind, encouraging, and brilliant. I am so grateful to have been in the DeLuca lab where my love for mitosis was born and my research foundation was built. Jake has been a terrific mentor. Her excitement and love for scientific research is contagious and her compassion towards her mentees throughout scientific failures and personal obstacles kept me here even after the hardest time in my life. In my DeLuca lab mates, I found a second family. Not many people would say they choose to hang out with their coworkers on a day off, but those are some of the best times I have had over the years. Keith, Jeanne, and Eric took a noob first year under their wings and taught me so much in the lab. Amanda and Rob have been my best friends over the last 5 years, providing valuable scientific insight and countless fun memories I will always cherish. Amy's addition to the lab a couple of years ago only added to the close-knit dynamic that made going to work every day something I enjoyed.

My committee members Steven, Susan, Erin, and Olve have provided valuable support and collaborations during my time here. Jacob Herman has been an incredible asset to my scientific growth over the years. Although we only overlapped for a few months in the lab, our continued scientific collaborations and friendship are very important to me.

My Fort Collins friends were critical for my mental well-being over the past 6 years. I am grateful for their support and company over the years. I am thankful for the friendship

that formed from cat-sitting for Jim Bamburg and Laurie Minamide and for the joy Sami, Toshi, Gracie, and Syd gave me over the years. I am thankful that Amanda brought Shugo into my life.

Finally, I was fortunate to always know that regardless of what happened here in graduate school, I always had a family at home that thought the world of me. I am grateful to each of them for taking time to come out and visit me. My parents went above and beyond the call of duty for parents. They sacrificed everything to get me to where I am today, and I could not have done this without them. Although my mom did not get to see me get to the finish line, she never doubted for a second that this day would come (even when I myself doubted it). Rozheen, Dawer, and Dereen have provided sibling support from afar. Without their personal sacrifices, as well as my dad's, to be there for my mom during her battle, I would have never been able to move across the country in pursuit of a PhD. I will always be grateful.

TABLE OF CONTENTS

CHAPTER 1: INTRODUCTION

1.1 The cell cycle: mitotic cell division

Once a cell has committed to entering the cell cycle, it prepares for DNA synthesis in G1 by growing in size, generating molecules it will need in the coming hours, including proteins and RNA (1). In S phase, the cell duplicates its entire genome and its centrosomes, again in preparation for mitosis (2,3). During G2, the cell completes its preparation by producing even more molecules needed for cell division, as well as the organelles that will be partitioned into the two new cells (1). To ensure the fidelity of the cell cycle, transitions from phase to phase are predominantly under the control of cyclin dependent kinases (CDK) and their activating cyclin counterparts (1,4). The expression and destruction of various cyclins at specific points in the cell cycle ensure activation of the correct CDK at the correct time, such that key substrate phosphorylations are synchronized with cell cycle progression. In conjunction with the timely activation of these CDK/cyclin enzyme complexes, the cell has numerous quality control mechanisms in place in the form of checkpoints that halt cell cycle progression into the next phase until sufficient completion of the previous phase has been assessed (5). These checkpoints include a restriction checkpoint early in G1, a G1/S phase checkpoint, a G2/M phase checkpoint, DNA damage checkpoints before and after S phase, and the mitotic spindle assembly checkpoint, which will be discussed in detail in subsequent sections (5). Cell cycle deregulation is a common theme found in many instances of human pathogenesis, including carcinogenesis, making it a very intriguing focus for therapeutic development (6).

Eukaryotic organisms rely on the process of mitosis for their growth and survival, during which a cell segregates its duplicated genome into two newly formed cells. This general principle is adhered to by all organisms from the simplest eukaryotes, including single-celled fungi, to the most complex of mammals. From the first records of researchers visualizing mitotic cells, the extraordinary morphological changes that occur have been apparent. The German biologist Walther Flemming is credited with being the first to coin the term “mitosis” from the Greek word for “thread” in 1882, reflecting the condensed nature of mitotic chromosomes, which differs vastly from interphase chromatin structure (7,8). We now know this is only a fraction of the dramatic structural reorganization that a mitotic cell must undergo. In addition to condensing chromatin, human mitotic cells break down their nuclear envelope, separate their centrosomes to opposite ends of the cell, and use the microtubules (MTs) nucleating from those centrosomes to physically drive the movement of sister chromatids, first to the spindle equator, then to opposite spindle poles, after which the single cell is split into two new cells at the cleavage furrow during cytokinesis (9) (Figure 1.1A).

1.2 Centromeres and the human kinetochore

Central to the process of mitosis are the kinetochores, the physical connections between the mitotic spindle and the sister chromatids. Kinetochores are large, proteinaceous complexes that assemble on centromeric heterochromatin and their

Figure 1.1. Overview of mitosis in human cells

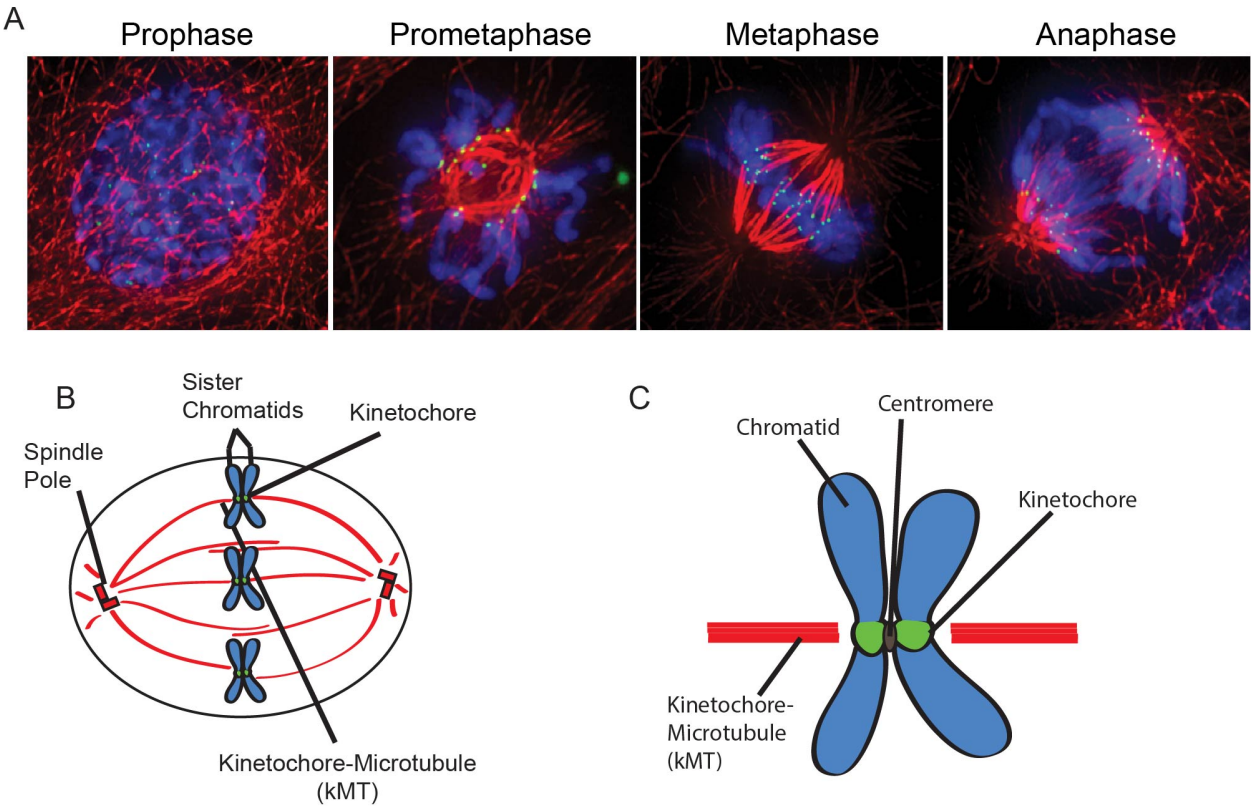

Figure 1.1. Overview of mitosis in human cells. A. Immunofluorescence images of HeLa cells undergoing mitosis. Cells are stained for DAPI (DNA) in blue, ACA (kinetochores) in green, and microtubules in red. B. A skeletal version of a mitotic cell with the spindle microtubules in red, kinetochores in green, and chromosomes in blue. C. A close-up view of a single chromosome consisting of two sister chromatids, two sister kinetochores, and a single centromere region.

molecular components are largely conserved amongst eukaryotes, excluding the unicellular flagellated kinetoplastids (10) (Figure 1.1B, C). As centromeres dictate the location of kinetochore assembly, there can be significant variation in kinetochore structure from species to species. Chromosomes may have monocentromeres, in which the centromere appears as a single primary constriction; polycentromeres, containing multiple primary constrictions; or holocentromeres, consisting of centromeres that run along the entire length of a chromosome (11). Monocentromeres are further divided into point and regional centromeres. Budding yeast is an example of an organism with a point centromere, encompassing only a single nucleosome at its centromere and its location is specified by a specific ~125 bp sequence of DNA (12,13). Human chromosomes have regional centromeres that do not appear to have a requirement for a specific DNA sequence. Instead, the DNA is composed of monomeric arrays of ~171 bp repetitive α-satellite sequences, which only share 50%-70% sequence identity. The monomers then comprise higher order repeats (HOR) that are themselves further repeated, capable of reaching up to five megabases in size (14,15).

While there is heterogeneity in the DNA sequences that dictate centromere identity, the commonality amongst the vast majority of eukaryotic centromeres is the enrichment of nucleosomes containing the histone H3 variant, CENP-A (16-18). This epigenetic factor has been shown to be essential for survival and kinetochore assembly (19-21). CENP-A containing nucleosomes allow for the formation of kinetochores at centromeres through recruitment of the constitutive-centromere-associated-network (CCAN), most of which is conserved in eukaryotes. In vertebrates, the CCAN is composed of 16 proteins that mostly remain associated with centromeric DNA throughout

the cell cycle. Through several key publications over the last few decades, it is now fairly well-understood how the subcomplexes within the CCAN support kinetochore function and formation. CENP-A nucleosomes directly bind to the protein CENP-C (22,23) and to the protein CENP-N, which is in complex with CENP-L (24). Additionally, adjacent histone H3-containing nucleosomes bind directly to the CENP-TW complex (25), which then forms a larger complex of CENP-T-W-S-X (26). Further inter-dependent interactions between these CCAN components leads to the recruitment of a CENP-H-I-K-M (27,28) and CENP-O-P-Q-U-R complex (29), ensuring structural stability at the foundation of the kinetochore. In addition to binding CENP-A-containing nucleosomes, the N-terminus of CENP-C directly binds to the kinetochore scaffold protein, Mis12, a component of the essential outer kinetochore Knl1-Mis12-Ndc80 (KMN) network, which will subsequently be discussed further (30,31). Thus, CENP-C helps bridge centromeres and kinetochores. Similarly, a second “arm” of the CCAN has also been shown to recruit KMN components separately from CENP-C. CENP-T directly binds to both the Ndc80 complex and the Mis12 complex, therefore contributing to its localization at kinetochores, independently of CENP-C (32,33) (Figure 1.2).

Unlike the centromeric DNA binding CCAN, vertebrate kinetochores are only assembled at the start of mitosis (G2/M phase) and are disassembled upon mitotic exit. Early electron microscopy data showed the kinetochore region as a disk-like structure composed of three distinct domains or layers (34-36). The innermost layer consists of centromeric chromatin and DNA-binding proteins and is cell-cycle independent. The middle layer appears less electron dense, and it connects the inner layer to the third layer, which is the electron dense outer layer that forms only during mitosis. In the absence of

Figure 1.2. The kinetochore is built from a bottom up approach.

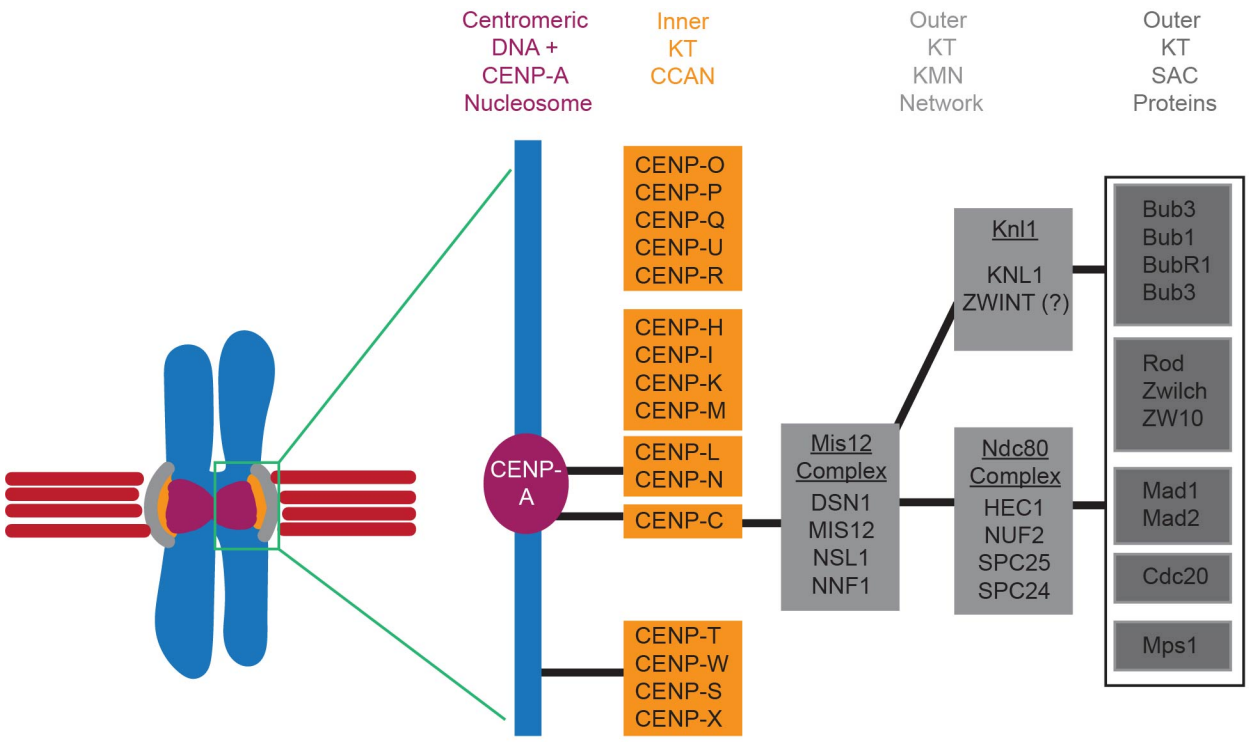

Figure 1.2. The kinetochore is built using a bottom up approach. CenpA containing nucleosomes provide a building block for the rest of the kinetochore. The inner kinetochore consists of the constitutive centromere associated network (CCAN) upon which the outer kinetochore Knl1-Mis12-Ndc80 (KMN) network is built. The KMN provides the binding site for the spindle assembly checkpoint proteins.

microtubule attachments, a meshwork termed the fibrous corona can be seen extending from the outer plate (37-39). The outer kinetochore is comprised of several key proteins involved in forming kinetochore-microtubule attachments, regulating the attachments that are formed, and in spindle assembly checkpoint signaling to ensure error-free cell division. Essential to all of these functions is the 10 subunit KMN network, named for the proteins from which it is comprised: the Knl1 complex, the Mis12 complex, and the Ndc80 complex (40,41) (Figure 1.2). The remaining focus will be on human kinetochores.

1.3 The Knl1-Mis12-Ndc80 (KMN) Network

The four subunit Mis12 complex, consisting of the MIS12, PMF1, NSL1, and DSN1 subunits, acts as a platform for the assembly of the other KMN components. The Mis12 complex recruits the Knl1 complex through direct binding of its NSL1 subunit to KNL1's C-terminus (42,43). Additionally, the Mis12 complex also recruits the Ndc80 complex through direct binding between NSL1 with the Ndc80 complex subunits, SPC24 and SPC25, in a non-competitive manner with KNL1 (43). As mentioned above, the Mis12 complex also forms a direct binding interaction between PMF1/DSN1 and the N-terminus of the CCAN component, CENP-C, thus connecting the inner kinetochore to the outer kinetochore (30,31,44). Depletion of the Mis12 complex results in chromosome alignment defects and thus segregation errors. Furthermore, while cells depleted of the Mis12 complex arrest in mitosis for ~8 hours as a result of the errors, decreased levels of checkpoint proteins suggest these cells may be partially compromised in their spindle assembly checkpoint (45).

The Knl1 complex consists primarily of the KNL1 protein, but some consider Zwint-1 a member of the complex as well, as it copurifies with the KMN network. KNL1 is the

largest outer kinetochore protein, with 2316 residues in humans. The majority of KNL1 is predicted to be intrinsically disordered and the protein has docking sites for several key mitotic factors (46). Only the C-terminus of KNL1 is predicted to be ordered, with two RWD motifs for Mis12 complex binding and a coiled coil domain for binding to the protein Zwint-1 (43). The very N-terminus of KNL1 contains a SILK and RVSF motif implicated in recruitment of the phosphatase PP1 to kinetochores (47). Additionally, the N-terminus has been reported to have a MT-binding domain, although KNL1 is not the predominant MT-binding component of the KMN (48). Just C-terminal to these motifs are the KI1 and KI2 (KI[DN]XXXF[LI]XXLK) motifs, which have been shown to aid in the recruitment of Bub1 and BubR1 to kinetochores (49,50). Following the KI motifs and extending into the middle of the protein, are the KNL1 MELT (M[ED][ILVM][ST]) motifs, which are critical for spindle assembly checkpoint function through recruitment of Bub3, Bub1, and BubR1 (51-53). KNL1 depletion results in chromosome segregation defects; while many chromosomes do in fact congress to the metaphase plate normally, some uncongressed chromosomes remain at the spindle poles (54,55). The misalignment phenotype resulting from KNL1 depletion is a matter of some question. KNL1 depletion does not abolish Ndc80 complex kinetochore localization, and Ndc80 is the key MT attachment factor (54). The motor protein CENP-E is required for polar ejection activity in which chromosomes at the pole are bound by the plus-end directed motor, which then walks toward the plus end of MTs that push out towards the spindle equator (56). CENP-E kinetochore recruitment requires Bub1 in some cell types and as KNL1 depletion results in loss of Bub1, possibly explaining the polar chromosome phenotype seen in KNL1 depletion (46,57,58). Additionally, it has been shown that Knl1 is required for Aurora B kinase

activity at the kinetochore (55), which is critical for the formation of correct kinetochore-MT attachments. As Bub1 and BubR1 are lost from kinetochores depleted of KNL1 (42), Kiyomitsu and colleagues found KNL1 depleted cells largely experienced faster mitosis, in which the spindle assembly checkpoint was abrogated, presumably due to the loss of BubR1. However, they also saw instances of checkpoint activation and mitotic arrest, likely due to the chromosome misalignment defects. As discussed in a review by Caldas and DeLuca, others have also seen sufficient spindle assembly checkpoint signaling even in the absence of KNL1 (46), perhaps due to a combination of weak cytosolic checkpoint function and the loss of PP1, which is implicated in checkpoint silencing.

The Ndc80 complex is the key binding module of MTs by the kinetochore (48,59,60). The heterotetrameric ~60 nm complex maintains a dumbbell shape comprised, on one end, of the C-terminal globular domains of SPC24 and SPC25 and, on the other end, of the N-terminal globular domains of NDC80 (HEC1) and NUF2 (61-63). The N-termini of SPC24/SPC25 and the C-termini of HEC1/NUF2 span the central region of the dumbbell in a coiled-coil tetramerization domain (64). This coiled-coil domain is interrupted by a ~40 amino acid “loop” in HEC1 that is important for regulation (65). The globular SPC24/SPC25 end consists of a RWD (RING finger, WD repeat, DEAD-like 113 helicase) fold, which connects the Ndc80 complex to the inner kinetochore through one of two different arms in the CCAN-outer kinetochore link: either the Mis12 complex bound to CENP-C or through CENP-T bound directly to SPC24/SPC25 or indirectly through another Mis12 complex. The globular domains of HEC1/NUF2 form calponin-homology (CH) domains, and the HEC1 CH domain contains a critical MT binding site referred to as the “toe” region. Mutations in this region completely abolish kinetochore-

MT binding in cells (63,66,67). An additional regulatory aspect is provided by the positively charged HEC1 unstructured “tail” domain located at its very N-terminus. In humans, this 80-amino-acid tail domain contains nine Aurora B kinase phosphorylation target sites that are thought to tune the binding affinity of HEC1 for MTs (48,59,68,69). Early in mitosis, phosphorylation at these sites is high, allowing for high kinetochore-MT turnover at a time when initial attachments are likely erroneous. As mitosis progresses and cells align at the metaphase plate, Aurora B kinase phosphorylation of these tail domain sites decreases and HEC1 binding affinity is strengthened or stabilized, allowing for robust, force-generating kinetochore-MT attachments. Depletion of Ndc80 complex components results in failure to form load-bearing kinetochore-MT attachments and a so-called “kinetochore-null” phenotype (40,60).

The KMN network is critical for high-fidelity mitotic cell division. These three complexes ensure the proper formation of kinetochore-microtubule attachments by physically binding the microtubules, as well as by recruiting several factors that perform regulatory and checkpoint functions. Errors that are not corrected during mitosis result in genetically aberrant daughter cells. While in a healthy organism most of these cells will be eliminated, genetic errors are heavily associated with many diseases and cancers. For that reason, cells have safeguards in place to prevent the persistence and transmission of such dangerous errors.

1.4 The spindle assembly checkpoint

The spindle assembly checkpoint (SAC) is a surveillance mechanism in the form of a signaling cascade that halts mitotic exit until kinetochore-MT attachments are properly formed at all sister chromatids in the cell. The SAC must be able to recognize

improperly attached or unattached kinetochores, and it must be able to send out a “wait anaphase” signal that can be amplified such that even a single unattached kinetochore can prevent mitotic exit. Over the course of several decades and from the contributions of several publications, we now have an extensive understanding of just how this is done.

The objective of the SAC is to inhibit the Anaphase Promoting Complex/Cyclosome (APC/C), an E3 ubiquitin ligase which, when active, will ubiquitinate the key mitotic regulators, cyclin B and securin, targeting them for proteasomal degradation (70-72). Loss of cyclin B leads to inactivation of the mitotic CDK1 and loss of securin leads to the activation of separase, which will cleave the Cohesin ring complexes responsible for keeping sister chromatids attached in mitosis (73-77). These two events result in mitotic exit, and it is imperative that they are prevented until all kinetochores are properly attached to the correct MTs, allowing for equal partitioning of the genome into the two newly formed daughter cells. To inhibit the APC/C, the SAC functions to interfere with the activation of the APC/C by its coactivator, Cdc20 (78).

The effector of the SAC is the mitotic checkpoint complex (MCC), comprised of Bub3, BubR1, Mad2, and Cdc20 (79-82) (Figure 1.3). Accumulation of these proteins that form the MCC occurs at the MELT (M[ED][ILVM][ST]) motifs of the outer kinetochore protein, KNL1. The kinase Mps1 phosphorylates the highly conserved MELT motifs (pMELT), creating a binding site for the Bub3-Bub1-BubR1-Bub3 tetrameric complex, which is central to SAC activity (51-53,83-85). To localize to kinetochores, the N-terminus of Mps1 kinase binds directly to the Ndc80 complex through the HEC1 CH domain. Competition between MTs and Mps1 for binding to the HEC1 CH domain allows for a mechanism of SAC activation that

Figure 1.3. The spindle assembly checkpoint inhibits mitotic exit in the presence of unattached kinetochores

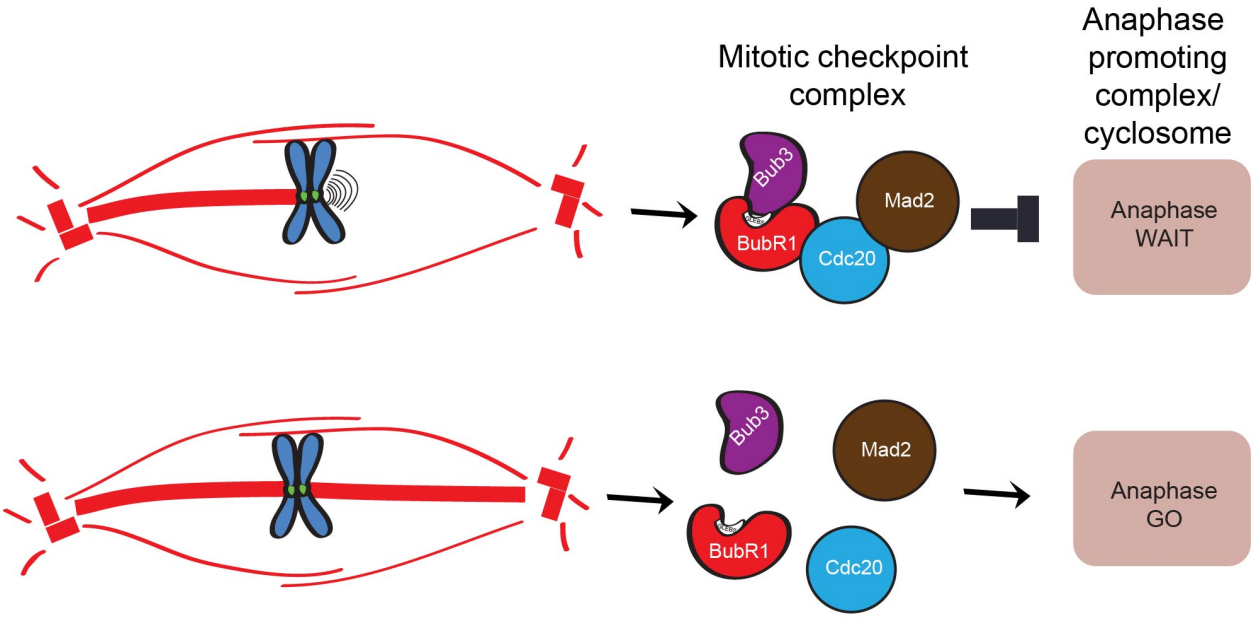

Figure 1.3. The spindle assembly checkpoint inhibits mitotic exit in the presence of unattached kinetochores. Schematic of the spindle assembly checkpoint. (Top) a sister chromatid is unattached to microtubules. This results in the formation of the mitotic checkpoint complex (MCC), which will localize to kinetochores and inhibit the anaphase promoting complex (APC/C), resulting in a mitotic arrest. (Bottom) Upon attachment of all kinetochores to spindle microtubules, the MCC will be disassembled and the APC/C will be activated by its co-activator, Cdc20. Anaphase may now commence.

is dependent on the attachment status of the kinetochore (86,87). In addition to nineteen candidate MELT motifs in human KNL1, the N-terminus of KNL1 also has two Lys-Ile (KI) motifs, each capable of directly binding to the tricopeptide repeat (TPR) of either Bub1 or BubR1 (42,49,50). However, while the KI motifs enhance Bub1 and BubR1 localization at kinetochores, they are not necessary for checkpoint function in the presence of the MELT motifs (50). Recruitment of the Bub proteins to KNL1 after Mps1 phosphorylation of the MELT repeats is a key step in the SAC signaling cascade. A single pMELT binds one Bub3-Bub1-BubR1-Bub3 tetramer (88). Bub3 recognizes the pMELT directly and Bub1 and BubR1 bind to Bub3 through their respective GLE2p-binding sequence (GLEBS) domains (89). Phosphorylation of kinetochore localized Bub1 by CDK1 and Mps1 then allows Bub1 to bind to and recruit Mad1, an essential SAC protein (90-92). Mad1 then recruits Mad2, a component of the MCC. Mad2 can adopt different conformational states (93-95). Soluble Mad2 not bound to kinetochores is usually in the inactive “open” state (O-Mad2), meaning it cannot incorporate into the MCC. When bound to Mad1 at the kinetochore, Mad2 takes on a “closed” conformation (C-Mad2) that is capable of incorporating into the MCC. Mad1-C-Mad2 at the kinetochore acts as a template, binding to O-Mad2 from the cytosol and promoting its conversion into an intermediate form of Mad2 (I-Mad2), which is then able to interact with Cdc20 (96-98). Once bound to Cdc20, Mad2 is in the “closed” state (Cdc20–C-Mad2) and can now interact with BubR1-Bub3 to form active MCC. There is evidence that Mad1 at the kinetochore is also phosphorylated by Mps1 kinase to increase the conversion rate of O-Mad2 to I-Mad2 (91,98).

Once MCC is formed at kinetochores, the complex must act to prevent APC/C activation. While Bub3's role in the MCC has mostly been considered as a targeting factor, there is recent evidence that it may have a more direct function in APC/C inhibition. Overlack and colleagues showed that Bub3 might enhance the ability of BubR1 to interact with the APC/C, thereby stimulating the MCC's inhibitory effects (99). BubR1 itself contains several domains involved in APC/C inhibition and these include two Lys-Glu-Asn (KEN) motifs (KEN boxes) (for Cdc20 and Mad2 binding), TPR motifs (implicated in Mad2, Cdc20, and APC/C binding), an "internal Cdc20-binding site" shown to contain an ABBA (Fx[ILV][FHY]x[DE]) motif (for Cdc20 binding), and two destruction box (D box) motifs (for Cdc20 binding) (100-103). These domains aid in BubR1's ability to bind Cdc20 by acting as a pseudo-substrate. Mad2 is a HORMA (Hop1, Rev7, Mad2) domain-containing protein that binds both BubR1 and Cdc20 directly (94,104,105). Cdc20 functions in two separate ways: as a component of the MCC with the goal of inhibiting the APC/C and as a coactivator of the APC/C. The Mad2-interacting motif (MIM) of Cdc20 is critical for its role in the SAC (106). Mad2 and BubR1 work synergistically in inhibiting APC/C activation by Cdc20 (107). Recent advancements in high resolution structures of the APC/C in complex with the MCC have revealed the presence of two Cdc20 molecules in the complex. One molecule is in complex with BubR1 and C-Mad2 as an inhibitor of the APC/C and the other molecule is bound to the APC/C, poised to be an activator. However, this would-be activating Cdc20 is positioned with significant orientation changes, preventing it from actually recognizing substrates for APC/C ubiquitination (108,109).

Upon formation of the correct kinetochore-MT attachments at each kinetochore, the SAC must be silenced in a timely manner (Figure 1.3). Classical experiments showed that laser ablation of the last unattached kinetochore in a cell resulted in anaphase onset after approximately ~17 minutes (110). Not only must kinetochores cease to generate MCC, but the cycling MCC in the cell must be disassembled. As kinetochores become stably attached in metaphase, Aurora B kinase activity at the kinetochore also decreases (55,69,111). This results in a loss of phosphorylation at the KNL1 SILK/RVSF motifs, allowing for the recruitment of the phosphatase, PP1 (47). Once localized to KNL1, PP1 can then dephosphorylate the MELT motifs, effectively reversing the signaling cascade that begins with Mps1 phosphorylation of the MELTs to recruit the Bub3-Bub1-BubR1-Bub3 tetrameric complex (112). Additionally, mammalian cells rely on the MT motor protein, Dynein, to remove checkpoint proteins from the kinetochore (113). While the details of this process remain to be refined, it is thought that the Dynein/Dynactin complex localizes to kinetochores through the adaptor protein, Spindly. Dynein then binds various checkpoint “cargoes” and, using end-on attached MTs as tracks, walks them to the spindle poles, aiding in checkpoint silencing (114). In order to disassemble preexisting MCC in the cytosol, cells rely on the joint efforts of the Thyroid receptor hormone interacting protein (TRIP13) and its adaptor p3comet. TRIP13 is a AAA-ATPase that catalyzes the conversion of C-Mad2 back into O-Mad2 (115,116). p31comet is structurally very similar to C-Mad2, which is thought to help block the conversion of O-Mad2 into additional C-Mad2 (117).

A fascinating question in the SAC field concerns the trigger that sets silencing in motion. As end-on attachment inevitably results in tension across sister kinetochores, it

has been difficult to assess if physical attachment itself or the pulling forces from the attached kinetochore-MTs leads to SAC satisfaction. This is further complicated by the fact that mammalian kinetochores are not bound to a single MT, but instead to a bundle of ~25 MTs which are continuously undergoing attachment/detachment cycles (118). This means that at any given time, some MTs in a bundle are attached while others are not. Historic experiments in which kinetochores were pulled on using a microneedle showed this was sufficient for SAC satisfaction, suggesting tension is the property the SAC monitors (119). However, even in this case, it is hard to prove that the microneedle interaction with the kinetochore does not satisfy the SAC simply by physical contact with the kinetochore, as a MT would. Through experiments combining a mutant Ndc80 HEC1 tail domain that is unable to be phosphorylated by Aurora B kinase (HEC1-9A) and manipulations to create monopolar spindles, two labs assessed attachments in the absence of tension across kinetochores (120,121). In these instances, the SAC was satisfied and silenced, even though biorientation was not achieved.

1.5 Error correction through phospho-regulation of attachments

The second safeguard cells use to prevent sustained accumulation of errors in mitosis is the error correction pathway. Kinetochore-MT attachments are conducted primarily through the Ndc80 complex in eukaryotes (122-124). Loadbearing, end-on attachments are critical for the fidelity of mitosis. The “master regulator” of kinetochore-microtubule attachment strength and error correction is the kinase Aurora B, which is the enzymatic component of the Chromosomal Passenger Complex (CPC) that localizes to both centromeres and kinetochores (125). Contrary to the prevailing model in which Aurora B localized at the centromere phosphorylates substrates at the kinetochore prior

to biorientation and tension, recent work has shown that a discrete population of Aurora B localizes to kinetochores to act on attachment factors locally (126,127). As a general rule, Aurora B activity at the kinetochore promotes kinetochore-microtubule turnover. One of the primary targets of Aurora B phosphorylation is the HEC1 N-terminal tail domain consisting of 80 amino acids, at least 9 of which have been shown to be sites of phosphorylation by Aurora B (48,59,68,69) (Figure 1.4A). Early experiments in which an antibody that bound the HEC1 tail domain was injected into cells resulted in hyper-stable attachments, leading to errors in mitosis (59). This was likely due to the loss of Aurora B access to the phospho-sites. This phenotype has been further proven using mutant versions of the HEC1 tail domain in which all 9 phosphorylation sites were mutated to alanine residues to prevent phosphorylation. The reverse experiment in which the 9 phosphorylation sites were mutated to aspartic acid showed a loss of stable attachments and tension across kinetochores (68,69,128).

Aurora B phosphorylation of substrates is usually high early in mitosis and decreases as chromosomes begin to align. This allows for high turnover of those initial attachments after nuclear envelope breakdown when the disordered kinetochores are likely making incorrect attachments (Figure 1.4A). Phosphatases at the kinetochore work to counteract Aurora B activity, maintaining a balance of attachment/detachment. The primary phosphatases at the kinetochore are PP2A and PP1, which will be discussed in detail in chapter 4 (129,130) (Figure 1.4B). As PP2A localizes to kinetochores in early mitosis while PP1 localizes later, it is generally thought that PP2A acts on kinetochore-MT attachment factors, while PP1 acts more in silencing of the SAC ((112,131,132). There is still much ambiguity regarding which substrates are dephosphorylated by each

Figure 1.4. The error correction pathway centers around the kinase Aurora B and the phosphatases

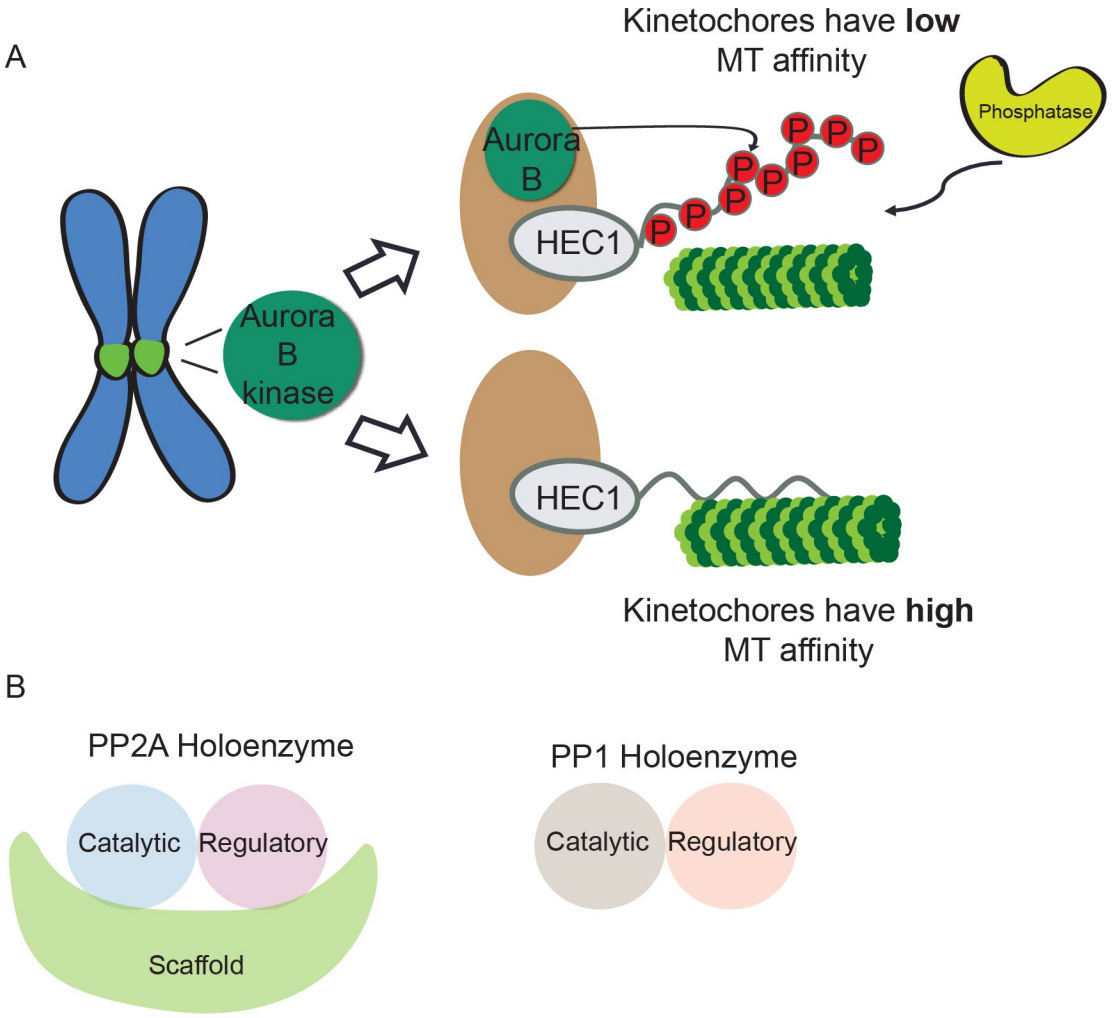

Figure 1.4. The error correction pathway centers around the kinase Aurora B and the phosphatases. A. Schematic of the erroc correction pathway, involving Aurora B kinase phosphorylation of the HEC1 N-terminal tail, decreasing the affinity between MTs and kinetochores. Upon decrease in Aurora B activity and increase in phosphatase activity, the HEC1 tail is dephosphorylated and its affinity for MTs is increased. B. Schematic of the PP2A and PP1 holoenzymes.

phosphatase. To further complicate the matter, each phosphatase can bind different regulatory proteins to create different holoenzymes that may act on different substrates (Figure 1.4B). As discussed earlier, PP1 localization to the kinetochore is largely through binding to the SILK/RVSF motif of KNL1. However, other proteins have also been implicated in PP1 kinetochore recruitment, including the SKA complex and the kinesin KIF18A (133,134). PP2A in complex with its B56 regulatory subunit is recruited to kinetochores through interaction with the BubR1 Kinetochore Attachment Regulatory Domain (KARD) after it is phosphorylated by the kinase PLK1 (131,135). Through the timely localization of different phosphatase holoenzymes to discrete locations in the cell, the activity of kinases involved in attachment can be regulated such that detachment is favored early in mitosis and attachment is favored as mitosis progresses.

An additional method of destabilizing erroneous attachments involves MT depolymerases of the Kinesin-13 family, such as microtubule depolymerase mitotic centromere-associated kinesin (MCAK) and KIF2B. These kinesins are nonmotile and they cause depolymerization of MTs through disassembling the tubulin dimers from the ends (136). MCAK is thought to reside at centromeres and inner kinetochores, where it predominantly works to correct kinetochore-MT attachments in metaphase, while KIF2B localizes to outer kinetochores and acts during prometaphase (137,138). Kinesin-13 members are very important for correcting merotelic attachments, in which a single kinetochore is attached to MTs from both spindle poles as these are not detected by the SAC (139). The kinesins are regulated by PLK1 and Aurora B kinase, but the details of the regulation remain a topic of investigation.

1.6 Mitotic aberrations in cancer cells

Chromosomal abnormalities are hallmarks of cancer cell genomes. One common type of abnormality is the gain or loss of whole chromosomes during cell division, known as aneuploidy (140). Theodor Boveri was one of the first cancer researchers to describe this phenomenon early in the twentieth century while working with sea urchin embryos, and it is still an area of great intrigue today (141). Particularly, the debate as to whether aneuploidy is a cause or by-product of cell transformation is far from settled. Nonetheless, the prevalence of aneuploidy in solid tumors has made mitosis an area of focus when trying to identify differences in primary and transformed cell lines that can be targeted for specific therapeutics.

Studies done in yeast and mouse embryonic fibroblast (MEF) cells have shown that aneuploidy is detrimental to cell fitness. Torres and colleagues generated haploid yeast strains with a single extra chromosome (142). Regardless of the specific chromosome that was in excess, all the aneuploid strains exhibited slower proliferation rates due to G1 delay, defects in DNA repair pathways, increased genomic instability, and increased sensitivity to drugs that target protein synthesis and folding. Williams and colleagues generated MEFs with an extra copy of one of four chromosomes (1, 13, 16, or 19) and found that all but one of the embryos (trisomy 19) died *in utero* (143). However, analysis of the generated MEF cell lines showed defects in proliferation and metabolic alterations. These and other studies raise the question of how seemingly detrimental karyotypes are tolerated, and perhaps selected for, in tumors. These cells must undergo significant changes to adapt to the altered functions that result from aneuploidy.

As aneuploidy results from aberrant cell division, it is important to consider what defects in mitosis may result in the mis-segregation of the genome (Figure 1.5). Many tumor cells have been shown to have more than the canonical two centrosomes (Figure 1.5A). This leads to multipolarity in early mitosis, resulting in many erroneous kinetochore-MT attachments. Interestingly, it has been reported that cancer cells exhibit centrosomal clustering as they near anaphase, giving the false representation of a bipolar spindle and dividing into two daughter cells that then have high levels of mis-segregation (144,145). Reduction in sister chromatid cohesion has also been implicated in increasing aneuploidy incidence (146) (Figure 1.5B). Premature separation of the sister chromatids before bipolar kinetochore-MT attachments can form is deleterious. An additional means of aneuploidy is defects in the SAC, as this would prevent sufficient timing for the formation of correct attachments (Figure 1.5C). In fact, a study looking at a subset of aneuploid colon cancer cell lines showed mutation of Bub1 and BubR1 correlating with a weakened SAC (147). However, mutations in SAC genes are actually relatively rare in studies looking at tumor cells (148). Perhaps the most common cause of chromosome mis-segregation in aneuploid cells is reportedly the persistence of lagging chromosomes, which result from merotelic kinetochore-MT attachments (Figure 1.5D) (139,149). Importantly, merotely occurs often in healthy cells as well, but the error correction machinery destabilizes these attachments, allowing for amphitelic attachments to replace them. Therefore, lagging chromosomes are often consequences of mis-regulation in the kinases and phosphatases involved in kinetochore-MT attachment strength.

Studying cell transformation model systems to better understand the mitotic defects that arise in cancers can help identify potential targets for therapeutic intervention.

Figure 1.5. Aneuploidy can arise from several different defects during mitosis

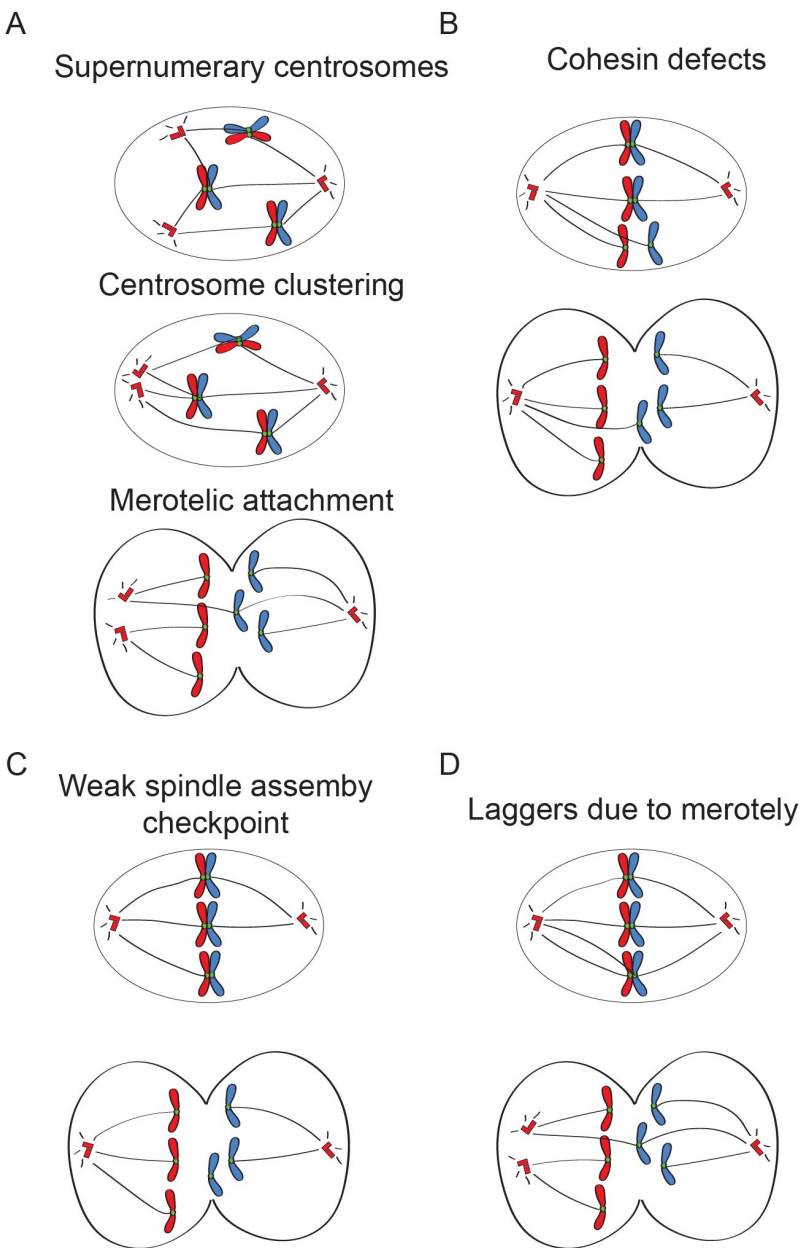

Figure 1.5. Aneuploidy can arise from several different defects during mitosis. A. Many cancer cells exhibit supernumerary centrosomes that cluster near metaphase, resulting in the impression of a bipolar spindle. B. Defects in the cohesin complex can result in premature sister chromatid separation. C. A weak or defective spindle assemby checkpoint can result in mitotic exit before all kinetochores become attached to spindle MTs. D. A merotelic attachment consists of a kinetochore is attached to MTs emanating from both spindle poles. This leads to lagging chromosomes in anaphase. This figure is modified from Gordon et. al., 2015.

As cancers are comprised of complex combinations of various mutations and genetic backgrounds, it is important to consider the vast differences between tumors. While much can be learned from studying patient tumor isolates, the variations in genetic backgrounds between patients and cells can complicate the interpretation of the results. Simultaneously, much can be learned from analyzing the results of single mutations which activate specific oncogenic signaling pathways. Therefore, we wanted to utilize a laboratory cell transformation system that consisted of cells originating from the same parental cell line.

Through the studies described below, we aimed to better understand the mitotic changes that occur upon cell transformation. To do this, a human papillomavirus (HPV) model system was initially used to assess mitotic aberrations that occur upon expression of HPV transforming proteins. Chapters three and four discuss a different approach to understanding mitosis in cancer cells. The work done in these two chapters is built upon initial cancer lethality screens performed by the lab of Dr. Patrick Paddison at the Fred Hutch Cancer Research Center. Through an RNAi screen targeting putative transcription factors in the human genome, Dr. Paddison's lab identified the mitotic protein BuGZ as essential for survival in glioblastoma multiforme stem cells (GSC), but dispensable in healthy neural crest stem cells (NSC) (150). The work in chapter three aims to characterize the function of BuGZ in mitosis. Similarly, a second RNAi screen targeting the human kinome revealed the mitotic protein BubR1 as essential in GSCs and dispensable in NSCs (151). The work in chapter four investigates which function of BubR1 becomes essential in transformed cells.

CHAPTER 2: SPINDLE ASSEMBLY CHECKPOINT SIGNALING AND SISTER CHROMATID COHESION ARE DISRUPTED BY HPV E6-MEDIATED TRANSFORMATION[1]

2.1 Introduction

A majority of cancer cells exhibit defects in chromosome segregation, which in many cases result in aneuploidy, a situation by which cells contain either too few or too many whole chromosomes (140). Although defects in regulating kinetochore–microtubule attachments are a well-demonstrated cause of chromosome segregation errors, it is unclear how oncogenic proteins induce such defects (139,152). Expression of E6 and E7 proteins isolated from high-risk human papillomavirus (HPV) strains 16 and 18 are sufficient to induce aneuploidy and other behaviors common to cancer cells (153). Thus, expression of these single proteins makes for a useful genetic model of possible mitotic defects that lead to chromosome segregation errors.

HPV E6 transforming protein is best known for functioning in complex with E6AP/UBE3A to polyubiquitinate p53 and target it for proteasomal degradation (154). By degrading p53, HPV-positive cells are able to bypass the senescence program usually activated by aneuploidy/polyploidy; however, p53 loss is not sufficient to cause chromosome segregation defects (155). HPV E7 transforming protein is instead best known for its sequestration of pRb, which accelerates the cell cycle. Upon inhibition of

[1] The work presented in this chapter was published as a research article in 2017 under the same title.

J.G.D. and J.A.H. conceived the idea for the project. J.A.H., E.P.K., and I conducted the experiments and analyzed the data. J.G.D., J.A.H., and I co-wrote the manuscript.

Shirnekhi, H. K., Kelley, E. P., DeLuca, J. G., and Herman, J. A. (2017) Spindle assembly checkpoint signaling and sister chromatid cohesion are disrupted by HPV E6-mediated transformation. Mol Biol Cell 28, 2035-2041.

pRb by E7, the transcription factor E2F is constitutively active, deregulating the G1- to S-phase transition (156). Thus HPV-positive cells exhibit unregulated cell cycling; however, unrestrained cell growth alone does not cause chromosome segregation defects either. Consequently, the molecular mechanisms by which E6 and E7 induce mitotic defects and chromosome segregation errors remain largely unexplained.

The correct segregation of chromosomes is a complex task accomplished by the entire mitotic machinery. Two major mitotic regulatory mechanisms are the spindle assembly checkpoint (SAC) and kinetochore–microtubule attachment error correction. The SAC ensures genetic fidelity by preventing mitotic exit until all kinetochores are properly attached to microtubules of the mitotic spindle and each sister kinetochore pair achieves biorientation at the spindle equator (157,158). Error correction instead employs phosphoregulation of microtubule-binding proteins and microtubule depolymerases to ensure that only properly bioriented kinetochore–microtubule attachments are stabilized (69,159,160).

Here we investigate how the fidelity of chromosome segregation is affected by expression of HPV proteins E6 and E7. Specifically, we analyzed cells' ability to generate and regulate kinetochore–microtubule attachments and to generate a robust SAC response. Through this characterization, we demonstrate that HPV16 E6 induces chromosome segregation errors by preventing proper chromosome congression, weakening the SAC, and compromising sister chromatid cohesion. These studies clarify how E6 contributes to chromosome segregation defects and aneuploidy and may help elucidate how such errors arise in other cancers.

2.2 Results

Expression of HPV16 E6 and E7 transforms RPE1 cells

We performed these studies in an hTert immortalized epithelial cell line, RPE1, a common tool to investigate mitotic processes in a nontransformed background. E6 and/or E7 genes from high-risk strain HPV16 were stably introduced into RPE1 cells using Moloney murine leukemia virus (MMLV)–based retroviral transduction (161). Gene expression was driven from a combination of the MMLV LTR and the HPV16 E6 endogenous p97 promoter (Figure 2.1A). Cells were termed RPE1, RPE16, RPE17, and RPE167 to denote which transgene each expressed. Polyclonal populations were negatively selected via neomycin resistance, and transgene expression was validated by PCR analysis of cDNA after 3 weeks of selection/outgrowth (Figure 2.1B). Expression of HPV proteins E6 and/or E7 was sufficient to cause changes in cell morphology; all cells were less elongated and contained dark staining nuclei, similar to transformed cells (Figure 2.1C). In addition to phenotypic changes, expression of E6 and/or E7 also conferred anchorage-independent growth to RPE1 cells. Most cells isolated from tumors can proliferate in a three-dimensional matrix and give rise to spherical colonies. This behavior is correlated with transformation, metastatic potential, and tumor-initiating ability (161-163). Nontransformed RPE1 cells were not able to proliferate in soft agar, and expression of either HPV protein conferred this behavior (Figure 2.1D). On average, RPE16 cells demonstrated limited growth (3 colonies/ field), whereas RPE17 cells grew more robustly (10 colonies/field), and combined expression was synergistic (21 colonies/field). E6 and E7 inactivate tumor suppressor genes to bypass cell cycle checkpoints, particularly the G1/S transition, which contributes to their tumorigenic

Figure 2.1. Expression and characterization of HPV16 E6 and E7 in RPE1 cells

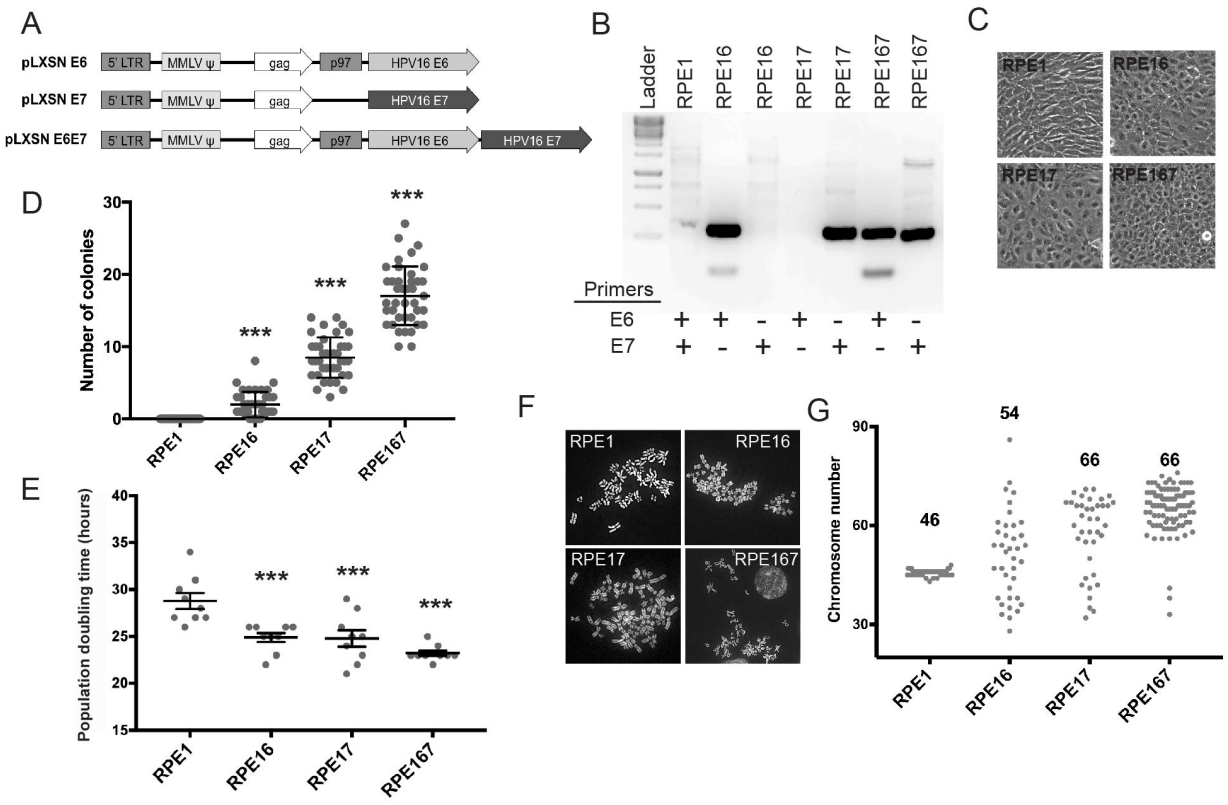

Figure 2.1. Expression and characterization of HPV16 E6 and E7 in RPE1 cells. A. Schematic of pLXSN expression cassettes used to produce HPV 16 E6 and E7 proteins in RPE1 cells. B. Reverse transcription PCR validation of gene expression in virally transduced cells. C. HPV proteins induce changes in cell morphology. D.,E. Expression of E6 and/or E7 increases cells' ability to grow independent of anchorage in soft agar D. and decreases population doubling time E. F., G. Chromosome spreads demonstrating the ability of E6 and E7 to induce aneuploidy in RPE1 cells; polyploidy is rarely observed. G. Chromosome numbers for each cell line and the population mode for each.

activities (154,156). In RPE1 cells expressing either E6 or E7, we observed a significant decrease in population doubling time (Figure 2.1E), which is in agreement with a shortened G1 due to loss of p53 and pRb activity (Figure 2.1E). Consistent with these oncogenic properties and with previous reports (153), expression of E6 and/or E7 also induced significant aneuploidy, with the modal chromosome number increasing by 10–20 chromosomes (Figure 2.1F). In contrast to previous reports, we rarely observed polyploid cells (164) and instead found a small population of hypodiploid cells.

E6 and E7 induce aneuploidy through unique chromosome segregation errors

In all transduced lines, aneuploid cells were commonly observed, whereas polyploid cells were not, suggesting that in this system, HPV proteins were acting on mitotic processes (e.g., spindle formation, SAC activity, kinetochore–microtubule attachments) rather than the cytokinesis machinery to induce chromosome segregation defects. To directly test this, we imaged E6/E7-transduced cells additionally expressing histone H2B–green fluorescent protein (GFP) progressing through mitosis and documented the various types of mitotic errors. E7 expression resulted in a small but significant increase in the instance of lagging chromosomes (~3%; Figure 2.2, A and B). Lagging chromosomes are common in cancer cells and usually arise from merotelic attachments, where a single kinetochore is bound to microtubules from both spindle poles (139,152). The mechanisms leading to merotelic attachments are well established, and thus we focused on E6 expression, which resulted in a more novel phenotype in which ~22% of cells had a small number (one to four) of chromosomes remaining at one or both of the spindle poles in a cell whose chromosomes were otherwise bioriented (Figure 2.2, A and B). This finding was further validated in an hTert immortalized lung fibroblast line

Figure 2.2. HPV proteins induce mitotic errors and delay mitotic duration

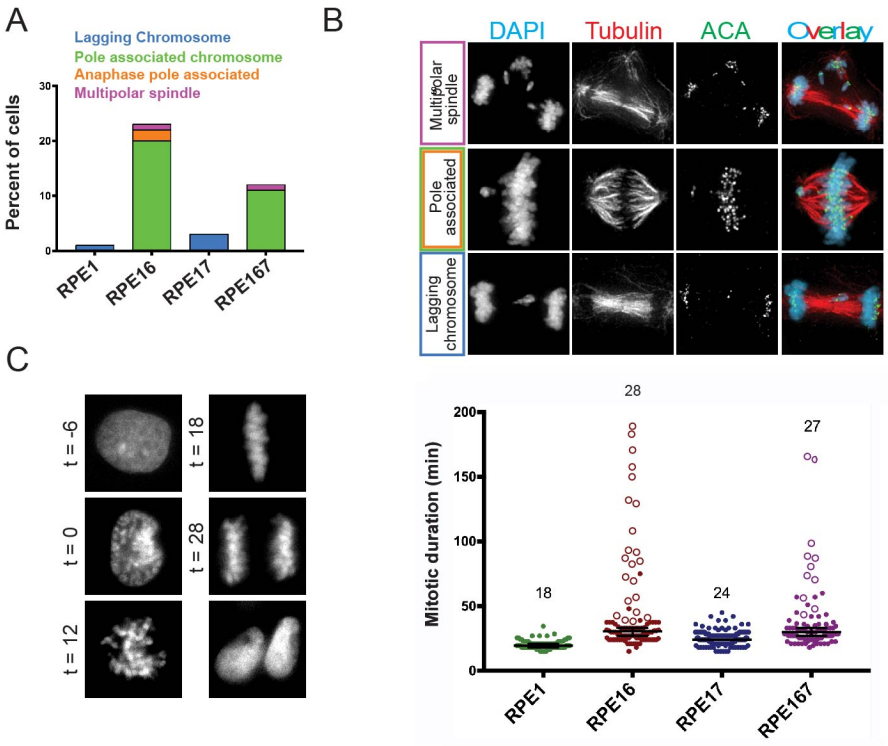

Figure 2.2. HPV proteins induce mitotic errors and delay mitotic duration. A. Chromosome alignment/segregation errors identified by live-cell filming of RPE cells expressing histone H2B-GFP to identify chromatin. At least 150 cells/line were quantified. B. High-resolution immunofluorescence staining of RPE16 and RPE17 cells demonstrating errors quantified in A. C. Left, representative images of a histone H2B-GFP–expressing RPE1 cell transiting mitosis (nuclear envelope breakdown to anaphase onset) with time shown in minutes.Right, median mitotic duration for each cell line. Open circles denote cells with pole-associated chromosomes.

(data not shown). Both E6- and E7-expressing cells took longer to progress through mitosis (nuclear envelope breakdown to anaphase onset) than control RPE1 cells (Figure 2.2C). HPV proteins increased the median mitotic duration by 25–35%, and this increase observed in E6-expressing cells was largely due to a small population that required 50-200 min to complete mitosis. This population was composed of RPE16 cells with pole-associated chromosomes that remained in mitosis for 80 min on average until the chromosome(s) migrated to the spindle equator and anaphase began (Figure 2.2C, open circles). Whereas most cells were eventually able to align all chromosomes, a small percentage of cells (~2%) initiated anaphase before the pole-associated chromosomes (termed anaphase pole associated) could congress to the metaphase plate (Figure 2.2A). This suggested that E6-expressing cells initially stimulated a functional checkpoint but failed to arrest cells in mitosis for prolonged periods despite the presence of uncongressed chromosomes.

E6 weakens spindle assembly checkpoint signaling by decreasing Mad2 levels at kinetochores

Robust SAC activity is essential for healthy and cancer cells alike; however, cancer transformation often alters SAC signaling (165). SAC amplification is more common in cancer, but in rare cases, tumor cells exhibit weakened checkpoint activity, resulting in aneuploidy (166-168). To test whether expression of E6 or E7 resulted in defective SAC signaling, we treated cells with 800 nM nocodazole for 16 h to depolymerize microtubules and activate the checkpoint. Under these conditions, 60%–70% of RPE1, RPE17, and RPE167 cells were arrested in mitosis, whereas only 40% of RPE16 cells remained in mitosis (Figure 2.3A). This trend was also observed in immortalized lung fibroblasts

expressing HPV16 proteins. Because a small population of RPE16 cells was observed to spend 100–200 min in mitosis, this data suggested that cells could generate a SAC response but could not sustain a mitotic arrest for prolonged periods; alternatively, RPE16 cells may enter mitosis less frequently. We observed the former via live-cell imaging, in which most RPE16 cells maintained a mitotic arrest for only ~3 h and nearly all cells exited mitosis within 8 h (Figure 2.3B). RPE167 cells began exiting mitosis at ~5 h in nocodazole, whereas RPE1 and RPE17 cells arrested for >8 h (Figure 2.3B).

Mad2 kinetochore levels correlate with a cell's ability to sustain a mitotic arrest in response to spindle poisons such as nocodazole and Taxol. Thus, we immunostained E6- and E7-transformed cells using Mad2 antibodies (169). Cells were treated with 10 μM nocodazole for 30 min after a double-thymidine block to generate completely unattached kinetochores and maximize Mad2 localization. Under these conditions, Mad2 kinetochore levels in RPE17 cells were similar to those in RPE1 cells, whereas levels were reduced by ~50% in RPE16 cells (Figure 2.3, C and D). The simultaneous expression of E6 and E7 resulted in an intermediate phenotype in which Mad2 levels were reduced by ~15% from RPE1 levels. These results indicate that failure to sustain SAC signaling is due in part to loss of kinetochore associated Mad2.

Kinetochore-associated Mad2 levels increase after inhibition of the 26S proteasome

HPV16 E6 binds to the ubiquitin ligase E6AP/UBE3A, causing polyubiquitination and subsequent degradation of noncanonical UBE3A targets, including p53 (154,170). To determine whether changes to the ubiquitin-mediated degradation machinery are responsible for loss of Mad2 at RPE16 kinetochores, we treated cells that had been

Figure 2.3. HPV E6-transformed cells exhibit defective SAC signaling and recruit less Mad2 to kinetochores

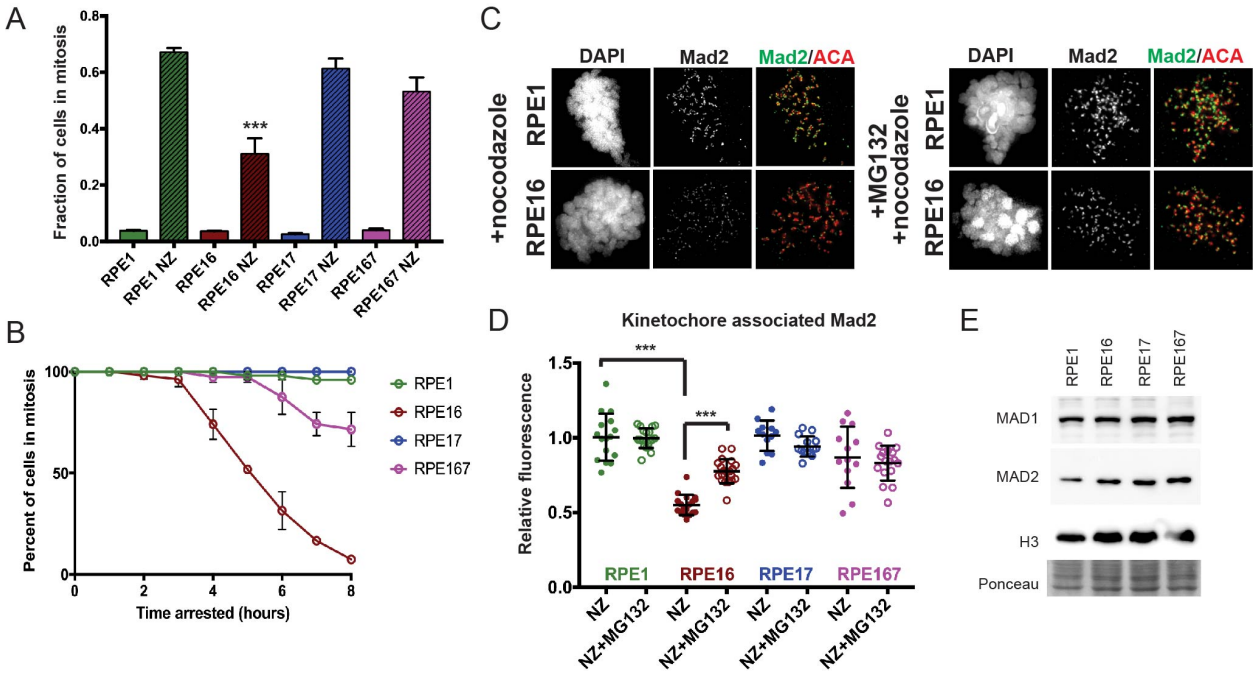

Figure 2.3. HPV E6-transformed cells exhibit defective SAC signaling and recruit less Mad2 to kinetochores. A. Mitotic index of control cells (solid) and cells arrested in 800 nM nocodazole for 16 h (striped) and then fixed. More than 200 cells analyzed among replicates. B. Quantification of time-lapse analysis of duration of mitotic arrest in nocodazole-treated cells. Only cells entering mitosis and exiting or arresting >8 h during the filming period were analyzed. Mean values and SD from three experiments with >60 cells analyzed. C. Representative images and D. quantification of kinetochore- associated Mad2 in each cell line arrested with nocodazole (solid circles) and in the presence of proteasome inhibitor MG132 (open circles). E. Total cellular levels of MAD2 and MAD1 determined by immunoblot with histone H3 loading control.

synchronized through a double-thymidine block with a proteasome inhibitor, MG132. Proteasome inhibition did not change Mad2 kinetochore levels in RPE1, RPE17, or RPE167 cells, but kinetochore levels increased in RPE16 cells from 50% to 80% of RPE1 cells. Thus, changes to the proteasomal degradation pathway in E6-expressing cells decrease Mad2 kinetochore levels and likely contribute to the inability of these cells to sustain a prolonged SAC arrest. It is unlikely that this is due to increased turnover of Mad2 itself in E6-expressing cells because, by immunoblot, total Mad2 levels are elevated compared with RPE1 (Figure 2.3E). The protein levels of Mad2's binding partner at kinetochores, Mad1, are also unchanged in E6-expressing cells (Figure 2.3E).

Cells expressing E6 are prone to cohesion fatigue likely due to elevated WAPL levels

The SAC defect in E6-expressing cells was obvious only because of the pole-associated chromosomes, which required sustained SAC activity. Pole-associated chromosomes are commonly observed when kinetochore–microtubule attachments are hyper-stabilized (55,69,121). To determine whether expression of E6 results in hyperstable attachments, we measured the distance between sister kinetochores of bioriented, aligned chromosomes in our cell lines. Interkinetochore distances of bioriented sister kinetochore pairs in control RPE1 cells were on average ~1.22 μm, and similar distances were measured on bioriented sister kinetochore pairs in RPE17 cells (~1.20 μm). Interkinetochore distances in RPE167 cells were shorter on average (~1.07 μm; Figure 2.4A). Of interest, interkinetochore distances of bioriented sister kinetochore pairs in RPE16 cells exhibited a bimodal distribution (Figure 2.4B). Most sister kinetochore pairs in RPE16 cells exhibited interkinetochore distances similar to those measured in

Figure 2.4. HPV E6-expressing cells cannot maintain robust sister chromatid cohesion during prolonged mitosis

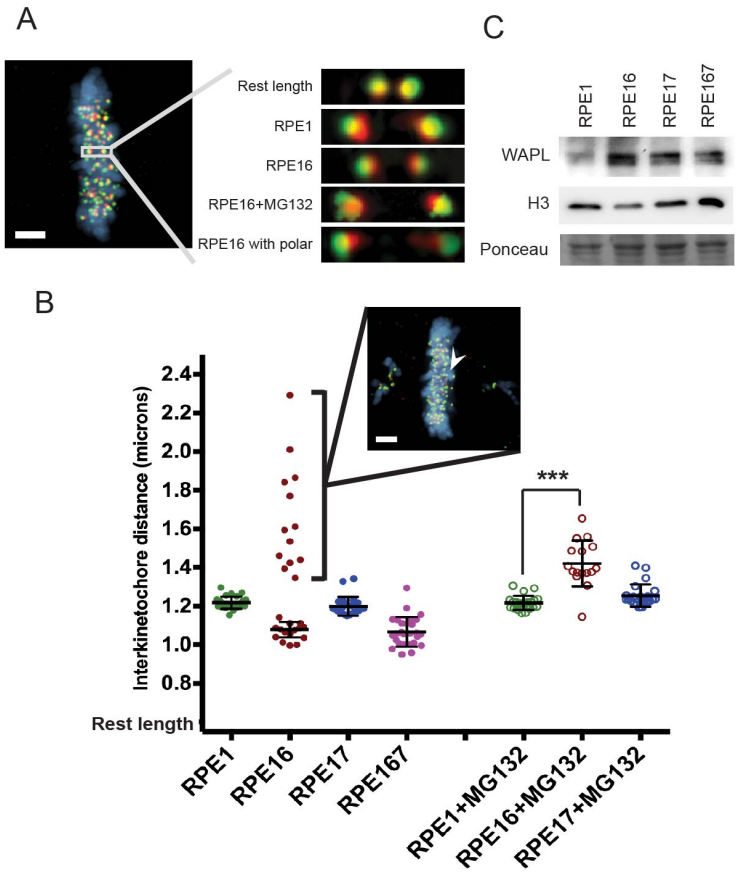

Figure 2.4. HPV E6–expressing cells cannot maintain robust sister chromatid cohesion during prolonged mitosis. A. Representative image of metaphase cell used to measure average interkinetochore distances and representative images of sister kinetochores for cell lines of interest. Interkinetochore distances measured between Hec1 foci (green) separated by ACA (red) staining. B. Average interkinetochore distance between bioriented sister kinetochores per cell for untreated RPE cells (solid circles) and MG132-treated cells (open circles). RPE16 cells that undergo delayed mitoses due to polar chromosomes (inset) or MG132 treatment (open circles) experience premature sister chromatid separation and abnormally long IKDs on bioriented sister kinetochores. C. Western blot of cellular WAPL levels in E6/E7-expressing cells.

RPE167 cells (~1.07 μm), but a small population of sister kinetochores in RPE16 cells had significantly longer interkinetochore distances (~1.63 μm), consistent with either kinetochore–microtubule attachment hyperstability or premature chromatid separation. This second population was entirely composed of RPE16 cells, with a few pole-associated chromosomes and an aligned metaphase plate from which interkinetochore distances were measured (Figure 2.4B). As mentioned, cells with this phenotype spent an average of 80 min in mitosis, which suggested that the increased interkinetochore distances might be due to cohesin fatigue and premature sister chromatid separation after a prolonged arrest rather than attachment hyperstability (171).

To understand whether this fatigue was unique to RPE16 cells, we again treated RPE1, RPE16, and RPE17 cells with MG132 to inhibit the proteasome. Previous studies demonstrated that such treatment prevents anaphase onset and prolongs the time cells spend in metaphase, eventually resulting in cohesin fatigue (171). We treated cells with 10 μM MG132 for 80 min (the average mitotic duration of RPE16 cells with polar chromosomes) and measured interkinetochore distances (Figure 2.4B). The average interkinetochore distance of aligned sister kinetochore pairs in RPE1 and RPE17 cells was largely unchanged from that in untreated cells (~1.22 and ~1.24 μm, respectively). In contrast, the average interkinetochore distance of aligned sister kinetochore pairs in RPE16 cells was significantly longer (~1.42 μm), supporting the idea that E6 expression results in perturbed cohesin function.

Consistent with this finding and previous studies, we found that E6-expressing and, to a lesser extent, E7-expressing cells increase protein levels of a cohesin antagonist, WAPL (Figure 2.4C). Although the average interkinetochore distance did not significantly

increase in E7 cells after 80 min in MG132, a small number of cells exhibited increased interkinetochore distances, suggesting that E7 cells may undergo fatigue sooner than RPE1 cells as well (Figure 2.4B).

2.3 Discussion

We determined that HPV E6 increases the incidence of mitotic slippage and premature sister chromatid separation; however, these defects result in aneuploidy only after mitotic delays. We found that E6 expression induced mitotic delays by compromising biorientation of one to four chromosomes that instead remained associated with spindle poles. Thus, in cycling cells, these combined perturbations increase genetic instability.

We found that pole-associated chromosomes are likely not the result of hyperstable kinetochore–microtubule attachments, despite such attachments being linked to aneuploidy (172). Although we did not determine the molecular mechanism responsible for this phenotype, it is possible that expression of E6 results in the mis-regulation of factors that contribute to chromosome congression, such as CENP-E, EB1, CLIP170, or adenomatous polyposis coli (APC; (173-175). APC is of particular interest because its depletion also results in loss of the protein Bub1, which functions to recruit Mad2 to kinetochores (176,177).

E6 expression weakens the ability of the SAC to sustain a robust arrest in response to misaligned chromosomes, in part due to decreased Mad2 levels at kinetochores. This is consistent with previous findings in RPE1 cells showing that Mad2 levels directly correlate with length of SAC arrest (169). However, E6 expression appears to increase total Mad2 protein levels, suggesting that this is instead a result of defective kinetochore recruitment. We also found that inhibition of the 26S proteasome partially rescued Mad2

kinetochore levels, indicating that a proteolytic event decreases Mad2 kinetochore recruitment. This proteolytic event does not appear to target Mad2 or its binding partner Mad1, as their cellular levels do not change when HPV proteins are expressed (Figure 2.3E). Checkpoint activity at kinetochores is regulated by many proteins and enzymatic reactions, and thus will require further study.

Expression of E6 also induced mild cohesion defects resulting in premature sister chromatid separation (observed by interkinetochore distances) during mitotic delays. Premature separation of sister kinetochores causes them to form merotelic attachments contributing to aneuploidy (171). This defect arises in part because of increased WAPL expression.

Chromosome segregation defects in RPE17 cells result from better understood phenomena. The most commonly observed error was lagging chromosomes at anaphase. It is possible that this error arises from cohesin fatigue. WAPL levels are increased in RPE17 cells, and a small number of cells demonstrated premature separation after an 80-min arrest. Moreover, E7's canonical activity of silencing pRB may also contribute to cohesin defects, as previously reported (178). In unperturbed RPE17 cells, however, we rarely observed abnormally long interkinetochore distances or prolonged mitotic delays. Thus, we suggest that defects in microtubule depolymerases, which have been well studied in multiple cancers, drive most chromosome segregation defects observed in E7 cells (160).

When expressing E6 and E7 together, it appears that phenotypes associated with cell proliferation are additive (doubling time, anchorage-independent growth), whereas in mitotic assays, E6 dominates the RPE167 phenotypes. Of interest, RPE167 followed the

same trends as RPE16 cells, but less dramatically. This is likely a result of HPV genomic structure. Both E6 and E7 are dicistronically transcribed from the internal p97 promoter, and translation of E7 is primarily dependent on precise splicing of the pre-mRNA (161,179). Owing to this splicing activity, RPE167 cells likely have lower soluble levels of E6 than those expressing E6 alone, despite being driven from the same promoter. We were unable to measure protein levels due to antibody detection capabilities via Western blotting.

It is well established that E6 and E7 inhibit tumor suppressor pathways, allowing aneuploid cells to persist rather than trigger senescence. We identified multiple ways in which these proteins contribute more directly to aneuploidy. E6 is of particular interest because it induced chromosome segregation errors not through a single defective pathway but instead by weakening multiple complementary pathways. In this case, chromosome congression defects delay mitosis, allowing aneuploidy to arise from cohesin fatigue and/or mitotic slippage. Although such subtle mitotic defects are more difficult to observe experimentally, they may be a key to understanding aneuploidy within cancer and its contributions to tumor evolution and heterogeneity.

Although failures in biorientation and mitotic slippage have been observed after experimental manipulations such as RNA interference, to our knowledge, they have not been documented as a result of cancer transformation. Decreased SAC activity has been suggested in some cancers due to their RNA transcription profiles; however, it has not been demonstrated that this directly contributes to aneuploidy (166). A key step in understanding the source of genetic instability will be to validate these findings in patient isolates for HPV-positive solid tumors.

2.4 Materials and methods

Cell culture and immunostaining

RPE1 (American Type Culture Collection) and derivative cell lines were cultured in DMEM/F-12 (Life Technologies) and supplemented with 1x penicillin/streptomycin and 10% fetal bovine serum (FBS) at 37°C in 5% CO2. For synchronization, cells were double thymidine blocked in the following manner: cells were treated with 2.5 mM thymidine for 16 h, followed by 8 h in regular medium, then 2.5 mM thymidine again for 16 h. After the second 16-h block, cells were washed out into regular medium for 10 h. In Mad2 quantification experiments, cells were treated with 10 μM nocodazole for 30 min after the 10 h. For Mad2 rescue experiments, cells were treated with 10 μM MG132 for 2 h at 8 h after release from the second thymidine block, followed by 30 min in 10 μM nocodazole before fixation. For Mad2 immunofluorescence, cells were first permeabilized with 1x PHEM (60 mM PIPES, 25 mM HEPES, 10 mM EGTA, 2 mM MgCl2)–0.5% TritonX for 2 min and then fixed with 4% paraformaldehyde for 20 min.

Western blotting

Cells were collected from the flasks with trypsin, pelleted in a table-top centrifuge, and raised in cold 1x phosphate-buffered saline (140 mM NaCl, 2.5 mM KCl, 1.6 mM KH2PO4, 15 mM Na2HPO4, pH 7.0), 2 mM dithiothreitol, and protease inhibitor cocktail (Thermo). Cells were sonicated on ice (Ultra Sonic Device), and lysates were clarified by centrifugation. Protein samples (40 μg) were run on 12% SDS–polyacrylamide gels and transferred to polyvinylidene difluoride membrane (Millipore). Blots were probed with the following antibodies: rabbit anti-Mad2 (Ted Salmon), 1:500; rabbit anti-Mad1 (GTX109519; GeneTex), 1:500; rabbit anti-WAPL (gift from Hongtao Yu), 1:500; and

rabbit anti–his- tone H3 (ab1791; Abcam), 1:500. Primary antibodies were detected using horseradish peroxidase–conjugated anti-mouse secondary antibody at a dilution of 1:10,000 (A00160; Gene Script) and visualized via chemiluminescence on an ImageQuant LAS 500 imager.

Viral transduction

MMLV-based retroviral particles were generated as previously de- scribed (Serrano et al., 1997). Briefly, packaging cells were transfected with pCMV-TAT and pCSIG to VSV-G pseudotype viruses and one of the following: pLXSN-HPV16E6, pLXSN-HPV16E7, or pLXSN-HPV16E6 (gifts from Denise Galloway). FuGENE 6 (Promega) transfection reagent was used at a 3:1 volume-to-mass ratio. Growth medium was replaced 24 h after transfection. Viral particle–containing supernatant media were harvested 48 and 72 h after transfection.

To perform viral transductions, RPE1 cells were grown in viral particle–containing supernatant medium for 24 h. This was repeated with fresh viral containing–supernatant medium for an additional 24 h. At 48 h after initial infection, cells were exposed to medium containing a negative selective pressure. Selection and outgrowth lasted ~3 weeks before a stable polyclonal population was established.

Reverse transcription PCR

Cells were grown to 80% confluency in two T75 flasks. RNA was extracted using the Qiagen RNeasy Midi Kit. The Qiagen OneStep RT-PCR Kit was used to visualize transcript expression. Primers were designed to amplify either 234 base pairs of E6 (forward, 5′-GCAACAGTTACTGCGACGTG-3′; reverse, 5′-GGACACAGTGGCTTTTGACAG-3′) or 200 base pairs of E7 (forward, 5′-

GACAGCTCAGAGGAGGAGG-3′; reverse, 5′-TGAGAACAGATGGGGCACAC-3′). Samples were run on a 1.8% agarose gel for band visualization.

Population doubling times

Each cell line was seeded at 50,000 cells in 12 wells of a 24-well plate. Three replicates of each cell line were counted using a hemocytometer 24, 48, and 72 hours after initial seeding. These data were fit to an exponential equation Y = Pier(t) with r=growth rate and t=time in hours.

Soft Agar Growth Assay

Culture dishes were coated with 1% agarose then 150,000 cells were mixed with into a 0.6% agar to form a second layer. Agar was hydrated with DMEM/F12 media to cover the agarose. Cells were incubated for six days when spheroid colonies were observed. An Olympus CK2 inverted compound microscope with a 10X/0.25 NA 160/0.17 Olympus objective was used to quantitate the number of colonies formed per field. A total of 20 frames were counted, and the average number of spheres per field was recorded.

Antibodies

Cells were stained with the following primary antibodies at these concentrations: rabbit anti Mad2 1:200 (a generous gift from Edward D. Salmon); human anti ACA 1:300 (Antibodies Incorporated 15-235); mouse anti Hec1 [9G3] 1:2000 (GeneTex; GTX70268); mouse anti alpha-tubulin [DM1a] 1:300 (Sigma T9026).

Chromosome Spreads

Cells were arrested in metaphase by treating with colcemid for 2 hours at a final concentration of 100ng/μL. Cells were harvested and resuspended in 75mM KCl for 40 minutes then fixed with a 3:1 Methanol:Acetic Acid solution. Cells were dropped onto

coverslips and mounted with prolong gold antifade reagent containing DAPI (ThermoFisher P36931).

Image acquisition and analysis

Images were acquired on a DeltaVision Personal DV (Applied Precision) imaging system equipped with a CoolSNAP HQ2 (Photometrics/Roper Scientific) camera with a 60X/1.42 NA PlanApochromat objective and SoftWorx acquisition software (Applied Precision). Interkinetochore distances were measured in SoftWoRx as the distance from Hec1 centroid to Hec1 centroid only measuring pairs that stained for both Hec1 and ACA within a single plane. Kinetochore intensities were also quantified using SoftWorRx, whereby the integrated fluorescence intensity minus the calculated background was determined for each kinetochore on max projected images. Values from HPV expressing cells were normalized to the average value obtained from RPE1 cells (Hoffman et al., 2001).

Live Cell Microscopy

Transformed cells expressing GFP-H2B were seeded at 500,000 cells and imaged the next day for 16 hours with or without immediate addition of 800nM nocodazole. Cells were imaged in a 37 °C environmental chamber (Pathology Devices Inc) in Leibovitz's L-15 media (Gibco) supplemented with 10% FBS, 7 mM HEPES and 4.5 g/l D-glucose (pH 7.0). Images were taken in 3 different z-stacks every 5 minutes at an exposure of 300 ms for a total of 16 hours. Images were acquired on a Nikon Eclipse Ti Microscope (Nikon Inc) equipped with an Andor Clara camera (Andor Inc) and a 40X/0.75NA Planfluorite DIC lens (Nikon Inc).

CHAPTER 3: BUGZ FACILITATES LOADING OF SPINDLE ASSEMBLY CHECKPOINT PROTEINS TO KINETOCHORES IN EARLY MITOSIS[2]

3.1 Introduction

During mitosis, cells must accurately divide their genomic content into two newly formed daughter cells. Central to the fidelity of this process is the spindle assembly checkpoint (SAC), a surveillance mechanism which monitors attachments between kinetochores and microtubules and halts mitotic progression until all attachments are correct (157). The effector of the SAC is the mitotic checkpoint complex (MCC), comprised of the proteins Bub3, BubR1, Mad2, and Cdc20 (79-81). This complex localizes to unattached or erroneously attached kinetochores and generates a diffusible "wait anaphase" signal, which inhibits the Anaphase Promoting Complex/Cyclosome (APC/C), an E3 ubiquitin ligase (70-72). When active, the APC/C ubiquitinates the key mitotic regulators cyclin B and securin, targeting them for proteasomal degradation and driving mitotic exit (73-77). In the presence of unattached or incorrectly attached kinetochores, the MCC functions to inhibit the activation of the APC/C by sequestering its activator, Cdc20 (78). Once all kinetochores are correctly attached, the SAC is silenced through both soluble MCC disassembly and reversal of the pathways leading to the formation of new MCCs (180).

[2] The work in this chapter is a manuscript prepared to be submitted in April 2020 under the same title. I have added additional sections where pertinent to this thesis.

J.G.D. and I conceived the idea for the project, designed experiments, analyzed the data, and prepared the manuscript. I conducted the experiments.

Formation of the MCC is initiated by localization of its components to unattached kinetochores. Central to this process is the essential mitotic kinase Mps1, which phosphorylates Met-Glu-Leu-Thr (MELT) repeats in the large kinetochore scaffolding protein KNL1 (51-53). These phosphorylated motifs create docking sites for the MCC component Bub3, which forms complexes with both BubR1 (also an MCC component) and Bub1 (88,89,107,181). Bub1 plays an important role in MCC formation by recruiting the SAC protein Mad1 to kinetochores in a phosphorylation dependent manner (91,92,98,182). Mad1, in turn, recruits the MCC component Mad2 to kinetochores, which adopts two conformational states. When soluble in the cytoplasm of mitotic cells, Mad2 exists in an "open" state (O-Mad2), in which it is inactive and unable to participate in MCC formation or function. After recruitment to kinetochore-associated Mad1 or kinetochore-associated Mad1-Mad2 complexes, Mad2 is converted to its "closed" state (C-Mad2), in which the protein is active and facilitates assembly of MCC complexes (94,96,183).

Bub1 and BubR1 associate with kinetochores by binding to Bub3 through conserved Gle2-binding-sequence (GLEBS) domains, also known as Bub3-binding domains (B3BD) (181,184,185). Bub3 is a WD40 protein that forms a seven-blade β-propeller structure, which interacts directly with GLEBS domains through a series of salt bridges (89). A large body of work has demonstrated that the recruitment of Bub1 and BubR1 to kinetochores is dependent on Bub3, although the minimal requirements differ in each case. Bub1 kinetochore recruitment requires its core GLEBS domain for Bub3 binding, as well as an additional loop region located between strands β1 and β2. In contrast, BubR1 kinetochore recruitment is dependent on its core GLEBS domain, its loop

region, a ~140 residue C-terminal extension region, and an interaction with Bub1 (49,57,84,181,186-189).

Previous studies have reported that Bub3 also associates with BuGZ, a recently identified, GLEBS-domain containing mitotic protein. BuGZ directly binds Bub3 and is required for Bub3 protein stability (150,190). Depletion of BuGZ results in chromosome segregation defects, which appear to be selectively lethal in transformed cells (150). BuGZ has been additionally implicated in mitotic spindle formation and in the activation of the mitotic kinase Aurora A (190-192). While BuGZ likely functions in numerous mitotic processes, its exact roles and contributions to these processes remain to be further investigated.

While the mechanisms for Bub3-mediated kinetochore recruitment of Bub1 and BubR1 to kinetochores are well-understood (84), the specific requirements for BuGZ's localization to kinetochores are not known. In addition, how Bub3 coordinates recruitment of its multiple GLEBS-domain-containing binding partners to kinetochores is an important outstanding question. In general terms, Bub3, Bub1, BubR1, and BuGZ all localize to kinetochores in early mitosis, when kinetochore-microtubule attachments are immature, and similarly, levels of all four proteins decrease as kinetochore-microtubule attachments are stabilized. The precise timing and the interdependence of their loading to and eviction from kinetochores, however, remains unknown. In this study, we investigate the requirements for BuGZ kinetochore loading, the temporal order for kinetochore loading of Bub3 and its binding partners, and the molecular composition of Bub3-containing subcomplexes during mitosis. We find that, unlike Bub1 and BubR1, BuGZ only requires its "core" GLEBS domain for kinetochore association. Additionally, we demonstrate that

BuGZ and Bub3 are loaded to kinetochores prior to Bub1 and BubR1 during mitosis, and that Bub3 forms a stable, soluble complex with BuGZ, but likely not with Bub1 and BubR1, prior to kinetochore loading. Our results suggest that BuGZ stabilizes Bub3 protein and facilitates Bub3 localization to kinetochores in early mitosis, which, in turn, facilitates proper Bub1 and BubR1 kinetochore loading. Additionally, we determine the phenotypic consequences of BuGZ depletion in cells. We find that cells depleted of BuGZ exhibit hyperstable kinetochore-MT attachments and mitotic delay.

3.2 Results

BuGZ's core GLEBS domain is sufficient for kinetochore localization

Bub1, BubR1, and BuGZ each contain a GLEBS domain that is required for binding to Bub3 (150,181,184,185,190). Previous work has carefully dissected the exact domain requirements for the kinetochore localization of Bub1 and BubR1 (84). Results from these studies have demonstrated that Bub1 requires its core GLEBS domain, as well as a loop domain that resides N-terminal to the GLEBS motif. The kinetochore localization of BubR1 requires its core GLEBS domain for Bub3 binding, as well as its loop domain and a C-terminal extension (CTE) domain (84) (Figure 3.1A). Additionally, the kinetochore localization of BubR1 is dependent on Bub1, likely through a direct interaction. Specifically, a Bub1 construct containing its CTE domain was shown to pull down BubR1 in immunoprecipitation experiments, while mutant Bub1 lacking the CTE failed to do so (84). We set out to identify the domain requirements for BuGZ kinetochore association, similar to what has been done for Bub1 and BubR1. Since the crystal structure of BuGZ has not yet been solved, it is not known if BuGZ contains the loop and C-terminal extension domains identified in Bub1 and BubR1. We therefore aligned the GLEBS

domains and surrounding sequences of BuGZ, Bub1, and BubR1 and predicted that amino acids 315-333 N-terminal to the BuGZ core GLEBS domain (344-376) (150) may be analogous to the loop domain in Bub1 and BubR1, and that amino acids 392-463 in BuGZ likely correspond to the C-terminal extension domain (84,150) (Figure 3.1A). Based on these predictions, we generated a series of BuGZ mutants and fragments and tested their ability to localize to kinetochores in HeLa cells (Figure 3.1B). Using this approach, we mapped the minimal kinetochore association domain of BuGZ to amino acids 352-376, which contains the GLEBS domain, but not the regions analogous to the loop and C-terminal extension domains in Bub1 and BubR1 (Figure 3.1C). In addition, the zinc finger domains were not required for kinetochore association, which confirms previous reports (150) (Figure 3.1C). Furthermore, replacing amino acids 323-333 in BuGZ with the loop domains of either Bub1 or BubR1 did not affect the ability of BuGZ to associate with kinetochores (Figure 3.1D). In contrast, previous results have demonstrated that substituting Bub1's loop domain with the loop domain from BubR1 resulted in decreased kinetochore localization of Bub1 (84). In the reverse experiment, replacing BubR1's loop domain with the Bub1 loop domain conferred to BubR1 the ability to load to kinetochores independently of Bub1 (84). In summary, our results suggest that BuGZ kinetochore localization requires only its core GLEBS domain, which is distinct from the requirements for both Bub1 and BubR1 kinetochore localization.

Temporal kinetochore localization of Bub3, BuGZ, Bub1, and BubR1

BuGZ, Bub1, and BubR1 all localize to kinetochores during mitosis, and in each case, this localization requires Bub3. To better understand how Bub3 facilitates loading

Figure 3.1. The core GLEBS domain of BuGZ is sufficient for kinetochore localization

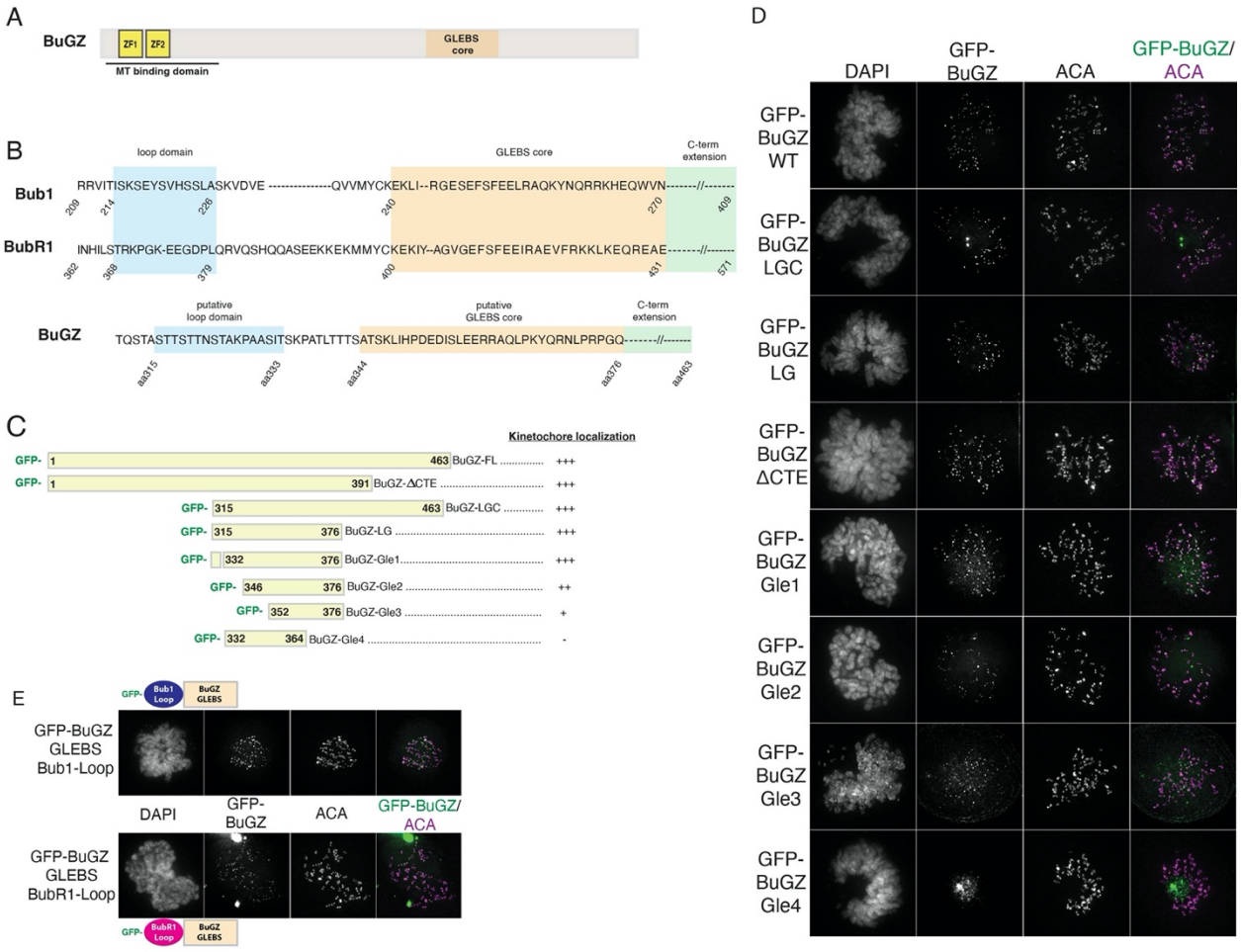

Figure 3.1.The core GLEBS domain of BuGZ is sufficient for kinetochore localization. A. Domain map of the human BuGZ. ZF1/2 are zinc finger domains 1 and 2. The microtubule binding domain overlaps with the zinc finger domains. The GLEBS core is the Gle2-binding-sequence containing two highly conserved glutamic acid residues. B Residue alignments of Bub1 and BubR1 depicting the loop domain, GLEBS core, and C-terminal extension (Overlack et al., 2013). BuGZ's GLEBS domain and surrounding regions are aligned with analogous domains in Bub1 and BubR1. Putative loop and C-terminal extension domains in BuGZ are indicated based on the alignments with Bub1 and BubR1. C Graphic depicting the GFP-BuGZ constructs used to test for kinetochore localization. D Immunofluorescence images of HeLa cells in early mitosis transfected with GFP-BuGZ constructs and analyzed for kinetochore localization. Cells are stained for DAPI and ACA (kinetochores). E. Immunofluorescence images of HeLa cells in early mitosis transfected with "loop swap" constructs consisting of the core GLEBS domain of ÅBuGZ fused to the loop domain of Bub1 (top)or BubR1 (bottom). Cells are stained for DAPI and ACA.

of each of its binding partners to kinetochores, we analyzed the timing of kinetochore association and eviction for each protein. Using viral transduction, we first generated RPE1 stable cell lines expressing mCherry-tagged Bub3, Bub1, BubR1, and BuGZ and imaged cells from nuclear envelope breakdown to anaphase onset. Consistent with previous studies, Bub3, Bub1, and BubR1 loaded onto kinetochores in early mitosis and protein levels decreased as chromosomes aligned (data not shown). mCherry-BuGZ exhibited a similar pattern, with high levels of the protein detected at kinetochores in early mitosis and low levels by late prometaphase (data not shown). To more precisely analyze the timing of kinetochore localization of each of the proteins, we imaged fixed HeLa cells and individually quantified the intensity levels of each protein throughout the phases of mitosis. While the general localization trends for all four proteins confirmed the live-cell data, we noted some interesting differences. Both BuGZ and Bub3 localized to kinetochores at high levels in prophase, and levels of both proteins remained high at kinetochores during nuclear envelope breakdown (Figure 3.2A, Figure 3.2B). However, BuGZ levels dropped significantly during early prometaphase, and the protein was completely evicted from kinetochores by late prometaphase (Figure 3.2B). In contrast, Bub3 levels at kinetochores remained high in prometaphase and a significant population remained at kinetochores during metaphase (Figure 3.2A). Bub1's localization dynamics differed somewhat from both BuGZ and Bub3. Kinetochore levels were low (but detectable) during prophase, kinetochore association increased during the process of nuclear envelope breakdown, and maximal levels were reached during prometaphase (Figure 3.2C). Similar to what was observed for Bub3, kinetochore association of Bub1 decreased in metaphase, but a significant population remained bound (Figure 3.2C). The

Figure 3.2. Maximal BuGZ kinetochore loading occurs in early mitosis.

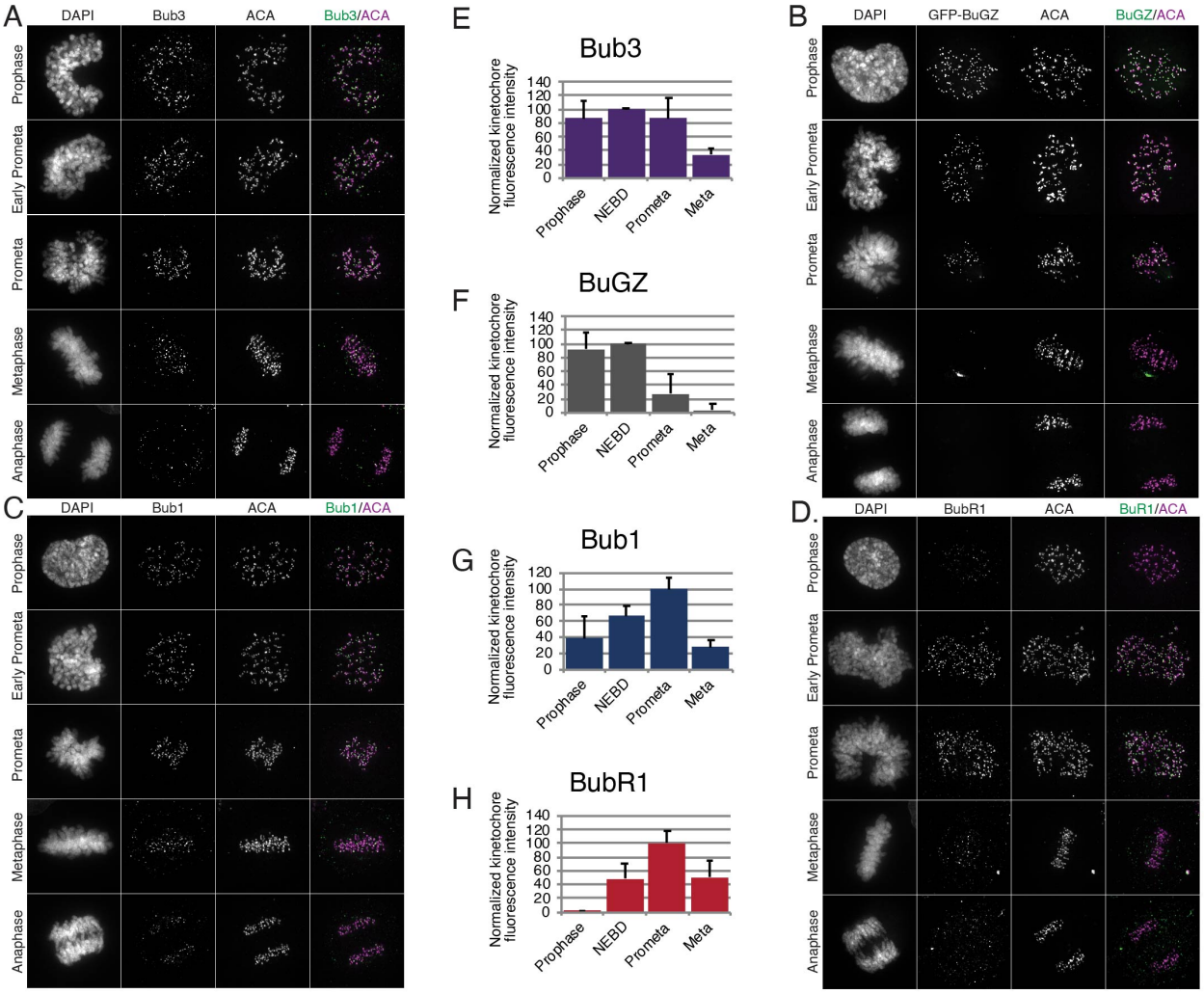

Figure 3.2. Maximal BuGZ kinetochore loading occurs in early mitosis. A.- D. Immunofluorescence images of mitotic HeLa cells in prophase, early prometaphase, prometaphase, metaphase, and anaphase. All cells are stained with DAPI and ACA as well as antibodies to a test checkpoint protein (Bub3, Bub1, or BubR1). In the case of BuGZ, cells were transfected with a GFP-BuGZ-WT construct. (E.-F.) Quantifications of immunofluorescence images from A-D. Kinetochore intensities were normalized to ACA levels.

localization dynamics of BubR1 were also distinct from the other proteins analyzed. Specifically, BubR1 was not readily detected at kinetochores in prophase, but levels increased during nuclear envelope breakdown and peaked during prometaphase (Figure 3.2D). Finally, in metaphase, kinetochore association of BubR1 decreased to about 50% of the maximal levels observed in prometaphase (Figure 3.2D). We next co-stained GFP-BuGZ expressing cells with Bub1 and BubR1 antibodies to directly visualize kinetochore localization of all three proteins simultaneously (Figure 3.3A). We found that kinetochores in prophase cells exhibited high levels of BuGZ and low levels of Bub1. In these cells, BubR1 was barely detectable (Figure 3.3A). On prometaphase kinetochores, Bub1 and BubR1 levels were high, while BuGZ levels were relatively low (Figure 3.3A). Finally, in metaphase, GFP-BuGZ was undetectable at kinetochores, while Bub1 and BubR1 levels persisted, albeit at lower levels than in prometaphase (Figure 3.3A). In light of the dependence of BuGZ, Bub1, and BubR1 kinetochore localization on Bub3, these localization data suggest a model in which a complex of Bub3-BuGZ loads onto kinetochores in prophase, prior to nuclear envelope breakdown, and prior to Bub1 and BubR1 loading. Then, in late prophase and during nuclear envelope breakdown Bub1 and BubR1 load to kinetochore associated Bub3, which we propose promotes the displacement of BuGZ from Bub3 and eviction from kinetochores.

Sub-complex analysis during mitosis

To better understand how Bub3 facilitates loading of each of its binding partners to kinetochores, we sought to identify and characterize Bub3-containing complexes in mitosis. First, we arrested HeLa cells in prometaphase using the microtubule depolymerizing drug nocodazole for 16 hr (Figure 3.4A). In this scenario, no kinetochore-

Figure 3.3. Co-staining for Bub1 and BubR1 in GFP-BuGZ expressing cells.

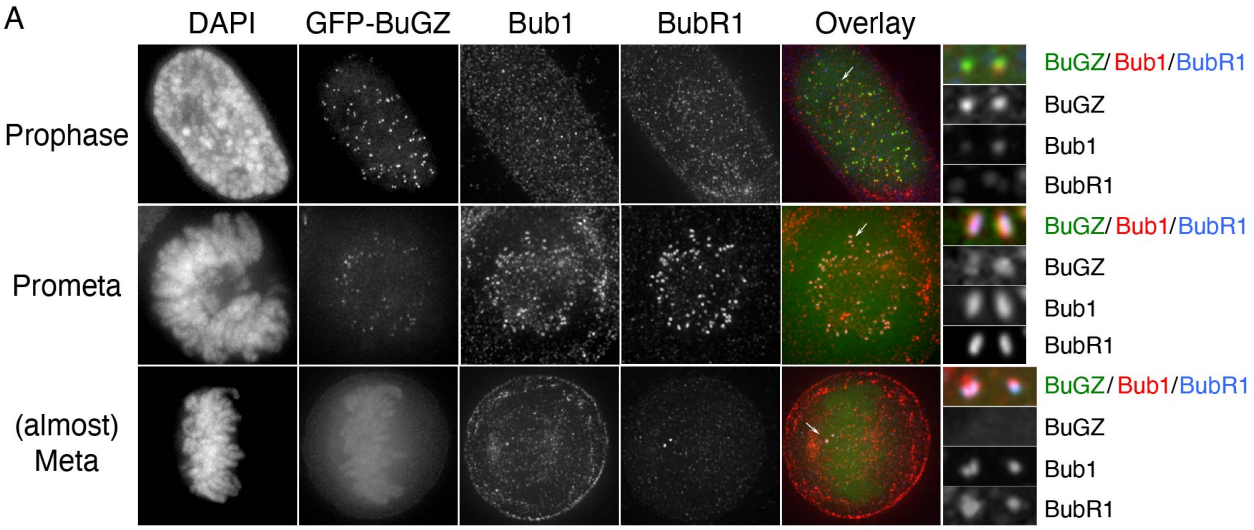

Figure 3.3. Co-staining for Bub1 and BubR1 in GFP-BuGZ expressing cells.
A. Immunofluorescence images of GFP-BuGZ expressing RPE1 cells in prophase, prometaphase, and late prometaphase/early metaphase. Cells are stained for DAPI, Bub1, and BubR1. Arrows point to the kinetochore pairs shown in the insets.

microtubule attachments are able to form, and the spindle assembly checkpoint is activated to generate MCC complexes capable of inhibiting the APC/C. Whole cell lysates were clarified and analyzed by size exclusion chromatography using a HiLoad 16/60 Superdex 200 column (Figure 3.4A). Western blot analysis of the fractions revealed a peak that eluted at approximately 500 kDa and included the proteins Bub3, BubR1, Mad2, and Cdc20, which likely corresponds to the MCC (Figure 3.4B) (79,193-196). Importantly, we did not detect BuGZ in this peak. In addition to its association with the MCC, we detected a large peak of Bub3 that co-eluted with BuGZ at approximately 240 kDa (Figure 3.4B). Interestingly, we also detected a peak of Bub3 at approximately 31 kDa which likely corresponds to the monomeric form of the protein. In this experiment, in which cells are arrested in 1 uM nocodazole overnight, MCCs are fully active and the complexes detected in the size exclusion eluates likely represent complexes that are both cytoplasmic and kinetochore associated. Thus, while these results clearly indicate that BuGZ is not a component of the MCC, it does not allow us to understand the nature of Bub3-containing complexes that are formed prior to kinetochore loading. In order to address this, we first arrested cells in G2 using the Cdk1 inhibiter, RO-3306, for 16 hours and then released the cells into media containing the drug reversine, which inhibits the checkpoint kinase Mps1 and prevents phosphorylation of KNL1 MELT motifs. This, in turn, prevents the loading of Bub3 and its co-factors to kinetochores (Figure 3.4C). The proteasome inhibitor MG132 was also included to prevent mitotic exit. As described above, cell lysates were clarified, subjected to size exclusion chromatography, and analyzed by Western blotting. As expected, we no longer detected a peak corresponding to the MCC. Instead, the majority of Mad2 eluted at ~26 kDa, indicative of monomeric Mad2, and a small peak of

Figure 3.4. In the absence of kinetochore loading, Bub3 is preferentially bound to BuGZ.

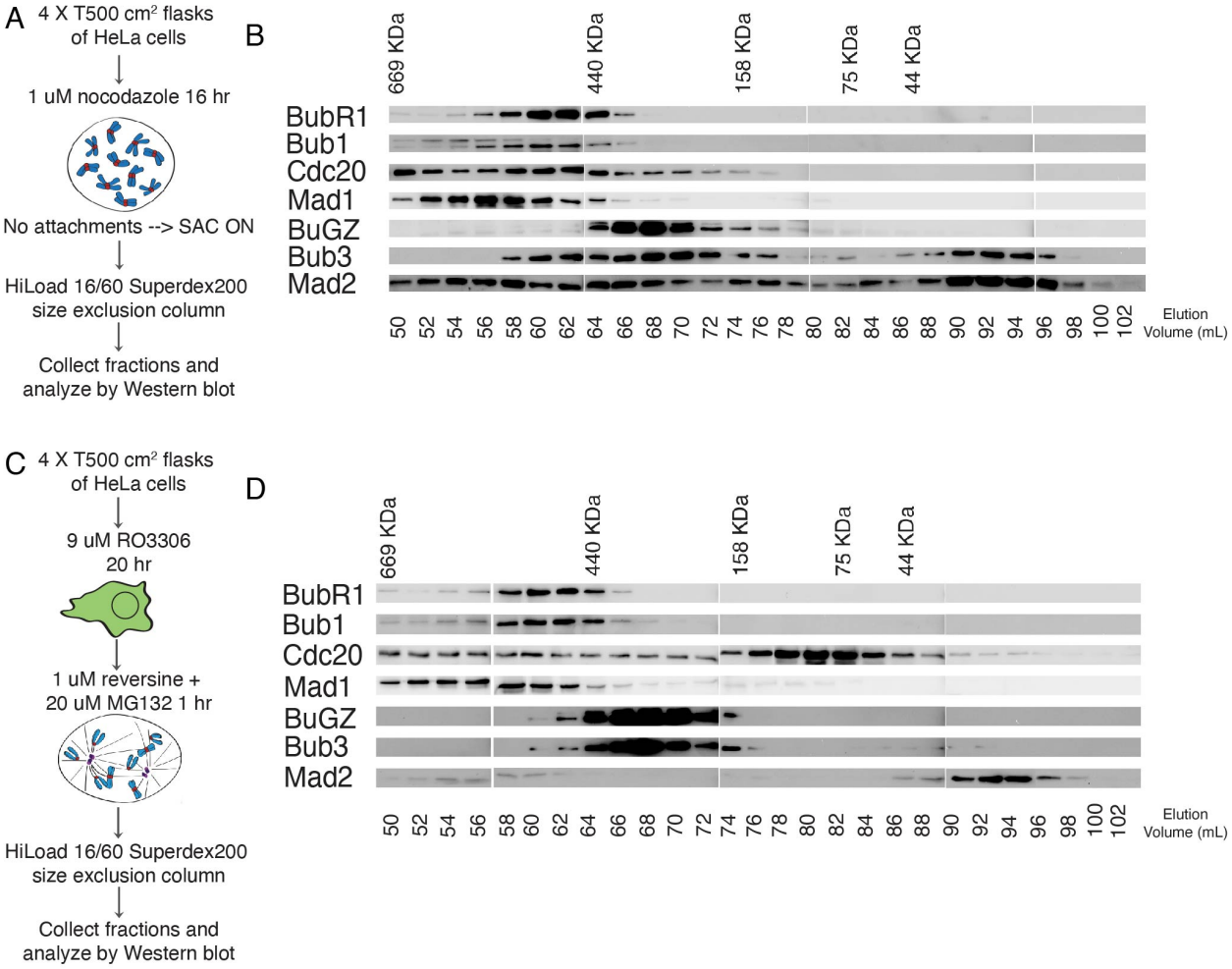

Figure 3.4. In the absence of kinetochore loading, Bub3 is preferentially bound to BuGZ. A. Schematic depicting the workflow for size exclusion chromatography fractionation of HeLa Kyoto cells arrested in nocodazole. (B.) Western blot images of nocodazole-arrested HeLa Kyoto cells probed with antibodies to BubR1, Bub1, Cdc20, Mad1, BuGZ, Bub3, and Mad2. Molecular weight standards are shown; the blots and fractions are labeled by their elution volume. C. Schematic depicting the workflow for size exclusion chromatography fractionation of HeLa Kyoto cells arrested in reversine and MG132. D. Western blot images of reversine/MG132-arrested HeLa Kyoto cells probed with antibodies to BubR1, Bub1, Cdc20, Mad1, BuGZ, Bub3, and Mad2. Molecular weight standards are shown; the blots and fractions are labeled by their elution volume.

Mad2 was found to co-elute with Mad1 (Figure 3.4D). Furthermore, under these conditions Bub3 eluted as a clear, monodispersed peak at ~260 kDa, where it co-migrated with the only detectable species of BuGZ (Figure 3.4D). Importantly, all of the Bub3 co-eluted with BuGZ, and no Bub3 was found to co-elute with either Bub1 or BubR1 (Figure 3.4D). Thus, under these conditions, it is likely that Bub3 is entirely bound by BuGZ in the cytoplasm. These results suggest that Bub1 and BubR1 do not form soluble complexes with Bub3, and that Bub1 and BubR1 do not load to kinetochores in complex with Bub3. Together with our localization data in Figure 3.2, these data support a model in which BuGZ and Bub3 form a complex in the cytoplasm in prophase, and prior to nuclear envelope breakdown, a complex of Bub3/BuGZ is loaded to kinetochores. After initial Bub3/BuGZ loading, Bub1 and BubR1 subsequently associate with kinetochore bound Bub3, resulting in eviction of BuGZ.

The results above suggest that Bub3 and BuGZ form a stable complex in mitotic cells. To further analyze this complex, and to determine the binding stoichiometry, we reconstituted the complex using recombinantly-expressed, purified human BuGZ and Bub3. Each protein was purified individually from Sf9 insect cells, which yielded high purity, single products. (Figure 3.5A). We first analyzed each protein individually using SEC-MALS, and while Bub3 eluted as a monomer at ~39 kDa (expected 37 kDa) (Figure 3.5B), BuGZ did not elute in a clear, monodispersed peak. Instead, BuGZ, whose molecular mass is ~50 kDa, eluted in a wide peak around ~340 kDa (Figure 3.5C). By SDS-PAGE, BuGZ appears to run as a single species, therefore the wide, 340 kDa peak could contain higher order, oligomeric complexes that perhaps form in cells (Figure 3.5C). In support of this idea, recent work from the Zheng lab has provided evidence for the

Figure 3.5. SEC-MALS-QELS data show a stable, multimeric complex between Bub3 and His-BuGZ.

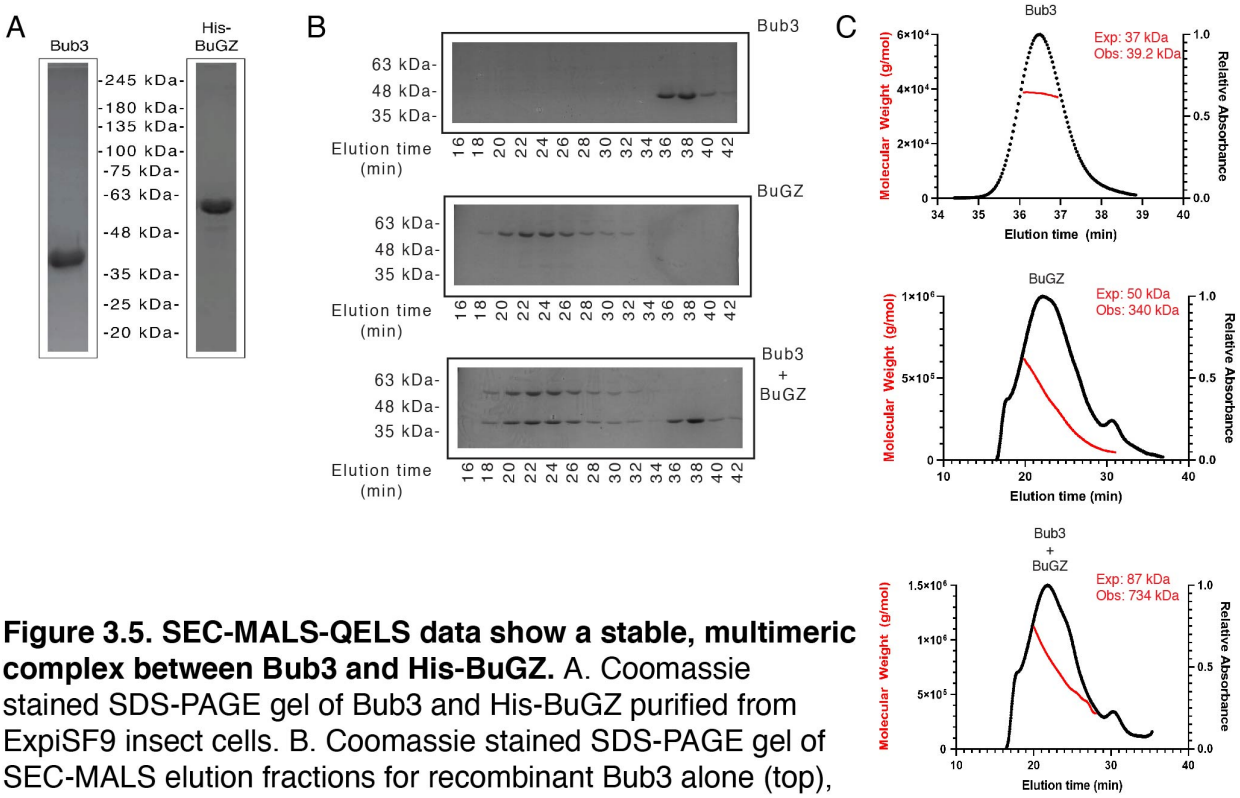

Figure 3.5. SEC-MALS-QELS data show a stable, multimeric complex between Bub3 and His-BuGZ. A. Coomassie stained SDS-PAGE gel of Bub3 and His-BuGZ purified from ExpiSF9 insect cells. B. Coomassie stained SDS-PAGE gel of SEC-MALS elution fractions for recombinant Bub3 alone (top), BuGZ alone (middle), and Bub3/BuGZ complex (bottom) runs. (C.) SEC-MALS profiles of recombinant Bub3 alone (top), BuGZ alone (middle), and Bub3/BuGZ complex (bottom). Expected (Exp) molar mass and observed (Obs) molar mass are indicated. Expected molar mass for the complex was calculated assuming 1:1 stoichiometry.

liquid-liquid phase separation of BuGZ, which is dependent on self-association of the disordered and low complexity regions of the protein (192) Pre-incubation of BuGZ and Bub3 and subsequent SEC-MALS analysis of the proteins together revealed a wide peak that corresponds to much larger complexes than expected for a 1:1 stoichiometry. The proteins co-elute at a peak of ~ 730 kDa, suggesting the addition of Bub3 led to even larger oligomeric complex formation (Figure 3.5D). This result suggests that BuGZ self-associates to form large oligomeric complexes. Although Bub3 can only bind a single GLEBS domain at a time, this mechanism may allow the association of several Bub3:BuGZ complexes through BuGZ self-association. In agreement with this, the Bub3-BuGZ peak in our size exclusion experiments using whole cell lysates (Figure 3.4D) also eluted at a large than expected size.

BuGZ depletion results in defective kinetochore-MT attachments

To better understand the importance of BuGZ's role in aiding in the stability and kinetochore recruitment of Bub3 during mitosis, we next aimed to reevaluate the phenotypic consequences of BuGZ depletion in HeLa cells. These experiments proved to be challenging, as we do not have an antibody specific to BuGZ for immunofluorescence experiments. Therefore, we are likely quantifying a mixture of cells with varying levels of BuGZ. By fixed cell analysis, depletion of BuGZ resulted in severe chromosome alignment defects in which BuGZ depleted cells formed ~40% less metaphase plates than their control counterparts (Figure 3.6A). Additionally, we observed an increase in the amount of multipolar spindle and "cruciform" phenotypes. The cruciform phenotype consists of a visible metaphase plate at the spindle equator with tufts of chromosomes at each pole. To better understand how the cruciform phenotype might

Figure 3.6. BuGZ depletion in HeLa cells results in chromosome alignment defects.

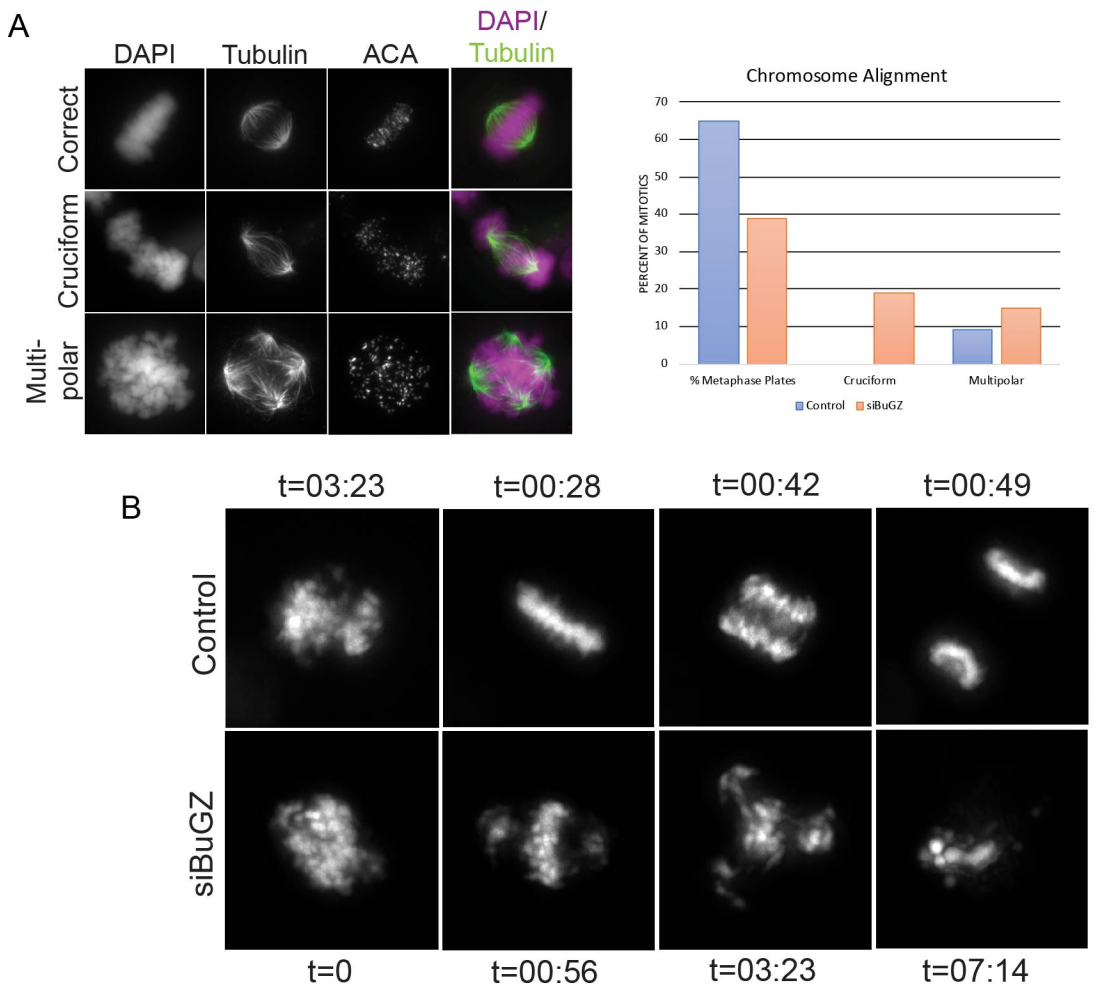

Figure 3.6. BuGZ depletion in HeLa cells results in chromosome alignment defects. A. (Left) Representative immunofluorescence images of phenotypes observed. Cells are stained for DAPI (DNA), Tubulin, and ACA (Kinetochores). (Right) Quantification of alignment in MG132-treated HeLa cells. B. Stills from live cell microscopy movies of control and BuGZ-depleted cells undergoing mitosis.

arise in BuGZ depleted cells, we performed live cell microscopy experiments to visualize BuGZ depleted cells undergoing mitosis (Figure 3.6B). Control cells entered mitosis and exited without errors within about an hour. When cells were treated with BuGZ siRNA, they often divided in a wild-type manner. However, about 10% of the mitotic cells imaged exhibiting a fascinating phenotype. These cells appeared to be bipolar at the start of filming, but they visibly struggled with forming a metaphase plate, depicting a clear cruciform phenotype. After several hours of spindle rotations and chromosome movements, the spindles would fracture, resulting in multi-polarity. Most of the time, these cells would die during mitosis.

Bipolar spindle formation is a result of a balance of plus- and minus-end directed motor forces (197), as well as kinetochore-associated forces. Hyper-stable attachments can thus result in an imbalance of these forces, causing spindle pole fragmentation and multipolarity (198). Therefore, we wanted to test the kinetochore-MT attachment stability in BuGZ depleted cells. Inter-kinetochore distances (IKDs) provide an indirect readout of attachment strength, as the distance between sister kinetochores will be longer if attachments are stronger. Control HeLa cells in metaphase had IKDs of ~1.3 um, while BuGZ depletion resulted in a striking increase of IKDs to ~2 um (Figure 3.7A, C). To further test attachment strength, we measured the density of cold-stabilized MTs in metaphase arrested cells. As all non-kinetochore attached MTs depolymerize upon cold treatment, this is also an indirect readout of the kinetochore-MT attachment status. We found that BuGZ depletion resulted in an ~40% increase in cold-stable MT polymers (Figure 3.7B, D). Together, this data suggest that kinetochore-MT attachments become

Figure 3.7. BuGZ depletion in HeLa cells results in hyperstable attachment phenotypes.

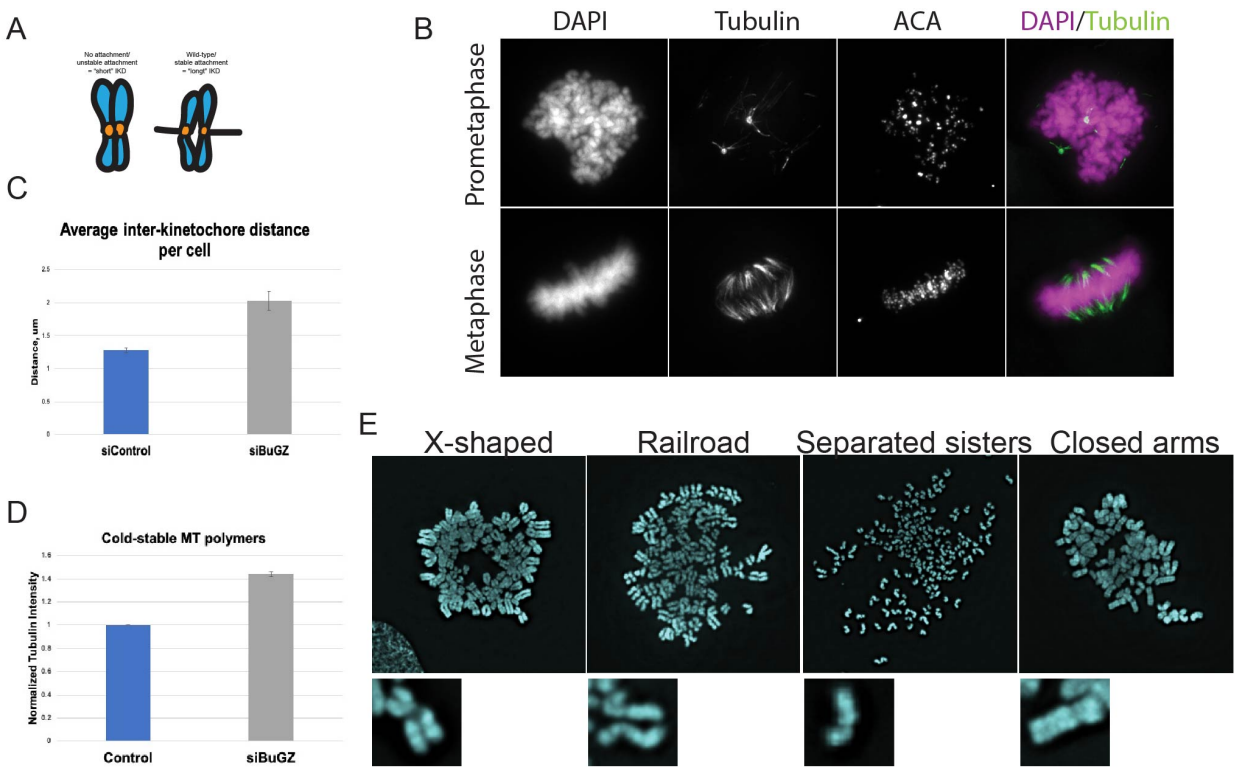

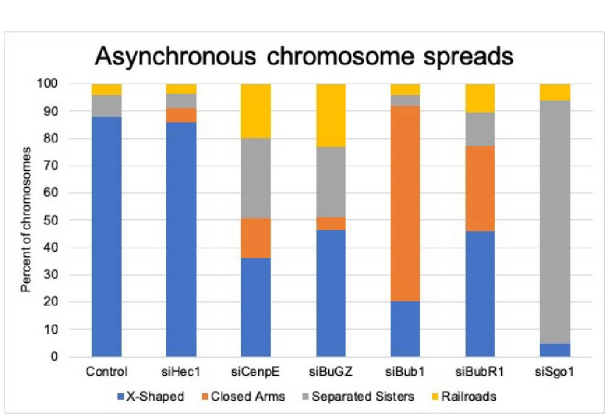

Figure 3.7. BuGZ depletion in HeLa cells results in hyperstable attachment phenotype. A. Schematic of IKDs. B. Representative images of cold-stabilized MTs in metaphase. C. Quantification of IKD in HeLa cells depleted of BuGZ. D. Quantification of cold-stable polymer density in cells depleted of BuGZ. E. Representative images of various categories used to analyze chromosome spreads. F. Quantification of chromosome spreads.

hyper-stabilized in BuGZ depleted cells, resulting in severe defects in chromosome alignment.

While the data suggest BuGZ is important for the maintenance of dynamic kinetochore-MT attachments and its depletion results in hyper-stabilized attachments, IKDs of ~2 um are very high, even for hyperstable attachments. IKDs greater than ~2 um are often indicative of defects in the cohesion between sister kinetochores. Sister chromatid cohesion is maintained by the cohesin complex (199). Defects in cohesion could be a result of defects in the cohesin complex itself, or it could be a result of cohesion fatigue, in which cells are arrested with kinetochores under tension for an extended period of time, resulting in weakening of cohesin complexes and premature separation of sister kinetochores (200). To better understand the large IKDs in BuGZ depleted cells, we analyzed their chromosome spreads. Sister chromatids were categorized as either X-shaped (wild-type), railroads (sisters remain together, but not visible attached), separated (single sister chromatids), or closed arms (cohesion along the length of sisters, not just at the centromere region). In addition to BuGZ depletion, we tested various other protein knockdowns that result in known defects. Shugoshin (Sgo1) depletion is known to lead to defective cohesin complexes. CenpE depletion is known to lead to a prolonged arrest in mitosis. HEC1 depletion is known to result in unattached or laterally attached kinetochores. Bub1 and BubR1 depletion were also tested to determine if the BuGZ depletion would mimic either of these, reflecting the possibility that BuGZ depletion results in defective Bub1 and BubR1 function due to decreased kinetochore localization. Overall, the BuGZ depleted chromosome spreads most closely resembled the CenpE depleted spreads (Figure 3.7E, F). This suggests that BuGZ depletion causes a prolonged mitotic

arrest, resulting in cohesion fatigue and lengthening of the IKDs. However, because the cold-stable MT data showed increased densities (Figure 3.7B, D), BuGZ depletion likely does still result in hyperstable attachments. The cohesion fatigue is likely an added consequence of a mitotic delay due to the formation of inappropriate kinetochore-MT attachments in BuGZ depleted cells.

3.3 Discussion

Recent work has established that BuGZ contributes to the fidelity of mitotic cell division; however, the mechanistic details of how it does so remain to be resolved (150,190-192). Here, we investigate a role for BuGZ in kinetochore loading of the checkpoint proteins Bub3, Bub1, and BubR1. The crystal structures of yeast Bub3 in complex with the GLEBS domains of yeast Bub1 or BubR1, reveal that each Bub3 can only bind a single GLEBS domain (88,89). Thus, the mechanisms by which BuGZ, Bub1, and BubR1 each localize to kinetochores through a direct interaction with Bub3 via their respective GLEBS domains are important to resolve. By temporally mapping the kinetochore localization patterns of BuGZ, Bub3, Bub1, and BubR1, we show here that BuGZ is loaded to kinetochores significantly earlier than Bub1 and BubR1, suggesting that Bub3 and BuGZ may first form a stable, cytoplasmic complex that is co-loaded to kinetochores. Depletion of BuGZ results in the proteolysis of Bub3, which further supports the idea that BuGZ and Bub3 form a stabilized complex prior to kinetochore loading (150,190). In further agreement with this hypothesis, through the biochemical fractionation of cell lysates generated from cells treated with various cell cycle-affecting drugs, we show here that when outer kinetochore assembly on the kinetochore scaffold KNL1 is inhibited with reversine, all detectable Bub3 is complexed with BuGZ, rather than

Figure 3.8. BuGZ aids in kinetochore loading of Bub3 and its binding partners.

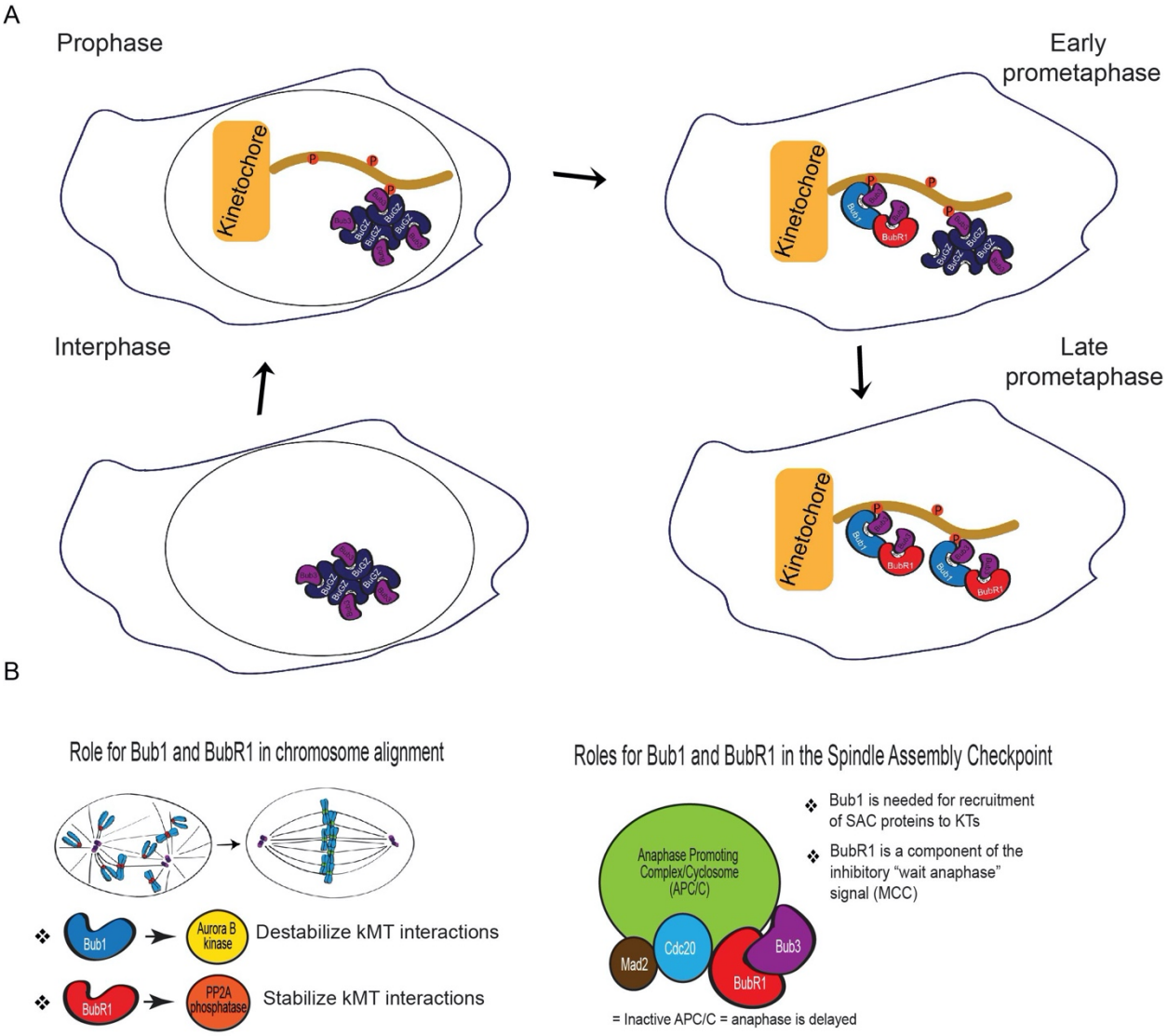

Figure 3.8. BuGZ aids in kinetochore loading of Bub3 and its binding partners. A. Model for BuGZ in mitosis. BuGZ first binds Bub3 in interphase cells. Together, the complex loads onto kinetochores in prophase. Bub3 moves from BuGZ to Bub1 and BubR1 upon nuclear envelope breakdown. BuGZ is fully gone by metaphase. B. Schematic of the roles of downstream Bub3 binding proteins, Bub1 and BubR1.

with Bub1 or BubR1. This supports a model in which BuGZ and Bub3 bind one another in the cytoplasm, independently of kinetochores prior to nuclear envelope breakdown. Upon the formation of the outer kinetochore, BuGZ and Bub3 then bind kinetochores and, through an unidentified mechanism, BuGZ is exchanged for Bub1 and BubR1 to allow for their association with Bub3 at kinetochores (Figure 3.8A).

If BuGZ is required for robust kinetochore loading of Bub3 and, consequently Bub1 and BubR1, then BuGZ depletion should presumably mimic depletion of these proteins as well. Unfortunately, as Bub3 is required for the kinetochore loading of both Bub1 and BubR1, these data can become quite muddled. Bub1 aids in the recruitment of Aurora B kinase to kinetochores, which is a critical component of the error correction machinery (Figure 3.8B). Aurora B kinase phosphorylates outer kinetochore substrates to weaken their affinity for MTs. BubR1 acts counter to Bub1 in that it recruits the phosphatase PP2A to kinetochores. PP2A then dephosphorylates outer kinetochore substrates to strengthen their affinity for MTs. Hyper-stabilization of kinetochore-MT attachments is a phenotype expected of cells depleted of Bub1, but depletion of BubR1 should result in loss of PP2A phosphatase as well, which could result in lower levels of hyper-stabilization. Both Bub1 and BubR1 are also required for the SAC. Bub1 is need for the recruitment of several SAC proteins to kinetochores and BubR1 plays a direct role in MCC formation (157). However, BuGZ depletion results in mitotic arrest, suggesting there is still enough Bub1 and BubR1 at kinetochores to allow for SAC activation in these cells. It will be important to generate cells with full BuGZ depletion or inducible deletion to determine just how much of Bub3, Bub1, and BubR1 are still localized to kinetochores in these conditions. These

levels can then be generated in cells with full BuGZ levels to ensure that the BuGZ depletion phenotype is indeed an indirect consequence of loss of Bub3, Bub1, or BubR1.

3.4 Materials and methods

Cell Culture and generation of stable cell lines

HeLa (American Type Culture Collection) and HeLa Kyoto cells were cultured in DMEM (VWR) supplemented with 10% FBS, 1% antibiotic/antimycotic solution, and 4 mM L-glutamine and maintained at 37°C in 5% CO_2. Stable RPE1 (parental from American Type Culture Collection) cell lines expressing mCherry-Bub3, mCherry-BuGZ, mCherry-Bub1, and mCherry-BubR1 were cultured in DMEM/F-12 (Life Technologies) and supplemented with 10% FBS, 1% antibiotic/antimycotic solution, and 2.5 mM L-glutamine and maintained at 37°C in 5% CO_2. Stable cell lines were generated using a lentiviral transduction system. Briefly, ~ 2 x 10^6 HEK 293T cells were seeded on poly-L-lysine treated 10 cm dishes. After 24 hr, cells were transfected with 12 ug of the donor plasmid containing a SAC protein gene, 8 ug of pPAX2 (packaging plasmid), and 3 ug of pMD2.G (packaging plasmid) using Lipofectamine 2000 (Thermo Fisher Scientific) per the manufacturer instructions. The media (DMEM, VWR) was replaced after 16 hr. After 48 hr, the media containing virus was harvested from the cells and used to infect RPE1 cells. Virus was tested for infectivity to produce the greatest percentage of infected cells. Infected cells were selected for using 0.2 mg/mL Hygromycin.

Plasmids and siRNAs

All GFP-BuGZ mutants were made by PCR amplification from the parental GFP-BuGZ construct, described in Toledo et al., 2014 (150). These were then cloned into a pEGFP-C2 vector through In-Fusion cloning. To generate the loop swap mutants with the

BuGZ core GLEBS domain, constructs were ordered as GeneArt fragments (ThermoFisher Scientific). Sequences of the loop swap constructs were (loop sequence is capitalized):

GeneArt fragment BuGZ LG^{Bub1loop}:

cggactcagatctcgagctccatggcttcaacaactagtacaacaaatATTTCTAAATCAGAATATT
CTGTGCACTCATCTTTGGCAagtaagcctgctacacttacaacaactagtgcaaccagtaagttga
tccatccagatgaggatatatccctggaagagagaagggcacagttacctaagtatcaacgtaatcttcctcggc
caggacagtgaggtaccgcgggcccgggatc

GeneArt fragment BuGZ LG^{BubR1loop}:

cggactcagatctcgagctccatggcttcaacaactagtacaacaaatACCAGAAAGCCTGGAAAG
GAAGAAGGAGATCCTCTAagtaagcctgctacacttacaacaactagtgcaaccagtaagttgatc
catccagatgaggatatatccctggaagagagaagggcacagttacctaagtatcaacgtaatcttcctcggcc
aggacagtgaggtaccgcgggcccgggatc

HeLa cells at ~70% confluency were transfected with 2 ug of each construct using Lipofectamine 2000 (Thermo Fisher Scientific) per the manufacturer's instructions. Cells were fixed after 24 hr. For protein purifications, BuGZ and Bub3 were cloned into a pFastBac plasmid per the Bac-to-Bac Baculovirus expression system (Invitrogen). Briefly, His-BuGZ and His-ZZ-Bub3 were PCR amplified and inserted into the pFastBac parental donor plasmid. These were transformed into MAX Efficiency DH10Bac (Invitrogen) cells for bacterial amplification and the recombinant bacmid DNA was isolated from a bacterial culture. Correct bacmid generation was confirmed by PCR. 2 ug of this bacmid DNA was then transfected into ExpiSf9 cells for generation of virus using ExpiFectamine reagent (Life technologies) per the manufacturer's instructions.

Immunofluorescence and Imaging

For fixed cell imaging, cells were grown on acid washed sterile coverslips. For the fixation procedure, cells were first rinsed with 1X PHEM buffer (60 mM PIPES, 25 mM HEPES, 10 mM EGTA, and 4 mM MgSO4) at 37°C. Cells were then either lysed first for 5 minutes in 0.5% TritonX followed by a 20-minute fixation in 4% paraformaldehyde or fixed first for 20 minutes in 4% paraformaldehyde buffer followed by a 5 minute lysis in 0.5% TritonX. After fixation, cells were washed 3 × 5 min in PHEM-T (PHEM buffer + 0.1% Triton X-100) and blocked in 10% boiled donkey serum (BDS) in PHEM for 1 h at room temperature. Primary antibodies were diluted in 5% BDS and added to coverslips overnight at 4°C. The primary antibodies used were: human anti-centromere antibody (Antibodies, Inc., 1:300), Mouse anti-Bub3 (BD Biosciences, 1:200), Rabbit anti-BubR1 (Bethyl, 1:500), Rabbit anti-Bub1 (Bethyl, 1:500), Mouse anti-Bub1 (Abcam, 1:500). After primary antibody incubation, cells were rinsed 3 x 5 min in PHEM-T and then incubated for 45 min at room temperature with secondary antibodies conjugated to Alexa Fluor 488, Alexa Fluor 568, or Alexa Fluor 647 (Jackson ImmunoResearch Laboratories) at 1:800 diluted in 5% BDS. Cells were rinsed 3 x 5 min in PHEM-T and quickly rinsed in PHEM followed by incubation in DAPI (2 ng/ml) diluted in PHEM for 30 s. Slides were rinsed 3 x 5 min in PHEM-T, quickly rinsed in PHEM, and then mounted onto glass slides with antifade solution (90% glycerol, 0.5% N-propyl gallate). Coverslips were sealed with nail polish and stored at 4°C. All fixed cell images were acquired on an IX71 inverted microscope (Olympus) incorporated into a DeltaVision Personal DV imaging system (GE Healthcare) using SoftWorx software (GE Healthcare). Slides were imaged using a 60X/1.42 NA differential interference contrast Plan Apochromat oil immersion lens

(Olympus) and a CoolSNAP HQ2 camera. For live-cell imaging, cells were maintained at 37°C using an environmental chamber (Precision Control) and in Leibovitz's L-15 media (Gibco) supplemented with 10% FBS, 7 mM HEPES and 4.5 g/l D-glucose (pH 7.0).

Size exclusion chromatography experiments

HeLa Kyoto cells were grown in 4-T500 cell culture dishes. To induce a prometaphase arrest, cells were grown to ~80% confluency then treated with 1 uM nocodazole (Tocris) for 16 hr. For reversine treatment, cells were also grown in 4-T500 cell culture dishes. Cells were grown to ~ 70% confluency, then treated with 9 uM of the CDK1 inhibitor, RO-3306 (Sigma-Aldrich, Thermo Fisher Scientific) for 20 hr. Then cells were washed out of RO-3306 using phosphate buffered saline (pH 7.0) and immediately put into DMEM medium containing 1 uM reversine (AdooQ BioScience) + 20 uM MG132 (Selleckchem) for 1 hr. Cells were then harvested and pelleted (1000 x g, 5 min). The pellets were resuspended in lysis buffer (25 mM Hepes (pH 7.4), 200 mM NaCl, 1 mM DTT, and protease inhibitor cocktail tablets (Thermo Scientific Pierce) and immediately stored on ice to prevent reformation of the mitotic spindle. Cells were lysed with sonication and clarified by ultracentrifugation at 35,000 RPM for 45 min at 4°C. The supernatant was loaded onto a HiLoad 16/60 Superdex 200 column (GE Healthcare) and all fractions were collected using an AKTA pure system. All fractions were analyzed by Western blotting. The antibodies probed with were: Rabbit anti-Mad2 (in-house, 1:500), Mouse anti-Bub3 (BD Biosciences, 1:300), Rabbit anti-BuGZ (GeneTex, 1:1000), Rabbit anti-Mad1 (GeneTex 1:500), Mouse anti-Cdc20 (Santa Cruz Biotechnology, 1:200), Mouse anti-Bub1 (Abcam, 1:500), and Rabbit anti-BubR1 (gift from Jakob Nilsson, 1:500). Horseradish peroxidase-conjugated secondary antibodies were used at 1:10,000

(Jackson ImmunoResearch Laboratories) and blots were imaged using an in-house HRP substrate and LAS500 imager.

Protein Purification

His-BuGZ and His-ZZ-Bub3 were individually expressed and purified from insect cells (ExpiSf9 cells; Life Technologies) maintained in ExpiSF CD Medium (Life Technologies). After bacmid generation (see above), 4 mL of ExpiSf9 cells at 2.5 x 10^6 cells/mL were transfected with 2 ug of bacmid DNA using ExpiFectamine reagent (Life Technologies) according to the manufacturer's instructions. After 5 days of growth, the cells were pelleted and 3 mL of the supernatant (P1) was used to infect 240 mL of ExpiSf9 cells grown to ~7 x 10^6 cells/mL. After 48 hr, the cells were harvested (1000 x g, 5 min), washed with phosphate buffered saline (pH 7.0), pelleted again (1000 x g, 5 min), resuspended in an equal volume of lysis buffer, drop frozen in liquid nitrogen, and stored at -80°C until the day of the purification. The lysis buffer for His-BuGZ was 20 mM phosphate buffer (pH 7.4), 1 mM $MgCl_2$, 1 mM BME, 0.01% Triton-X, 500 mM NaCl, 10 % Glycerol, 1 mM PMSF. The lysis buffer for His-ZZ-Bub3 was 25 mM Hepes (pH 7.4), 1 mM BME, 300 mM NaCl, 10% glycerol, 1 mM PMSF. For purification, 25 mL of additional lysis buffer supplemented with protease inhibitor cocktail tablets (Thermo Scientific Pierce) was added to the frozen cell pellet and the pellet was rapidly thawed in a 37°C water bath then incubated on ice. Cells were lysed by passage through an M110-L Microfluidizer using an H10Z reaction chamber at 18,000 psi (Microfluidics). The lysate was clarified with a 45-minute ultracentrifuge spin at 35,000 RPM and the supernatant (supplemented with 20 mM Imidazole) was run over a 5 mL HisTrap HP column (GE Healthcare) using an AKTA Pure system. His-tagged protein was then eluted with the

respective lysis buffer supplemented with 500 mM Imidazole. Peak fractions were collected and pooled. For His-ZZ-Bub3, the pooled fractions were dialyzed overnight into SEC buffer (25 mM Hepes (pH 7.4), 200 mM NaCl, 1 mM BME, and 10% glycerol). The next day, the His-ZZ-Bub3 was incubated with HRV3C protease (purified in house) rocking overnight at 4°C to cleave the His-ZZ tag off of Bub3. SDS-PAGE was used to confirm the cleavage reaction. Since His-ZZ is similar in size to Bub3, the sample was run over first GST beads, then Nickel beads, and the flow-throughs were saved and concentrated to ~700 uL and run on a Superose6 Increase 10/300 (GE Healthcare) sizing column. Peak fractions were collected, pooled, concentrated, and drop frozen in liquid nitrogen to be stored at -80°C. For His-BuGZ purification, the pooled peak fractions from the HisTrap HP column (GE Healthcare) were dialyzed overnight into lysis buffer containing lower salt (25 mM NaCl). The next day, the sample was run on a MonoS cation exchange column (GE Healthcare) and peak fractions were collected, pooled, and concentrated to ~700 uL. This was then run on a Superose6 Increase 10/300 (GE Healthcare) sizing column and peak fractions of His-BuGZ were collected, pooled, concentrated, and drop frozen in liquid nitrogen to be stored at -80°C.

SEC-MALS-QELS

His-BuGZ and Bub3 proteins purified from ExpiSf9 cells were diluted to 10 uM stocks using buffer containing 25 mM Hepes (pH 7.4), 200 mM NaCl and 1 mM BME. A Wyatt Technologies Dawn Heleos-II multi-angle light scattering apparatus in conjunction with an Optilab T-rex differential refractive index detector were paired with a Superose6 Increase 10/300 (GE Healthcare) sizing column. 500 uL of each sample was run through the column using an AKTA Pure system and analyzed by the detectors. All fractions were

collected and run on SDS-PAGE to confirm peaks and protein composition. Data was analyzed using ASTRA processing software (Wyatt Technologies).

CHAPTER 4: BUBR1 IS REQUIRED FOR KINETOCHORE-MICROTUBULE ATTACHMENT STABILITY IN CANCER CELLS

4.1 Introduction

Cancer lethality screens performed by the lab of Dr. Patrick Paddison at the Fred Hutch Cancer Research Center have shed light on proteins that become selectively required in transformed cells. Glioblastoma multiforme is the most aggressive and common form of primary brain cancer in adults and even with standard of care treatments, 90% of adults do not survive 2 years after diagnosis (151). Dr. Paddison's lab performed a side-by-side shRNA screen of the entire human kinome in patient-derived Glioblastoma stem cells (GSCs) and healthy neural crest stem cells (NSCs). The top glioblastoma-specific hit was the mitotic protein, BubR1 (151).

BubR1 is a highly conserved, multidomain protein with many functions (Figure 4.1A). As a component of the MCC, it is critical for proper checkpoint function (157). Several of BubR1's domains are implicated in its checkpoint role, including the KEN boxes, TPR motifs, ABBA motif, and two destruction box (D box) motifs (100-103). The majority of these domains act as pseudo-substrates to bind CDC20 and prevent it from activating the APC/C. BubR1 additionally contains a GLE2p-binding sequence (GLEBS) domain which is used to bind directly to Bub3 (89). Shortly after the GLEBS domain is a helical extension domain that BubR1 uses to dimerize with Bub1, which is thought to be critical for the kinetochore localization of BubR1 (84). Interestingly, it has been postulated that the kinetochore localization of BubR1 may not be necessary for its checkpoint function or for cell viability. Malureanu and colleagues have shown that a mutant BubR1 containing just the two KEN boxes, TPR motifs, and one of the D-boxes was able to

rescue cell viability and sustain mitotic checkpoint functionality in MEFs (188). Importantly, this construct lacked the entire C-terminal half of BubR1 and therefore could not localize to kinetochores.

A more recently appreciated role for BubR1 is in stabilization of kinetochore-MT attachments. Using amino acids 647-697, consisting of the kinetochore attachment regulatory domain (KARD), BubR1 binds to and recruits the phosphatase, PP2A-B56 (135). This KARD-PP2A interaction is dependent on PLK1 kinase phosphorylation of the KARD domain at three sites. Once at the kinetochore, this phosphatase is thought to counteract Aurora B kinase substrate phosphorylation in order to strengthen kinetochore-MT attachments. In agreement with this, BubR1 mutations in the KARD domain result in the loss of chromosome alignment and kinetochore-MT attachments in HeLa cells (135).

Both kinetochore-MT attachments and SAC signaling are processes that are dependent on a delicate balance between kinases and phosphatases at the kinetochore. At the beginning of mitosis, kinase activity dominates these processes, while phosphatase activity wins out as mitosis progresses. The primary kinases involved in these processes are Aurora B and Mps1. While much is known about the kinases and their substrate, relatively little is understood about the phosphatases that act on those same substrates. The primary phosphatases during mitosis are PP2A and PP1 (129,130). The PP2A holoenzyme is comprised of three subunits: a constant catalytic component, a constant scaffold component, and a variable regulatory subunit. Of the 4 structurally distinct regulatory subunit families (B55, B56, PR72, and Striatin), B56 is the primary regulatory subunit of the PP2A holoenzyme thought to act on kinetochore substrates. Within the B56 family, there are 5 separate isoforms (B56α, β, γ, δ and ε). Isoforms γ and

δ are kinetochore-localized, while α and ε are centromere localized, and β has a mixed localization pattern (201). The PP1 holoenzyme consists of a variable catalytic subunit (PPP1Cα, PPP1Cβ, and PPP1Cγ) bound to a variable regulatory subunit (>180 possibilities) (129). Both PP1 and PP2A localize to their sites of action through interacting with short linear motifs (SLiMs). The most well characterized SLiM for PP1 is the RVxF motif (e.g. found in KNL1 N-terminus) and for PP2A-B56 is the LxxIxE motif (e.g. found in BubR1 KARD) (202).

One of the primary reasons for the lack of understanding concerning which phosphatases act on which substrates is that PP1 and PP2A-B56 are involved in a feedback loop in which they regulate one other. Phosphorylation of the KNL1 MELT repeats leads to BubR1 recruitment to kinetochores, where PLK1 phosphorylates the BubR1 KARD, leading to PP2A-B56 recruitment. The RVSF motif of KNL1 is phosphorylated by Aurora B kinase and this phosphorylation event inhibits PP1 docking. Early in mitosis, PP2A-B56 is thought to counteract Aurora B phosphorylation to promote PP1 docking, but kinase activity “wins out” until Aurora B phosphorylation activity is decreased, at which time PP2A-B56 dephosphorylates the RVSF and permit PP1 loading to kinetochores. Once at kinetochores, it is thought that PP1 dephosphorylates the pMELTs, leading to loss of the pMELT-BubR1 interaction and therefore loss of PP2A-B56 (203).

The results of the shRNA lethality screen in GSCs and NSCs indicated that BubR1 may be a suitable target for selectively killing cancer cells while leaving healthy cells unharmed. However, very intriguingly, Ding and colleagues found that not all patient-derived GSCs were sensitive to BubR1 depletion. In fact, a closer look revealed that only

those GSCs which had short distances between sister kinetochores (quantified as inter-kinetochore distance, or IKD) were sensitive to the depletion of BubR1 (151). IKDs are usually short early in mitosis and become longer as stable kinetochore-MT attachments are formed, representing an indirect readout of kinetochore-MT attachment strength. This is exciting for two reasons: it appears that IKD measurements could serve as a biomarker for cancers that may be sensitive to BubR1-directed therapeutics and perhaps different oncogenic signaling pathways respond differently to BubR1 loss. Of primary interest is which of BubR1's functions are needed in cancer cells that are sensitive to the depletion of BubR1.

HeLa cells are sensitive to the loss of BubR1

Discrepancies in the requirement of BubR1 for chromosome alignment have been seen across many labs. Early work in the DeLuca lab showed a requirement for BubR1 in chromosome alignment in cervical cancer HeLa cells, but no significant requirement in retinal pigment epithelial (RPE1) cells. While both HeLa and RPE1 cells align their chromosomes efficiently in metaphase, depletion of BubR1 resulted in severe defects in this alignment in the HeLa cells but not in the RPE1 cells (Figure 4.1B). Importantly, as BubR1 depletion results in a checkpoint override phenotype, these cells were arrested in metaphase using the proteasome inhibitor, MG132. Metaphase cells were then assessed for alignment. Notably, while HeLa cells are a cancer cell line, RPE1 cells are a diploid, non-cancerous immortal cell line. This data is in agreement with the results Ding and colleagues found in comparing GSC and NSC sensitivity to the loss of BubR1 (151).

Figure 4.1. BubR1 depletion differentially affects cancer cells.

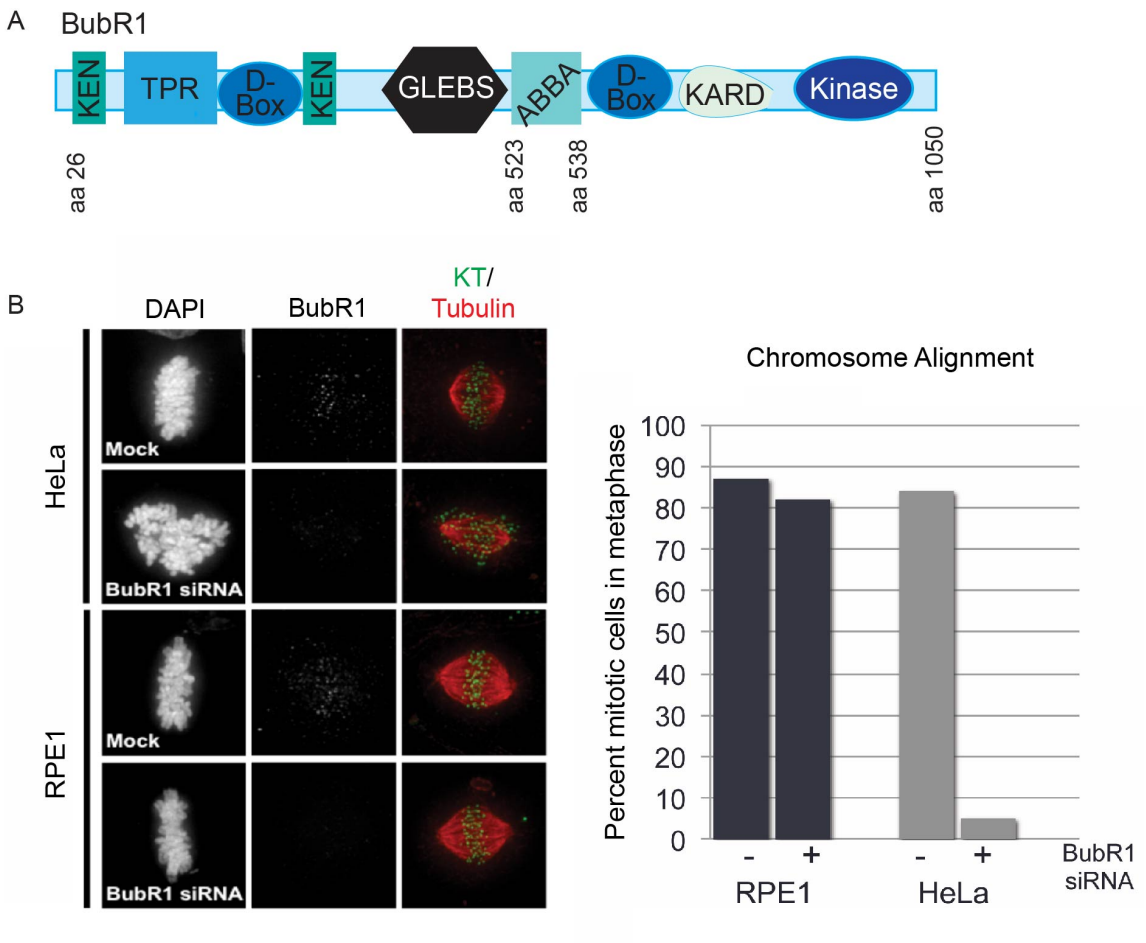

Figure 4.1. BubR1 depletion differentially affects cancer cells. A. Domain architecture of the human BubR1 protein. B. (Left) Representative fixed cell images of HeLa and RPE1 cells depleted of BubR1. DAPI represents the DNA, BubR1 staining confirms the siRNA knockdown, kinetochores (KT) are labeled with ACA staining and Tubulin labels the spindle. (Right) Quantification of the percent of metaphase arrested cells with aligned chromosomes. Data in figure B was collected by Betsy Beuchler.

4.2 Results

Phosphorylation changes in HeLa cells upon depletion of BubR1

As HeLa and GSC cells depleted of BubR1 exhibit severe chromosome alignment defects, the role of BubR1 in recruiting PP2A-B56 to kinetochores is likely at play. PP2A-B56 is thought to counteract Aurora B phosphorylation of outer kinetochore substrates, namely the HEC1 N-terminal tail, to stabilize kinetochore-MT attachments (135). However, there are multiple recruitment factors for both PP2A and PP1 phosphatase to the kinetochore and centromere. It is therefore important to establish that the BubR1-mediated pool of PP2A-B56 directly dephosphorylates the HEC1 tail domain. Additionally, the HEC1 tail domain contains at least 9 different phosphorylation sites. While Aurora B is the primary kinase acting on the HEC1 tail, it has been shown that a single site (serine 69) is selectively phosphorylated by a different kinase, Aurora A (69,204), making it feasible that different phosphatases may also work on different sites. To test this, HeLa cells were depleted of BubR1 using siRNA and cells were stained for phospho-specific antibodies to three different phosphorylation sites in the HEC1 tail domain (pSerine 44, pSerine 55, and pSerine 69) (Figure 4.2). As phosphorylation of HEC1 is very sensitive to the MT attachment status of the kinetochore, cells were treated with the MT depolymerizing drug, Nocodazole, such that no visible MTs remained in the spindle. Immunofluorescence and quantification showed that all 3 phosphorylations sites significantly increased in signal upon BubR1 depletion in HeLa cells (Figure 4.2A-C). Thus, the BubR1-recruited pool of PP2A-B56 at the kinetochore regulates at least 3 sites in the HEC1 tail.

Figure 4.2. HeLa cells depleted of BubR1 exhibit changes in phosphorylation of substrates.

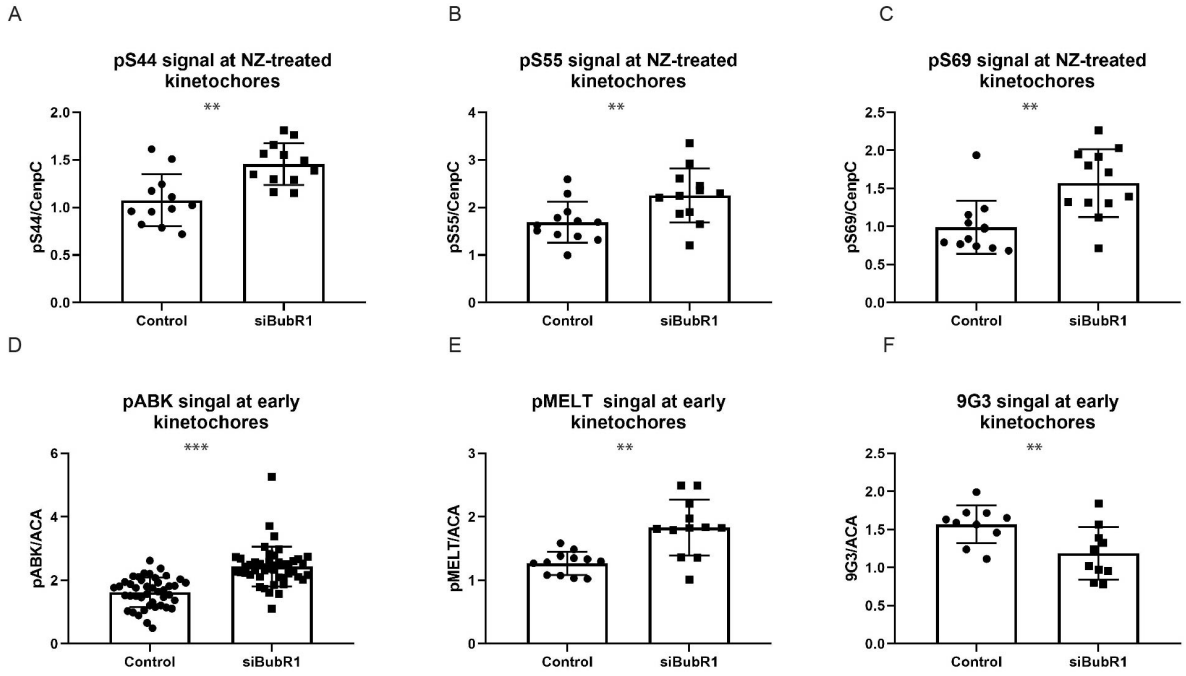

Figure 4.2. HeLa cells depleted of BubR1 exhibit changes in phoshorylation of substrates. A. Quantification of HEC1 phospho-Serine44 staining in control and BubR1 depleted HeLa cells treated with Nocodazole for 30 minutes prior to fixing.B. Quantification of HEC1 phospho-Serine55 staining in control and BubR1 depleted HeLa cells treated with Nocodazole for 30 minutes prior to fixing. C. Quantification of HEC1 phospho-Serine69 staining in control and BubR1 depleted HeLa cells treated with Nocodazole for 30 minutes prior to fixing. D. Quantification of phospho-ABK staining in control and BubR1 depleted early HeLa cells. D. Quantification of phospho-MELT staining in control and BubR1 depleted early HeLa cells. E. Quantification of 9G3 staining in control and BubR1 depleted early HeLa cells. All data points represent average signal per single cell.

In addition to phospho-specific antibodies targeting the HEC1 tail domain, various other potential PP2A-B56 substrates at the kinetochore were tested upon BubR1 depletion. For these experiments, cells were synchronized with a double thymidine block to enrich for mitotic cells. Cells were then fixed and only those cells that had just broken down their nuclear envelope were analyzed for phospho-signals. At this stage, there should be essentially no kinetochore-MT attachments. Upon BubR1 depletion by siRNA, antibodies specific to phospho-Aurora B and phospho-MELT showed significantly increased signals, suggesting that this pool of PP2A-B56 recruited to kinetochores acts on these substrates (Figure 4.2D, 4.2E).

To confirm that the integrity of the kinetochore was not severely disrupted upon BubR1 depletion, we next quantified pan-NDC80 complex levels at the kinetochore using the HEC1-specific antibody, 9G3 (59). To our surprise, there was a small but significant decrease in the amount of HEC1 at kinetochores of BubR1 depleted cells. It is not yet clear why BubR1 depletion might decrease HEC1 levels at kinetochores (Figure 4.2F). Nevertheless, this finding suggests that the increased pHEC1 levels seen upon BubR1 depletion quantified in Figure 4.2A-C are an underestimate since total HEC1 levels are lower in these cells.

Phosphorylation changes in HeLa cells upon inhibition of PP1 recruitment to KNL1

As mentioned earlier, PP2A-B56 at the kinetochore is thought to counteract Aurora B by dephosphorylating the KNL1 RVSF motif to allow for PP1 recruitment later in mitosis when Aurora B activity is decreased (47,203). Therefore, depletion of BubR1 indirectly results in loss of PP1 from kinetochores as well. Any changes in phosphorylation of substrates upon BubR1 depletion could be a result of either loss of PP2A-B56 (directly)

or PP1 (indirectly). To better parse through which phosphatase is responsible for HEC1 tail phosphorylation, the phosphorylation status must be assessed upon PP1-RVSF inhibition. By mutating the RVSF motif of KNL1 into 4 alanine residues (AAAA), PP1-KNL1 interaction is inhibited (47). Stable cell lines expressing siRNA-resistant GFP-KNL1-WT or GFP-KNL1-RVSF/AAAA were generated using the Flp-In T-Rex HeLa System (Figure 4.3A). Endogenous KNL1 was depleted with siRNA and exogenous construct expression was induced with doxycycline addition. Cells were again treated with nocodazole to ensure uniform attachment status across all kinetochores and fixed and stained with the 3 HEC1 tail domain phospho-antibodies (pSerine 44, pSerine 55, and pSerine 69). As a control, cells were also stained with a phospho-specific antibody to the phosphorylated RVSF motif (pRVSF). If the endogenous KNL1 knockdown is efficient, cells expressing GFP-KNL1-RVSF/AAAA should have no pRVSF signal while GFP-KNL1-WT cells should have normal signal. Expression of the GFP-KNL1-RVSF/AAAA resulted in significant increase in all 3 HEC1 tail phosphorylation sites (Figure 4.3B-D). While this would suggest that PP1 does indeed act on the HEC1 tail domain, the results are brought into question by the fact that pRVSF signal does not dampen in GFP-KNL1-RVSF/AAAA expressing cells but instead stays just as high as control and GFP-KNL1-WT cells (Figure 4.3E). This would suggest that perhaps the knockdown of endogenous HEC1 is insufficient. Further experiments are needed for clarification.

Kinetochore-MT attachment stability is defective in BubR1 depleted HeLa cells

Regardless of whether the effect seen upon BubR1 depletion is due to PP2A-B56 directly dephosphorylating the HEC1 tail or to the inability of PP1 to localize to KNL1 (in which case PP1 is the true phosphatase that dephosphorylates the HEC1 tail), we can

Figure 4.3. Inhibiting the PP1-KNL1 interaction results in increased phospho-HEC1.

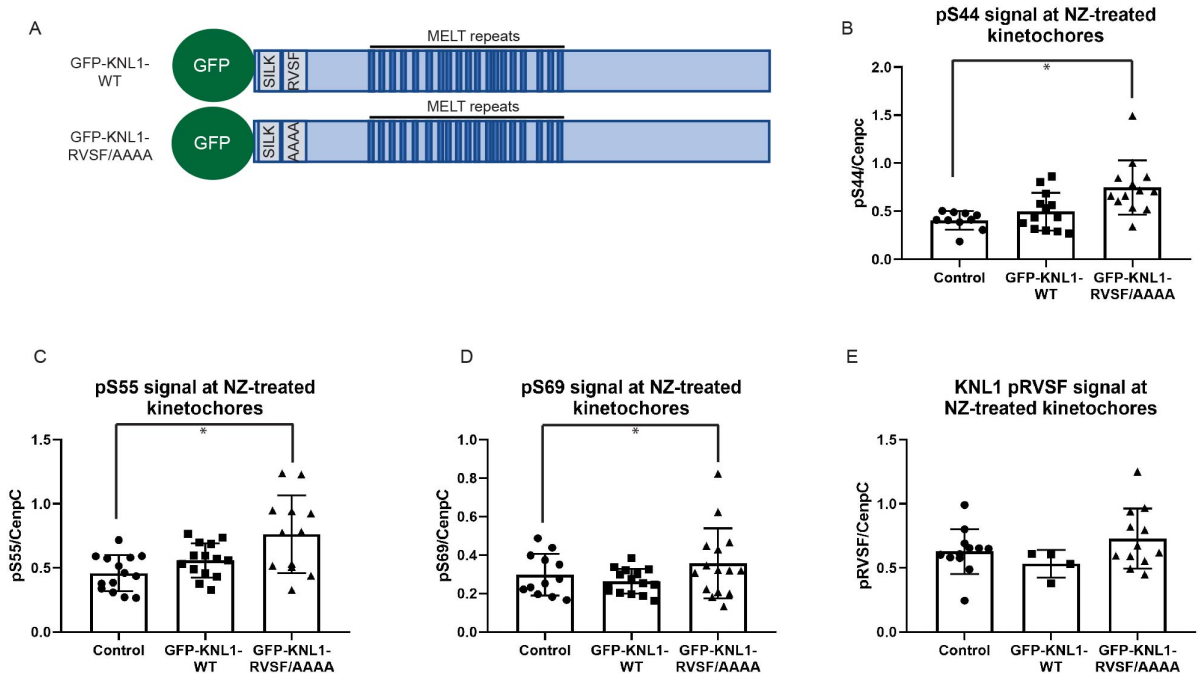

Figure 4.3. Inhibiting the PP1-KNL1 interaction results in increased phospho-HEC1. A. Schematic of the constructs used to generate inducible KNL1 HeLa FlpIn stable cell lines. Constructs are resistant to siRNA treatment. B. Quantification of HEC1 phospho-Serine44 staining in control, siKNL1 + GFP-KNL1-WT, and siKNL1+ GFP-KNL1-RVSF/AAAA cells treated with Nocodazole for 30 minutes prior to fixing. C.Quantification of HEC1 phospho-Serine55 staining in control, siKNL1 + GFP-KNL1-WT, and siKNL1+ GFP-KNL1-RVSF/AAAA cells treated with Nocodazole for 30 minutes prior to fixing. D. Quantification of HEC1 phospho-Serine69 staining in control, siKNL1 + GFP-KNL1-WT, and siKNL1+ GFP-KNL1-RVSF/AAAA cells treated with Nocodazole for 30 minutes prior to fixing. E. Quantification of KNL1 phospho-RVSF staining in control, siKNL1 + GFP-KNL1-WT, and siKNL1+ GFP-KNL1-RVSF/AAAA cells treated with Nocodazole for 30 minutes prior to fixing.

assess if the phosphorylation status of the HEC1 tail is the cause of the kinetochore-MT attachment defects seen in cancer cells that are sensitive to the loss of BubR1. Kinetochore-MT attachment stability can be assessed by cold treatment. Cold treatment of cells will result in the depolymerization of all MTs in the cell, other than those that are stabilized by attachment to kinetochores. To determine if the increased phosphorylation of the HEC1 tail is responsible for the alignment defects seen in BubR1 depleted HeLa cells, we asked if expressing a phospho-null mutant of HEC1 can rescue attachment defects seen upon BubR1 depletion. In this case, all 9 phosphorylation sites in the HEC1 tail domain were mutated to alanine residues (68). Cells were then cold treated for 13 minutes on ice to depolymerize all non-kinetochore bound MTs and fixed and stained for kinetochores and microtubules. Deconvolved images were scored for their attachment status. When quantifying cells that have been arrested in metaphase, we found that control HeLa cells displayed very high attachment (~97%) while BubR1 depletion resulted in only ~48% of kinetochores forming end-on attachment (Figure 4.4A, 4.4B). When we attempt to rescue the BubR1 depletion with a GFP-HEC1-9A construct, we find the percent attachment increases to ~93%, showing an impressive rescue. However, when we attempt to rescue the BubR1 depletion with a GFP-HEC1-WT construct, in which the tail phosphorylation sites are not mutated at all, we still find a significant rescue in end-on attachment, albeit to a lesser degree (~74%) (Figure 4.4A, 4.4B). This is peculiar because without BubR1, a WT HEC1 tail domain still would not be dephosphorylated without the PP2A-B56 complex. However, multiple labs have described tail domain-mediated oligomerization of the Ndc80 complex, making it feasible that simply over-expressing WT HEC1 might still increase attachment status by increasing oligomerization (205).

Figure 4.4. A non-phosphorylatable HEC1 tail domain rescues attachment defects seen upon BubR1 depletion.

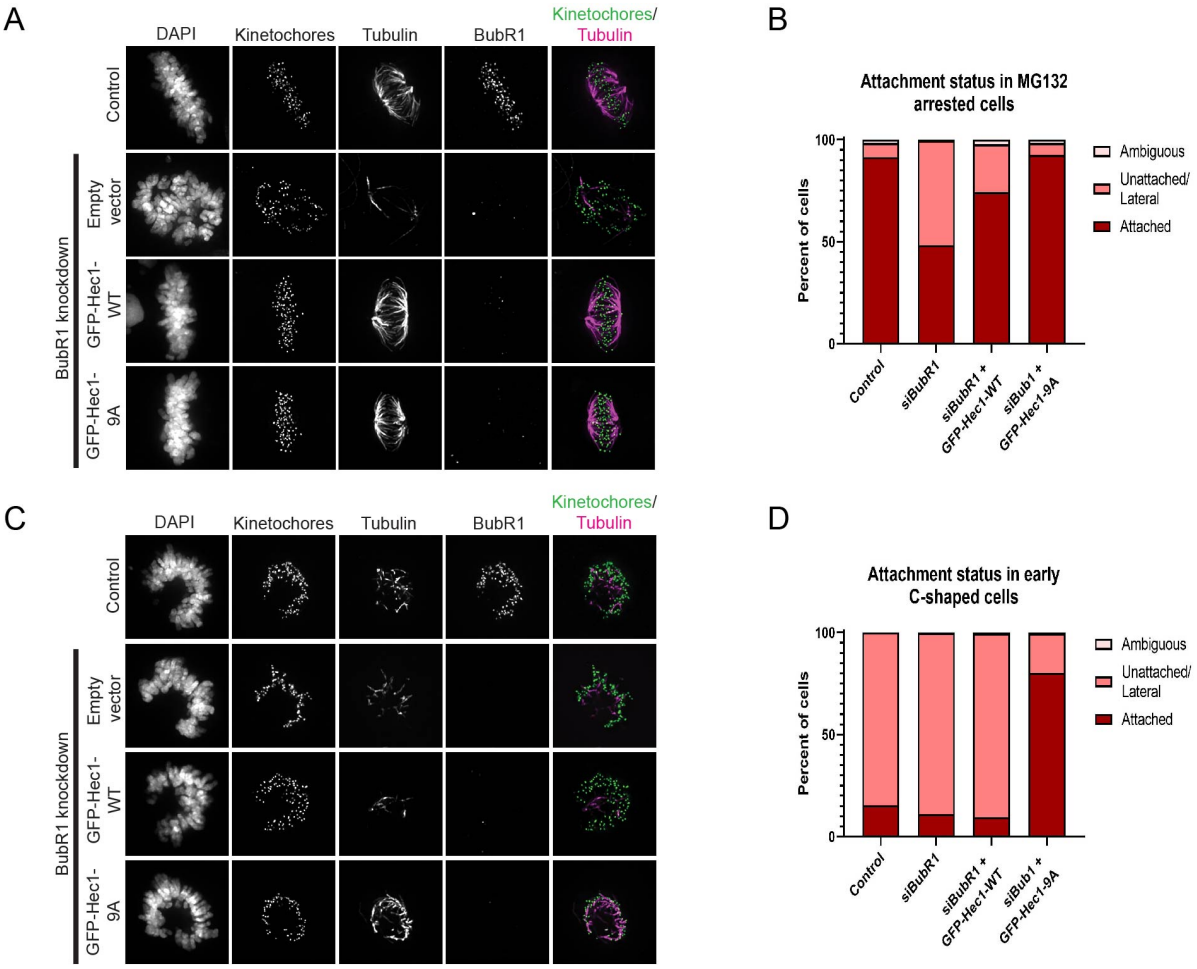

Figure 4.4. A non-phosphorylatable HEC1 tail domain rescues attachment defects seen upon BubR1 depletion. A. Representative images of cold-treated HeLa cells stained for DAPI (DNA), Kinetochores (either ACA or GFP-HEC1), Tubulin, and BubR1. B. Quantification of kinetochore-MT attachment status in MG132 arrested cells. C. Representative images of cold-treated HeLa cells stained for DAPI (DNA), Kinetochores (either ACA or GFP-HEC1), Tubulin, and BubR1. D. Quantification of kinetochore-MT attachment status in early, C-shaped cells.

Additionally, as we see an ~25% decrease in total HEC1 (9G3) levels in BubR1 depleted cells (Figure 4.2F), perhaps a partial rescue is achieved simply by increasing those levels back to WT amounts.

To further test the dependence of the BubR1 depletion phenotype on the HEC1 tail domain phosphorylation state, we measured attachment in early mitotic cells. During prometaphase, most kinetochores are not stable attached to MTs, meaning we may be able to see more differences between the different cell treatments. For this experiment, only cells found immediately after nuclear envelope breakdown were quantified. As expected, control HeLa cells display very little attachment this early in mitosis (~15%) (Figure 4.4C, 4.4D). Depletion of BubR1 resulted in even less attachment (~11%), although it is unclear if this is significant yet. Rescue of the BubR1 depletion with GFP-HEC1-WT was insufficient, with attachment at only ~10%. However, attachment was increased to ~80% upon BubR1 depletion and simultaneous expression of GFP-HEC1-9A (Figure 4.4C, 4.4D). Thus, preventing phosphorylation of the HEC1 tail domain overrides the defective attachment phenotype of BubR1 depletion.

Generating a cell transformation system

To directly assess the oncogenic pathways that lead to BubR1 sensitivity, Dr. Jacob Herman created a laboratory cell transformation model system using retroviral transduction (unpublished). Beginning with primary retinal pigment epithelial (ARPE19) cells, he first created an intermediary cell line in which multiple tumor suppressor pathways were inactivated and telomerase was activated (206,207) (Figure 4.5A). This cell line was termed ARPE19-T53D4. From here, three additional cell lines were generated, each expressing a unique oncogene: $HRAS^{V12}$ (ARPE19-RAS^{V12}), MEK^{DD}

(ARPE19- MEK^{DD}), or AKT^{myr} (ARPE19-AKT^{myr}). $HRas^{V12}$ was chosen because Ding and colleagues previously showed that this mutation is sufficient to cause sensitivity to the loss of BubR1 (151). MEK^{DD} and AKT^{myr} were chosen because each of these mutations represents a unique oncogenic pathway downstream of RAS activation. MEK^{DD} leads to hyperactivation of the MAP kinase (MAPK) pathway, while AKT^{myr} leads to hyperactivation of the PI3 kinase (PI3K) pathway (208,209). Expression of the transgenes was confirmed using RT-PCR (data not shown).

We performed initial experiments using only the parental ARPE19 cell line and the transformed ARPE19-RAS^{V12} cell line. First, to ensure that the ARPE19-RAS^{V12} transformed cell line was indeed sensitive to BubR1 depletion, the alignment status of cells depleted of BubR1 was analyzed. Cells were arrested in metaphase using the drug MG132 for 45 minutes and alignment was quantified (Figure 4.5B). When the parental ARE19 cells were depleted of BubR1, there was not a significant increase in the number of cells with unaligned chromosomes. However, upon BubR1 depletion in the ARPE19-RAS^{V12} cells, the incidence of unaligned cells was significantly increased, confirming that these cells require BubR1 for proper chromosome alignment.

When Ding and colleagues analyzed the inter-kinetochore distances (IKDs) of GSCs that were sensitive to the loss of BubR1, they found that they were significantly shorter than those of NSCs and GSCs that were not sensitive to the loss of BubR1 (151). As ARPE19-RAS^{V12} cells are also sensitive to BubR1 depletion, we asked if they have defects in their IKDs (Figure 4.5C, 4.5D). When comparing the IKDs of parental ARPE19 cells to those of ARPE19-RAS^{V12} cells, we found that the ARPE19-RAS^{V12} cells had significantly shorter IKDs. These shorter distances can be reflective of weaker

Figure 4.5. ARPE19 cell transformation system recapitulates BubR1 sensitivity seen in Glioblastoma cells.

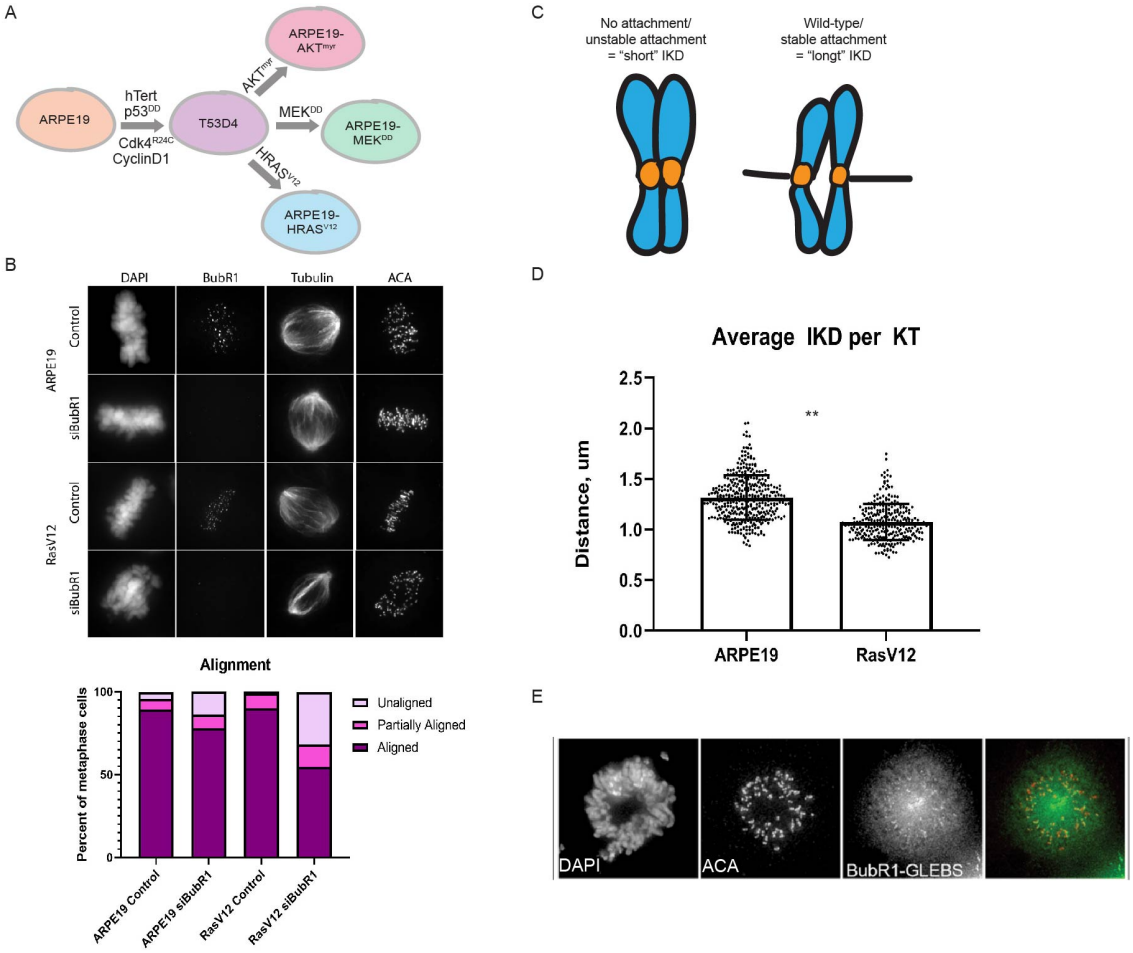

Figure 4.5. ARPE19 cell transformation system recapitulates BubR1 sensitivity seen in Glioblastoma cells. A. Schematic of cell lines generated by Jacob Herman. B. (Top) Representative immunofluorescence images. (Bottom) Quantification of perentage of cells aligned after 45 minutes in MG132 drug to arrest cells in metaphase. C. Illustration depicting inter-kinetochore stretch upon stable kinetochore-microtubule attachment D. Quantificaiton of average inter-kinetochore distance in APRE19 and RasV12 cells. Each data point is a single kinetochore pair. E. Fixed HeLa cells transiently transfected with a fragment of BubR1 containing just the GLEBS domain (GFP-BubR1-GLEBS). Cells were costained for ACA (kinetochore marker) and DAPI (DNA).

attachments between kinetochores and MTs, further suggesting that BubR1 is required in these cell lines to bring in PP2A-B56 to strengthen attachments that are already weak before any perturbations.

4.3 Discussion

We show here that HeLa cells display defective chromosome alignment upon BubR1 depletion. To better understand what substrates the pool of PP2A-B56 that BubR1 recruits may be acting on, we utilized phospo-specific antibody staining upon BubR1 depletion. We find that at least three sites in the HEC1 tail domain are substrates of PP2A-B56, although more work is needed to determine if this is a direct or indirect effect. Additionally, we show that BubR1 depletion results in a ~50% loss of end-on kinetochore-MT attachments, which is rescued upon expressing a mutant GFP-HEC1-9A construct. Additionally, through the cell lines created by Jacob Herman, we now have a laboratory cell culture transformation system with which to analyze the effect of different oncogenic pathways on the sensitivity to BubR1 depletion.

The discrepancy between why some cell lines require BubR1 for chromosome alignment while others do not can be explained with this cancer-specific phenotype that we and others have seen (151). It is likely that although BubR1 recruits the phosphatase PP2A-B56 to kinetochores in all cells, this specific pool only becomes necessary when a cell line already has weak attachments to begin with. As there are other pathways to recruiting the phosphatases to kinetochores, it is possible that there is enough phosphatase activity in these non-sensitive cells to tolerate the loss of the BubR1-recruited PP2A-B56 pool. The ARPE19-Ras^{V12} cells display shorter IKDs inherently, with no BubR1 perturbations, suggesting they may not be able to withstand even a partial hit

to their phosphatase activity. It remains to be determined if the cause of the inherently weak attachments in these cells is increased Aurora B kinase activity or decreased phosphatase activity.

As BubR1's role in the SAC is required in all cell types, it is unlikely that BubR1 depletion can provide therapeutic potential. However, evidence in the field suggests BubR1 may be able to perform its SAC function independent of kinetochore localization (188). BubR1 localizes to kinetochores using its GLE2p-binding sequence (GLEBS), with which it binds to the kinetochore protein Bub3 (89). A possible option for therapeutic development is to competitively inhibit the Bub3-BubR1-GLEBS interaction. This may be possible using GLEBS peptide fragments to compete the full length BubR1 from Bub3. Preliminary experiments show that overexpression of fragments of the BubR1 GLEBS domain do indeed localize to kinetochores (Figure 4.5E). Whether or not BubR1 kinetochore localization is required for attachment has been variable, but it is likely that this is because only cells sensitive to the loss of BubR1 (a subset of transformed cells) would show a phenotype upon inhibition of the kinetochore localization of BubR1 (187,188). Harris and colleagues showed a mutant BubR1 that could not localize to kinetochores resulted in an alignment defect, while Malureanu and colleagues showed that a BubR1 mutant that did not localize to kinetochores did not result in an alignment phenotype. This may be explained by the fact that Harris and colleagues used cancerous HeLa cells, while Malureanu and colleagues used primary MEFs. Ding and colleagues also performed similar experiments in MEFs and showed that a point mutation in the GLEBS domain of BubR1, which prevents its kinetochore localization, does not affect cell viability (151).

In the future, it will be important to directly test the hypothesis that BubR1 is primarily required in these cancer cells because it recruits PP2A-B56. To do so, we can tether the phosphatase to kinetochores in the ARPE19-Ras^{V12} cells and ask if they now tolerate BubR1 depletion. As tethering a phosphatase may interfere with its activity, we can alternatively perform knockdown/rescue experiments utilizing mutants designed in the Kops lab in which the KARD domain of BubR1 is mutated to mimic or inhibit phosphorylation (135). This would result in an artificial excess or lack of PP2A-B56 at kinetochores.

4.4 Materials and methods

Cell culture and generation of stable cell lines

ARPE19 cells (American Type Culture Collection) and derivative cell lines were cultured in DMEM/F-12 (Life Technologies) and supplemented with 1x penicillin/streptomycin and 10% fetal bovine serum (FBS) at 37°C in 5% CO2. For synchronization, cells were double-thymidine blocked in the following manner: cells were treated with 2.5 mM thymidine for 16 h, followed by 8 h in regular medium, then 2.5 mM thymidine again for 16 h. After the second 16-h block, cells were washed out into regular medium for 10 h. For metaphase arrest, cells were treated with 10 uM MG132 (Selleckchem) for 45 minutes before fixation. For nocodazole treatment, cells were treated with 10 uM nocodazole (Tocris) for 30 minutes prior to fixation and 10 hr after thymidine release. For cold-stable treatment, cells were treated with ice-cold DMEM/F12 medium and placed on ice for 13 minutes prior to fixation. To generate Flp-In T-REx HeLa inducible stable cell lines expressing GFP-KNL1-WT and GFP-KNL1-RVSF/AAAA, the host cells were grown to 50% confluency and transfected with 4.5 µg pOG44

recombinase-containing plasmid and 0.5 µg pcDNA5.FRT.TO-GFP-KNL1 plasmids using Lipofectamine 3000 (Thermo Fisher Scientific) per manufacturer instructions. After 48 h, cells were switched to media containing 100 µg/mL hygromycin (EMD Millipore) and grown in selection media for 2 wk. Hygromycin-resistant foci were expanded and tested for inducible GFP-KNL1 construct expression. Cell lines expressing GFP fusion proteins were cultured in DMEM supplemented with 10% FBS, 1% antibiotic/antimycotic solution, 2 mM L-glutamine, and 100 µg/ml hygromycin and maintained at 37°C in 5% CO2. Gene expression was induced with 1 µg/ml doxycycline (Sigma-Aldrich) for 12–24 h. For the retroviral generation of ARPE19 cell lines (done by Dr. Jacob Herman): Phoenix packaging cells were transfected with pCMV-TAT and pCSIG to VSV-G psuedotype viruses in addition to a donor plasmid of choice described below. The combination of plasmids were transfected at a 3:1 volume to DNA mass ratio using Fugene 6 (Promega) transfection reagent. Growth medium was replaced 24 hours after transfection. Viral particle-containing supernatant media were harvested 48 and 72 hours after transfection, centrifuged, aliquoted, and used or frozen at -80°C. To perform viral infections, target cells were grown in 6 cm or 24-well cell culture dishes in viral particle-containing supernatant media for 24 hours. This was repeated with fresh viral containing-supernatant media for 24 more hours. 48 hours after initial infection cells were exposed to media containing a negative selective pressure.

Plasmids and siRNAs

To silence BUBR1 cells were transfected with siRNA (Qiagen) using Lipofectamine 3000 (Thermo Fisher Scientific) according to manufacturer instructions and fixed 48 hours later. BUBR1 siRNA sequence: 5’-GAGAAUACCUAAUAUGUGATT-3’. For BubR1

knockdown and GFP-HEC1 rescue experiments, 2 ug of GFP-HEC1 DNA was transfected concurrently. To inactivate tumor suppressor pathways in ARPE19 cells (done by Dr. Jacob Herman), viral particles were generated using two dually encoding plasmids: pbabe-hTERT+p53DD (Addgene plasmid # 11128) and pbabe-cyclinD1+CDK4R24C (Addgene plasmid # 11129), which were gifts from Christopher Counter. After infection with these donor plasmids cells were infected with viral particles containing one of the following donor plasmids: pLXSN-H-Ras_V12 (Addgene plasmid # 39516), a gift from Julian Downward; 901-pLNCX-myr-HA-Akt, (Addgene plasmid # 9005) a gift from William Sellers; or pBabe-Puro-MEK-DD (Addgene plasmid # 15268) was a gift from William Hahn.

Immunofluorescence and Imaging

For fixed cell imaging, cells were grown on acid washed sterile coverslips. For the fixation procedure, cells were first rinsed with 1X PHEM buffer (60 mM PIPES, 25 mM HEPES, 10 mM EGTA, and 4 mM MgSO4) at 37°C. Cells were then either lysed first for 5 minutes in 0.5% TritonX followed by a 20-minute fixation in 4% paraformaldehyde or fixed first for 20 minutes in 4% paraformaldehyde buffer followed by a 5 minute lysis in 0.5% TritonX. After fixation, cells were washed 3 × 5 min in PHEM-T (PHEM buffer + 0.1% Triton X-100) and blocked in 10% boiled donkey serum (BDS) in PHEM for 1 h at room temperature. Primary antibodies were diluted in 5% BDS and added to coverslips overnight at 4°C. The primary antibodies used were: human anti-centromere antibody (Antibodies, Inc., 1:300), Rabbit anti-BubR1 (Bethyl, 1:500), DM1α mouse anti-tubulin (Sigma, 1:1000), Guinea pig anti CENPC (MBL International, 1:500), Rabbit anti pABK (made in-house, 1:500), Rabbit anti pMELT (Cell Signaling Technology, 1:500), rabbit

anti pRVSF (a gift from Iian Cheeseman, 1:500), Rabbit anti pHEC1-S44 (made in-house, 1:2000), Rabbit anti pHEC1-S55 (made in-house, 1:300), Rabbit anti pHEC1-S69 (made in-house, 1:2000). After primary antibody incubation, cells were rinsed 3 x 5 min in PHEM-T and then incubated for 45 min at room temperature with secondary antibodies conjugated to Alexa Fluor 488, Alexa Fluor 568, or Alexa Fluor 647 (Jackson ImmunoResearch Laboratories) at 1:800 diluted in 5% BDS. Cells were rinsed 3 x 5 min in PHEM-T and quickly rinsed in PHEM followed by incubation in DAPI (2 ng/ml) diluted in PHEM for 30 s. Slides were rinsed 3 x 5 min in PHEM-T, quickly rinsed in PHEM, and then mounted onto glass slides with antifade solution (90% glycerol, 0.5% N-propyl gallate). Coverslips were sealed with nail polish and stored at 4°C. All fixed cell images were acquired on an IX71 inverted microscope (Olympus) incorporated into a DeltaVision Personal DV imaging system (GE Healthcare) using SoftWorx software (GE Healthcare). Slides were imaged using a 60X/1.42 NA differential interference contrast Plan Apochromat oil immersion lens (Olympus) and a CoolSNAP HQ2 camera. For live-cell imaging, cells were maintained at 37°C using an environmental chamber (Precision Control) and in Leibovitz's L-15 media (Gibco) supplemented with 10% FBS, 7 mM HEPES and 4.5 g/l D-glucose (pH 7.0).

CHAPTER 5: DISCUSSION AND FUTURE PROSPECTIVE

5.1 Transformed cells display inherent defects in cell division

The cellular changes that arise upon cell transformation are wide-reaching. Cancers are conglomerations of several different altered signaling pathways that result in unique signatures for different types of cancers. Mitosis is a promising target for therapeutic development, as evidenced by the fact that two different cancer screens targeting two different types of proteins (transcription factors and kinases) resulted in mitotic proteins as top hits. While deregulation of factors outside of mitosis likely drive cancer initiation, defects during the mitotic process result in the aneuploidy that is so characteristic of most tumor cells, likely contributing to the progression of the cancer. The work described here, as well as a growing body of evidence, shows that mitosis in cancer cells displays regulatory and mechanistic differences when compared to healthy cells. Therefore, a better understanding of the fundamental changes that occur during mitosis in a transformed cell type can provide valuable direction for cancer therapies.

As a step toward furthering this understanding, we used human papillomavirus (HPV) and cervical cancer as an initial model system. We found that the SAC was weakened upon HPV E6 expression in cultured cells. This weakened SAC combined with the increase in the incidence of polar chromosomes meant that these cells could not sustain a checkpoint arrest for an extended period of time, even in the presence of kinetochore-MT attachment errors. Consequently, these cells had a higher incidence of aneuploidy, as they exited mitosis prematurely. While a weakened SAC is certainly a mechanism of generating aneuploidy, loss of function mutations in checkpoint proteins

are relatively rare in cancers. In fact, many cancers exhibit overexpression of SAC proteins. Along these lines, inhibiting the checkpoint with ~90% BubR1 or Mad2 depletion in cancer cells has been shown to be lethal after just 2-3 cell divisions, due to massive chromosome losses (165). Importantly, we have shown that the HPV E6 expressing cells have a weaker checkpoint, but they can still produce a significant arrest, likely explaining why these cells survive under normal conditions. Without the increased instance of persistent polar attachments, the weaker checkpoint might not lead to significant cell division errors. As it stands, the increased incidence of attachment errors in combination with a weaker checkpoint in these cells likely results in tolerable small, incremental increases in aneuploidy over time. Thus, kinetochore-MT attachment defects are likely the driving contributor to oncogenesis in this system.

5.2 Targeting mitotic proteins in cancer cells

Mitosis has long been a general therapeutic target for cancer treatments. As many cancer cells are not inhibited by the restriction checkpoints that are usually in place, they cycle through the cell cycle at a faster rate. Therefore, at any given time, more cancer cells will be in mitosis than their healthy counterparts. This has led to the widespread use of drugs that target microtubules with the aim of activating the spindle assembly checkpoint for a prolonged amount of time, resulting in cell death. Taxanes and vinca alkaloids are the primary drug categories used for these purposes (210,211). However, these drugs do not discriminate between healthy and transformed cells. Instead, more targeted approaches are necessary.

Through RNAi cancer lethality screens performed in Glioblastoma brain cancer cells, we now have two potential candidates for targeted therapeutics (150,151). BubR1

and BuGZ are both GLEBS-domain containing mitotic proteins with roles in regulating kinetochore-MT attachment, although this is less well-understood for BuGZ. We show here that kinetochore-MT attachments are weakened in BuR1 depleted cells, presumably due to the loss of the PP2A-B56 phosphatase. In fact, phosphorylation of the HEC1 tail domain is upregulated in these cells, suggesting that PP2A-B56 is needed specifically to dephosphorylate HEC1. Therefore, Ras-transformed cells have an added requirement for BubR1 at kinetochores, to strengthen attachments. As proper kinetochore-MT attachments are a result of a delicate kinase/phosphatase balance, this added requirement is likely due to either upregulation of Aurora B activity or downregulation of phosphatase activity in these cells. To answer this, we will perform RNA sequencing on the ARPE19 cell lines to determine if there is significant change in kinase or phosphatase pathways upon cell transformation. This may provide additional therapeutic targets involved in the same pathways at work here.

Intriguingly, the cancer lethality screen that produced BuGZ as a top hit was performed in the same cell type as the kinase screen that identified BubR1 as a top hit. While both proteins are intricately connected in mitosis as they both bind to Bub3, their functions appear to differ greatly. BubR1 depletion resulted in weakened kinetochore-MT attachments, but we show that BuGZ depletion results in hyperstable attachments. Therefore, BubR1 is needed to counteract Aurora B kinase activity at the kinetochore, while BuGZ is needed to promote Aurora B activity. This suggests that two separate kinetochore-MT attachment defects occur in Glioblastoma cancer cells. As only a subset of Glioblastoma patient isolates were sensitive to BubR1 loss, it will be important to determine if the same cells that are sensitive to BubR1 loss are also sensitive to BuGZ

loss. As patient tumors are genetically complex, the cell transformation model system we now have will greatly aid in determining the specific oncogenic signaling pathways that result in a requirement for either BubR1 or BuGZ. Excitingly, we show here that BuGZ and BubR1 might represent a means of targeting features that are distinct to cancer cells, thereby leaving healthy cells unharmed.

REFERENCES

1. Schafer, K. A. (1998) The cell cycle: a review. *Vet Pathol* **35**, 461-478

2. Howard, A., and Pelc, S. R. (1986) Synthesis of Desoxyribonucleic Acid in Normal and Irradiated Cells and Its Relation to Chromosome Breakage. *International Journal of Radiation Biology and Related Studies in Physics, Chemistry and Medicine* **49**, 207-218

3. Bettencourt-Dias, M., and Glover, D. M. (2007) Centrosome biogenesis and function: centrosomics brings new understanding. *Nat Rev Mol Cell Biol* **8**, 451-463

4. Grana, X., and Reddy, E. P. (1995) Cell cycle control in mammalian cells: role of cyclins, cyclin dependent kinases (CDKs), growth suppressor genes and cyclin-dependent kinase inhibitors (CKIs). *Oncogene* **11**, 211-219

5. Barnum, K. J., and O'Connell, M. J. (2014) Cell cycle regulation by checkpoints. *Methods Mol Biol* **1170**, 29-40

6. Vermeulen, K., Van Bockstaele, D. R., and Berneman, Z. N. (2003) The cell cycle: a review of regulation, deregulation and therapeutic targets in cancer. *Cell Prolif* **36**, 131-149

7. Flemming, W. (1882) *Zellsubstanz, Kern und Zelltheilung*, Vogel, Leipzig,

8. Vagnarelli, P. (2013) Chromatin reorganization through mitosis. *Adv Protein Chem Struct Biol* **90**, 179-224

9. Gheghiani, L., and Gavet, O. (2014) Deciphering the spatio-temporal regulation of entry and progression through mitosis. *Biotechnol J* **9**, 213-223

10. Akiyoshi, B., and Gull, K. (2014) Discovery of unconventional kinetochores in kinetoplastids. *Cell* **156**, 1247-1258

11. Wong, C. Y. Y., Lee, B. C. H., and Yuen, K. W. Y. (2020) Epigenetic regulation of centromere function. *Cell Mol Life Sci*

12. Bloom, K. S., and Carbon, J. (1982) Yeast centromere DNA is in a unique and highly ordered structure in chromosomes and small circular minichromosomes. *Cell* **29**, 305-317

13. Biggins, S. (2013) The composition, functions, and regulation of the budding yeast kinetochore. *Genetics* **194**, 817-846

14. Manuelidis, L. (1978) Chromosomal localization of complex and simple repeated human DNAs. *Chromosoma* **66**, 23-32

15. Aldrup-Macdonald, M. E., and Sullivan, B. A. (2014) The past, present, and future of human centromere genomics. *Genes (Basel)* **5**, 33-50

16. Earnshaw, W. C., and Rothfield, N. (1985) Identification of a family of human centromere proteins using autoimmune sera from patients with scleroderma. *Chromosoma* **91**, 313-321

17. Palmer, D. K., O'Day, K., Wener, M. H., Andrews, B. S., and Margolis, R. L. (1987) A 17-kD centromere protein (CENP-A) copurifies with nucleosome core particles and with histones. *J Cell Biol* **104**, 805-815

18. Sullivan, K. F., Hechenberger, M., and Masri, K. (1994) Human CENP-A contains a histone H3 related histone fold domain that is required for targeting to the centromere. *J Cell Biol* **127**, 581-592

19. Howman, E. V., Fowler, K. J., Newson, A. J., Redward, S., MacDonald, A. C., Kalitsis, P., and Choo, K. H. (2000) Early disruption of centromeric chromatin organization in centromere protein A (Cenpa) null mice. *Proc Natl Acad Sci U S A* **97**, 1148-1153

20. Oegema, K., Desai, A., Rybina, S., Kirkham, M., and Hyman, A. A. (2001) Functional analysis of kinetochore assembly in Caenorhabditis elegans. *J Cell Biol* **153**, 1209-1226

21. Liu, S. T., Rattner, J. B., Jablonski, S. A., and Yen, T. J. (2006) Mapping the assembly pathways that specify formation of the trilaminar kinetochore plates in human cells. *J Cell Biol* **175**, 41-53

22. Saitoh, H., Tomkiel, J., Cooke, C. A., Ratrie, H., 3rd, Maurer, M., Rothfield, N. F., and Earnshaw, W. C. (1992) CENP-C, an autoantigen in scleroderma, is a component of the human inner kinetochore plate. *Cell* **70**, 115-125

23. Carroll, C. W., Milks, K. J., and Straight, A. F. (2010) Dual recognition of CENP-A nucleosomes is required for centromere assembly. *J Cell Biol* **189**, 1143-1155

24. Carroll, C. W., Silva, M. C., Godek, K. M., Jansen, L. E., and Straight, A. F. (2009) Centromere assembly requires the direct recognition of CENP-A nucleosomes by CENP-N. *Nat Cell Biol* **11**, 896-902

25. Hori, T., Amano, M., Suzuki, A., Backer, C. B., Welburn, J. P., Dong, Y., McEwen, B. F., Shang, W. H., Suzuki, E., Okawa, K., Cheeseman, I. M., and Fukagawa, T. (2008) CCAN makes multiple contacts with centromeric DNA to provide distinct pathways to the outer kinetochore. *Cell* **135**, 1039-1052

26. Nishino, T., Takeuchi, K., Gascoigne, K. E., Suzuki, A., Hori, T., Oyama, T., Morikawa, K., Cheeseman, I. M., and Fukagawa, T. (2012) CENP-T-W-S-X forms a unique centromeric chromatin structure with a histone-like fold. *Cell* **148**, 487-501

27. Basilico, F., Maffini, S., Weir, J. R., Prumbaum, D., Rojas, A. M., Zimniak, T., De Antoni, A., Jeganathan, S., Voss, B., van Gerwen, S., Krenn, V., Massimiliano, L., Valencia, A., Vetter, I. R., Herzog, F., Raunser, S., Pasqualato, S., and Musacchio, A. (2014) The pseudo GTPase CENP-M drives human kinetochore assembly. *Elife* **3**, e02978

28. Klare, K., Weir, J. R., Basilico, F., Zimniak, T., Massimiliano, L., Ludwigs, N., Herzog, F., and Musacchio, A. (2015) CENP-C is a blueprint for constitutive centromere-associated network assembly within human kinetochores. *J Cell Biol* **210**, 11-22

29. Hori, T., Okada, M., Maenaka, K., and Fukagawa, T. (2008) CENP-O class proteins form a stable complex and are required for proper kinetochore function. *Mol Biol Cell* **19**, 843-854

30. Przewloka, M. R., Venkei, Z., Bolanos-Garcia, V. M., Debski, J., Dadlez, M., and Glover, D. M. (2011) CENP-C is a structural platform for kinetochore assembly. *Curr Biol* **21**, 399-405

31. Screpanti, E., De Antoni, A., Alushin, G. M., Petrovic, A., Melis, T., Nogales, E., and Musacchio, A. (2011) Direct binding of Cenp-C to the Mis12 complex joins the inner and outer kinetochore. *Curr Biol* **21**, 391-398

32. Gascoigne, K. E., Takeuchi, K., Suzuki, A., Hori, T., Fukagawa, T., and Cheeseman, I. M. (2011) Induced ectopic kinetochore assembly bypasses the requirement for CENP-A nucleosomes. *Cell* **145**, 410-422

33. Hara, M., Ariyoshi, M., Okumura, E. I., Hori, T., and Fukagawa, T. (2018) Multiple phosphorylations control recruitment of the KMN network onto kinetochores. *Nat Cell Biol* **20**, 1378-1388

34. Brinkley, B. R., and Stubblefield, E. (1966) The fine structure of the kinetochore of a mammalian cell in vitro. *Chromosoma* **19**, 28-43

35. Jokelainen, P. T. (1967) The ultrastructure and spatial organization of the metaphase kinetochore in mitotic rat cells. *J Ultrastruct Res* **19**, 19-44

36. McEwen, B. F., Hsieh, C. E., Mattheyses, A. L., and Rieder, C. L. (1998) A new look at kinetochore structure in vertebrate somatic cells using high-pressure freezing and freeze substitution. *Chromosoma* **107**, 366-375

37. Ris, H., and Witt, P. L. (1981) Structure of the mammalian kinetochore. *Chromosoma* **82**, 153-170

38. Rieder, C. L. (1982) The formation, structure, and composition of the mammalian kinetochore and kinetochore fiber. *Int Rev Cytol* **79**, 1-58

39. Cooke, C. A., Bazett-Jones, D. P., Earnshaw, W. C., and Rattner, J. B. (1993) Mapping DNA within the mammalian kinetochore. *J Cell Biol* **120**, 1083-1091

40. Cheeseman, I. M., Niessen, S., Anderson, S., Hyndman, F., Yates, J. R., 3rd, Oegema, K., and Desai, A. (2004) A conserved protein network controls assembly of the outer kinetochore and its ability to sustain tension. *Genes Dev* **18**, 2255-2268

41. Varma, D., and Salmon, E. D. (2012) The KMN protein network--chief conductors of the kinetochore orchestra. *J Cell Sci* **125**, 5927-5936

42. Kiyomitsu, T., Obuse, C., and Yanagida, M. (2007) Human Blinkin/AF15q14 is required for chromosome alignment and the mitotic checkpoint through direct interaction with Bub1 and BubR1. *Dev Cell* **13**, 663-676

43. Petrovic, A., Pasqualato, S., Dube, P., Krenn, V., Santaguida, S., Cittaro, D., Monzani, S., Massimiliano, L., Keller, J., Tarricone, A., Maiolica, A., Stark, H., and Musacchio, A. (2010) The MIS12 complex is a protein interaction hub for outer kinetochore assembly. *J Cell Biol* **190**, 835-852

44. Petrovic, A., Keller, J., Liu, Y., Overlack, K., John, J., Dimitrova, Y. N., Jenni, S., van Gerwen, S., Stege, P., Wohlgemuth, S., Rombaut, P., Herzog, F., Harrison, S. C., Vetter, I. R., and Musacchio, A. (2016) Structure of the MIS12 Complex and Molecular Basis of Its Interaction with CENP-C at Human Kinetochores. *Cell* **167**, 1028-1040 e1015

45. Kline, S. L., Cheeseman, I. M., Hori, T., Fukagawa, T., and Desai, A. (2006) The human Mis12 complex is required for kinetochore assembly and proper chromosome segregation. *J Cell Biol* **173**, 9-17

46. Caldas, G. V., and DeLuca, J. G. (2014) KNL1: bringing order to the kinetochore. *Chromosoma* **123**, 169-181

47. Liu, D., Vleugel, M., Backer, C. B., Hori, T., Fukagawa, T., Cheeseman, I. M., and Lampson, M. A. (2010) Regulated targeting of protein phosphatase 1 to the outer kinetochore by KNL1 opposes Aurora B kinase. *J Cell Biol* **188**, 809-820

48. Cheeseman, I. M., Chappie, J. S., Wilson-Kubalek, E. M., and Desai, A. (2006) The conserved KMN network constitutes the core microtubule-binding site of the kinetochore. *Cell* **127**, 983-997

49. Krenn, V., Wehenkel, A., Li, X., Santaguida, S., and Musacchio, A. (2012) Structural analysis reveals features of the spindle checkpoint kinase Bub1-kinetochore subunit Knl1 interaction. *J Cell Biol* **196**, 451-467

50. Krenn, V., Overlack, K., Primorac, I., van Gerwen, S., and Musacchio, A. (2014) KI motifs of human Knl1 enhance assembly of comprehensive spindle checkpoint complexes around MELT repeats. *Curr Biol* **24**, 29-39

51. London, N., Ceto, S., Ranish, J. A., and Biggins, S. (2012) Phosphoregulation of Spc105 by Mps1 and PP1 regulates Bub1 localization to kinetochores. *Curr Biol* **22**, 900-906

52. Shepperd, L. A., Meadows, J. C., Sochaj, A. M., Lancaster, T. C., Zou, J., Buttrick, G. J., Rappsilber, J., Hardwick, K. G., and Millar, J. B. (2012) Phosphodependent recruitment of Bub1 and Bub3 to Spc7/KNL1 by Mph1 kinase maintains the spindle checkpoint. *Curr Biol* **22**, 891-899

53. Yamagishi, Y., Yang, C. H., Tanno, Y., and Watanabe, Y. (2012) MPS1/Mph1 phosphorylates the kinetochore protein KNL1/Spc7 to recruit SAC components. *Nat Cell Biol* **14**, 746-752

54. Cheeseman, I. M., Hori, T., Fukagawa, T., and Desai, A. (2008) KNL1 and the CENP-H/I/K complex coordinately direct kinetochore assembly in vertebrates. *Mol Biol Cell* **19**, 587-594

55. Caldas, G. V., DeLuca, K. F., and DeLuca, J. G. (2013) KNL1 facilitates phosphorylation of outer kinetochore proteins by promoting Aurora B kinase activity. *J Cell Biol* **203**, 957-969

56. Kapoor, T. M., Lampson, M. A., Hergert, P., Cameron, L., Cimini, D., Salmon, E. D., McEwen, B. F., and Khodjakov, A. (2006) Chromosomes can congress to the metaphase plate before biorientation. *Science* **311**, 388-391

57. Johnson, V. L., Scott, M. I., Holt, S. V., Hussein, D., and Taylor, S. S. (2004) Bub1 is required for kinetochore localization of BubR1, Cenp-E, Cenp-F and Mad2, and chromosome congression. *J Cell Sci* **117**, 1577-1589

58. Ciossani, G., Overlack, K., Petrovic, A., Huis In 't Veld, P. J., Koerner, C., Wohlgemuth, S., Maffini, S., and Musacchio, A. (2018) The kinetochore proteins CENP-E and CENP-F directly and specifically interact with distinct BUB mitotic checkpoint Ser/Thr kinases. *J Biol Chem* **293**, 10084-10101

59. DeLuca, J. G., Gall, W. E., Ciferri, C., Cimini, D., Musacchio, A., and Salmon, E. D. (2006) Kinetochore microtubule dynamics and attachment stability are regulated by Hec1. *Cell* **127**, 969-982

60. DeLuca, J. G., Dong, Y., Hergert, P., Strauss, J., Hickey, J. M., Salmon, E. D., and McEwen, B. F. (2005) Hec1 and nuf2 are core components of the kinetochore outer plate essential for organizing microtubule attachment sites. *Mol Biol Cell* **16**, 519-531

61. Ciferri, C., De Luca, J., Monzani, S., Ferrari, K. J., Ristic, D., Wyman, C., Stark, H., Kilmartin, J., Salmon, E. D., and Musacchio, A. (2005) Architecture of the human ndc80-hec1 complex, a critical constituent of the outer kinetochore. *J Biol Chem* **280**, 29088-29095

62. Wei, R. R., Sorger, P. K., and Harrison, S. C. (2005) Molecular organization of the Ndc80 complex, an essential kinetochore component. *Proc Natl Acad Sci U S A* **102**, 5363-5367

63. Ciferri, C., Pasqualato, S., Screpanti, E., Varetti, G., Santaguida, S., Dos Reis, G., Maiolica, A., Polka, J., De Luca, J. G., De Wulf, P., Salek, M., Rappsilber, J., Moores, C. A., Salmon, E.

D., and Musacchio, A. (2008) Implications for kinetochore-microtubule attachment from the structure of an engineered Ndc80 complex. *Cell* **133**, 427-439

64. DeLuca, J. G., and Musacchio, A. (2012) Structural organization of the kinetochore-microtubule interface. *Curr Opin Cell Biol* **24**, 48-56

65. Maiolica, A., Cittaro, D., Borsotti, D., Sennels, L., Ciferri, C., Tarricone, C., Musacchio, A., and Rappsilber, J. (2007) Structural analysis of multiprotein complexes by cross-linking, mass spectrometry, and database searching. *Mol Cell Proteomics* **6**, 2200-2211

66. Wilson-Kubalek, E. M., Cheeseman, I. M., Yoshioka, C., Desai, A., and Milligan, R. A. (2008) Orientation and structure of the Ndc80 complex on the microtubule lattice. *J Cell Biol* **182**, 1055-1061

67. Alushin, G. M., Ramey, V. H., Pasqualato, S., Ball, D. A., Grigorieff, N., Musacchio, A., and Nogales, E. (2010) The Ndc80 kinetochore complex forms oligomeric arrays along microtubules. *Nature* **467**, 805-810

68. Guimaraes, G. J., Dong, Y., McEwen, B. F., and Deluca, J. G. (2008) Kinetochore-microtubule attachment relies on the disordered N-terminal tail domain of Hec1. *Curr Biol* **18**, 1778-1784

69. DeLuca, K. F., Lens, S. M., and DeLuca, J. G. (2011) Temporal changes in Hec1 phosphorylation control kinetochore-microtubule attachment stability during mitosis. *J Cell Sci* **124**, 622-634

70. Tugendreich, S., Tomkiel, J., Earnshaw, W., and Hieter, P. (1995) CDC27Hs colocalizes with CDC16Hs to the centrosome and mitotic spindle and is essential for the metaphase to anaphase transition. *Cell* **81**, 261-268

71. He, X., Patterson, T. E., and Sazer, S. (1997) The Schizosaccharomyces pombe spindle checkpoint protein mad2p blocks anaphase and genetically interacts with the anaphase-promoting complex. *Proc Natl Acad Sci U S A* **94**, 7965-7970

72. Sivakumar, S., and Gorbsky, G. J. (2015) Spatiotemporal regulation of the anaphase-promoting complex in mitosis. *Nat Rev Mol Cell Biol* **16**, 82-94

73. King, R. W., Peters, J. M., Tugendreich, S., Rolfe, M., Hieter, P., and Kirschner, M. W. (1995) A 20S complex containing CDC27 and CDC16 catalyzes the mitosis-specific conjugation of ubiquitin to cyclin B. *Cell* **81**, 279-288

74. Irniger, S., Piatti, S., Michaelis, C., and Nasmyth, K. (1995) Genes involved in sister chromatid separation are needed for B-type cyclin proteolysis in budding yeast. *Cell* **81**, 269-278

75. Sudakin, V., Ganoth, D., Dahan, A., Heller, H., Hershko, J., Luca, F. C., Ruderman, J. V., and Hershko, A. (1995) The cyclosome, a large complex containing cyclin-selective ubiquitin ligase activity, targets cyclins for destruction at the end of mitosis. *Mol Biol Cell* **6**, 185-197

76. Cohen-Fix, O., Peters, J. M., Kirschner, M. W., and Koshland, D. (1996) Anaphase initiation in Saccharomyces cerevisiae is controlled by the APC-dependent degradation of the anaphase inhibitor Pds1p. *Genes Dev* **10**, 3081-3093

77. Funabiki, H., Kumada, K., and Yanagida, M. (1996) Fission yeast Cut1 and Cut2 are essential for sister chromatid separation, concentrate along the metaphase spindle and form large complexes. *EMBO J* **15**, 6617-6628

78. Hwang, L. H., Lau, L. F., Smith, D. L., Mistrot, C. A., Hardwick, K. G., Hwang, E. S., Amon, A., and Murray, A. W. (1998) Budding yeast Cdc20: a target of the spindle checkpoint. *Science* **279**, 1041-1044

79. Fraschini, R., Beretta, A., Sironi, L., Musacchio, A., Lucchini, G., and Piatti, S. (2001) Bub3 interaction with Mad2, Mad3 and Cdc20 is mediated by WD40 repeats and does not require intact kinetochores. *EMBO J* **20**, 6648-6659

80. Sudakin, V., Chan, G. K., and Yen, T. J. (2001) Checkpoint inhibition of the APC/C in HeLa cells is mediated by a complex of BUBR1, BUB3, CDC20, and MAD2. *J Cell Biol* **154**, 925-936

81. Hardwick, K. G., Johnston, R. C., Smith, D. L., and Murray, A. W. (2000) MAD3 encodes a novel component of the spindle checkpoint which interacts with Bub3p, Cdc20p, and Mad2p. *J Cell Biol* **148**, 871-882

82. Chao, W. C., Kulkarni, K., Zhang, Z., Kong, E. H., and Barford, D. (2012) Structure of the mitotic checkpoint complex. *Nature* **484**, 208-213

83. Zhang, G., Lischetti, T., and Nilsson, J. (2014) A minimal number of MELT repeats supports all the functions of KNL1 in chromosome segregation. *J Cell Sci* **127**, 871-884

84. Overlack, K., Primorac, I., Vleugel, M., Krenn, V., Maffini, S., Hoffmann, I., Kops, G. J., and Musacchio, A. (2015) A molecular basis for the differential roles of Bub1 and BubR1 in the spindle assembly checkpoint. *Elife* **4**, e05269

85. Hoyt, M. A., Totis, L., and Roberts, B. T. (1991) S. cerevisiae genes required for cell cycle arrest in response to loss of microtubule function. *Cell* **66**, 507-517

86. Hiruma, Y., Sacristan, C., Pachis, S. T., Adamopoulos, A., Kuijt, T., Ubbink, M., von Castelmur, E., Perrakis, A., and Kops, G. J. (2015) CELL DIVISION CYCLE. Competition between MPS1 and microtubules at kinetochores regulates spindle checkpoint signaling. *Science* **348**, 1264-1267

87. Ji, Z., Gao, H., and Yu, H. (2015) CELL DIVISION CYCLE. Kinetochore attachment sensed by competitive Mps1 and microtubule binding to Ndc80C. *Science* **348**, 1260-1264

88. Primorac, I., Weir, J. R., Chiroli, E., Gross, F., Hoffmann, I., van Gerwen, S., Ciliberto, A., and Musacchio, A. (2013) Bub3 reads phosphorylated MELT repeats to promote spindle assembly checkpoint signaling. *Elife* **2**, e01030

89. Larsen, N. A., Al-Bassam, J., Wei, R. R., and Harrison, S. C. (2007) Structural analysis of Bub3 interactions in the mitotic spindle checkpoint. *Proc Natl Acad Sci U S A* **104**, 1201-1206

90. Li, R., and Murray, A. W. (1991) Feedback control of mitosis in budding yeast. *Cell* **66**, 519-531

91. London, N., and Biggins, S. (2014) Mad1 kinetochore recruitment by Mps1-mediated phosphorylation of Bub1 signals the spindle checkpoint. *Genes Dev* **28**, 140-152

92. Ji, Z., Gao, H., Jia, L., Li, B., and Yu, H. (2017) A sequential multi-target Mps1 phosphorylation cascade promotes spindle checkpoint signaling. *Elife* **6**

93. Luo, X., Fang, G., Coldiron, M., Lin, Y., Yu, H., Kirschner, M. W., and Wagner, G. (2000) Structure of the Mad2 spindle assembly checkpoint protein and its interaction with Cdc20. *Nat Struct Biol* **7**, 224-229

94. Luo, X., Tang, Z., Rizo, J., and Yu, H. (2002) The Mad2 spindle checkpoint protein undergoes similar major conformational changes upon binding to either Mad1 or Cdc20. *Mol Cell* **9**, 59-71

95. Mapelli, M., Massimiliano, L., Santaguida, S., and Musacchio, A. (2007) The Mad2 conformational dimer: structure and implications for the spindle assembly checkpoint. *Cell* **131**, 730-743

96. De Antoni, A., Pearson, C. G., Cimini, D., Canman, J. C., Sala, V., Nezi, L., Mapelli, M., Sironi, L., Faretta, M., Salmon, E. D., and Musacchio, A. (2005) The Mad1/Mad2 complex as a template for Mad2 activation in the spindle assembly checkpoint. *Curr Biol* **15**, 214-225

97. Hara, M., Ozkan, E., Sun, H., Yu, H., and Luo, X. (2015) Structure of an intermediate conformer of the spindle checkpoint protein Mad2. *Proc Natl Acad Sci U S A* **112**, 11252-11257

98. Faesen, A. C., Thanasoula, M., Maffini, S., Breit, C., Muller, F., van Gerwen, S., Bange, T., and Musacchio, A. (2017) Basis of catalytic assembly of the mitotic checkpoint complex. *Nature* **542**, 498-502

99. Overlack, K., Bange, T., Weissmann, F., Faesen, A. C., Maffini, S., Primorac, I., Muller, F., Peters, J. M., and Musacchio, A. (2017) BubR1 Promotes Bub3-Dependent APC/C Inhibition during Spindle Assembly Checkpoint Signaling. *Curr Biol* **27**, 2915-2927 e2917

100. Lara-Gonzalez, P., Scott, M. I., Diez, M., Sen, O., and Taylor, S. S. (2011) BubR1 blocks substrate recruitment to the APC/C in a KEN-box-dependent manner. *J Cell Sci* **124**, 4332-4345

101. Di Fiore, B., Davey, N. E., Hagting, A., Izawa, D., Mansfeld, J., Gibson, T. J., and Pines, J. (2015) The ABBA motif binds APC/C activators and is shared by APC/C substrates and regulators. *Dev Cell* **32**, 358-372

102. Diaz-Martinez, L. A., Tian, W., Li, B., Warrington, R., Jia, L., Brautigam, C. A., Luo, X., and Yu, H. (2015) The Cdc20-binding Phe box of the spindle checkpoint protein BubR1 maintains the mitotic checkpoint complex during mitosis. *J Biol Chem* **290**, 2431-2443

103. Lischetti, T., Zhang, G., Sedgwick, G. G., Bolanos-Garcia, V. M., and Nilsson, J. (2014) The internal Cdc20 binding site in BubR1 facilitates both spindle assembly checkpoint signalling and silencing. *Nat Commun* **5**, 5563

104. Fang, G., Yu, H., and Kirschner, M. W. (1998) The checkpoint protein MAD2 and the mitotic regulator CDC20 form a ternary complex with the anaphase-promoting complex to control anaphase initiation. *Genes Dev* **12**, 1871-1883

105. Tipton, A. R., Wang, K., Link, L., Bellizzi, J. J., Huang, H., Yen, T., and Liu, S. T. (2011) BUBR1 and closed MAD2 (C-MAD2) interact directly to assemble a functional mitotic checkpoint complex. *J Biol Chem* **286**, 21173-21179

106. Kim, S. H., Lin, D. P., Matsumoto, S., Kitazono, A., and Matsumoto, T. (1998) Fission yeast Slp1: an effector of the Mad2-dependent spindle checkpoint. *Science* **279**, 1045-1047

107. Musacchio, A. (2015) The Molecular Biology of Spindle Assembly Checkpoint Signaling Dynamics. *Curr Biol* **25**, R1002-1018

108. Alfieri, C., Chang, L., Zhang, Z., Yang, J., Maslen, S., Skehel, M., and Barford, D. (2016) Molecular basis of APC/C regulation by the spindle assembly checkpoint. *Nature* **536**, 431-436

109. Yamaguchi, M., VanderLinden, R., Weissmann, F., Qiao, R., Dube, P., Brown, N. G., Haselbach, D., Zhang, W., Sidhu, S. S., Peters, J. M., Stark, H., and Schulman, B. A. (2016) Cryo-EM of Mitotic Checkpoint Complex-Bound APC/C Reveals Reciprocal and Conformational Regulation of Ubiquitin Ligation. *Mol Cell* **63**, 593-607

110. Rieder, C. L., Cole, R. W., Khodjakov, A., and Sluder, G. (1995) The checkpoint delaying anaphase in response to chromosome monoorientation is mediated by an inhibitory signal produced by unattached kinetochores. *J Cell Biol* **130**, 941-948

111. Krenn, V., and Musacchio, A. (2015) The Aurora B Kinase in Chromosome Bi-Orientation and Spindle Checkpoint Signaling. *Front Oncol* **5**, 225

112. Rosenberg, J. S., Cross, F. R., and Funabiki, H. (2011) KNL1/Spc105 recruits PP1 to silence the spindle assembly checkpoint. *Curr Biol* **21**, 942-947

113. Howell, B. J., McEwen, B. F., Canman, J. C., Hoffman, D. B., Farrar, E. M., Rieder, C. L., and Salmon, E. D. (2001) Cytoplasmic dynein/dynactin drives kinetochore protein transport to the spindle poles and has a role in mitotic spindle checkpoint inactivation. *J Cell Biol* **155**, 1159-1172

114. Gassmann, R., Holland, A. J., Varma, D., Wan, X., Civril, F., Cleveland, D. W., Oegema, K., Salmon, E. D., and Desai, A. (2010) Removal of Spindly from microtubule-attached kinetochores controls spindle checkpoint silencing in human cells. *Genes Dev* **24**, 957-971

115. Eytan, E., Wang, K., Miniowitz-Shemtov, S., Sitry-Shevah, D., Kaisari, S., Yen, T. J., Liu, S. T., and Hershko, A. (2014) Disassembly of mitotic checkpoint complexes by the joint action of the AAA-ATPase TRIP13 and p31(comet). *Proc Natl Acad Sci U S A* **111**, 12019-12024

116. Miniowitz-Shemtov, S., Eytan, E., Kaisari, S., Sitry-Shevah, D., and Hershko, A. (2015) Mode of interaction of TRIP13 AAA-ATPase with the Mad2-binding protein p31comet and with mitotic checkpoint complexes. *Proc Natl Acad Sci U S A* **112**, 11536-11540

117. Yang, M., Li, B., Tomchick, D. R., Machius, M., Rizo, J., Yu, H., and Luo, X. (2007) p31comet blocks Mad2 activation through structural mimicry. *Cell* **131**, 744-755

118. McEwen, B. F., Heagle, A. B., Cassels, G. O., Buttle, K. F., and Rieder, C. L. (1997) Kinetochore fiber maturation in PtK1 cells and its implications for the mechanisms of chromosome congression and anaphase onset. *J Cell Biol* **137**, 1567-1580

119. Nicklas, R. B. (1967) Chromosome micromanipulation. II. Induced reorientation and the experimental control of segregation in meiosis. *Chromosoma* **21**, 17-50

120. Etemad, B., Kuijt, T. E., and Kops, G. J. (2015) Kinetochore-microtubule attachment is sufficient to satisfy the human spindle assembly checkpoint. *Nat Commun* **6**, 8987

121. Tauchman, E. C., Boehm, F. J., and DeLuca, J. G. (2015) Stable kinetochore-microtubule attachment is sufficient to silence the spindle assembly checkpoint in human cells. *Nat Commun* **6**, 10036

122. He, X., Rines, D. R., Espelin, C. W., and Sorger, P. K. (2001) Molecular analysis of kinetochore-microtubule attachment in budding yeast. *Cell* **106**, 195-206

123. Wigge, P. A., and Kilmartin, J. V. (2001) The Ndc80p complex from Saccharomyces cerevisiae contains conserved centromere components and has a function in chromosome segregation. *J Cell Biol* **152**, 349-360

124. DeLuca, J. G., Moree, B., Hickey, J. M., Kilmartin, J. V., and Salmon, E. D. (2002) hNuf2 inhibition blocks stable kinetochore-microtubule attachment and induces mitotic cell death in HeLa cells. *J Cell Biol* **159**, 549-555

125. Carmena, M., Wheelock, M., Funabiki, H., and Earnshaw, W. C. (2012) The chromosomal passenger complex (CPC): from easy rider to the godfather of mitosis. *Nat Rev Mol Cell Biol* **13**, 789-803

126. Posch, M., Khoudoli, G. A., Swift, S., King, E. M., Deluca, J. G., and Swedlow, J. R. (2010) Sds22 regulates aurora B activity and microtubule-kinetochore interactions at mitosis. *J Cell Biol* **191**, 61-74

127. Broad, A. J., DeLuca, K. F., and DeLuca, J. G. (2020) Aurora B kinase is recruited to multiple discrete kinetochore and centromere regions in human cells. *J Cell Biol* **219**

128. Welburn, J. P., Vleugel, M., Liu, D., Yates, J. R., 3rd, Lampson, M. A., Fukagawa, T., and Cheeseman, I. M. (2010) Aurora B phosphorylates spatially distinct targets to differentially regulate the kinetochore-microtubule interface. *Mol Cell* **38**, 383-392

129. Nilsson, J. (2019) Protein phosphatases in the regulation of mitosis. *J Cell Biol* **218**, 395-409

130. Saurin, A. T. (2018) Kinase and Phosphatase Cross-Talk at the Kinetochore. *Front Cell Dev Biol* **6**, 62

131. Foley, E. A., Maldonado, M., and Kapoor, T. M. (2011) Formation of stable attachments between kinetochores and microtubules depends on the B56-PP2A phosphatase. *Nat Cell Biol* **13**, 1265-1271

132. Moura, M., Osswald, M., Leca, N., Barbosa, J., Pereira, A. J., Maiato, H., Sunkel, C. E., and Conde, C. (2017) Protein Phosphatase 1 inactivates Mps1 to ensure efficient Spindle Assembly Checkpoint silencing. *Elife* **6**

133. Sivakumar, S., Janczyk, P. L., Qu, Q., Brautigam, C. A., Stukenberg, P. T., Yu, H., and Gorbsky, G. J. (2016) The human SKA complex drives the metaphase-anaphase cell cycle transition by recruiting protein phosphatase 1 to kinetochores. *Elife* **5**

134. De Wever, V., Nasa, I., Chamousset, D., Lloyd, D., Nimick, M., Xu, H., Trinkle-Mulcahy, L., and Moorhead, G. B. (2014) The human mitotic kinesin KIF18A binds protein phosphatase 1 (PP1) through a highly conserved docking motif. *Biochem Biophys Res Commun* **453**, 432-437

135. Suijkerbuijk, S. J., Vleugel, M., Teixeira, A., and Kops, G. J. (2012) Integration of kinase and phosphatase activities by BUBR1 ensures formation of stable kinetochore-microtubule attachments. *Dev Cell* **23**, 745-755

136. Desai, A., Verma, S., Mitchison, T. J., and Walczak, C. E. (1999) Kin I kinesins are microtubule-destabilizing enzymes. *Cell* **96**, 69-78

137. Maney, T., Hunter, A. W., Wagenbach, M., and Wordeman, L. (1998) Mitotic centromere-associated kinesin is important for anaphase chromosome segregation. *J Cell Biol* **142**, 787-801

138. Manning, A. L., Ganem, N. J., Bakhoum, S. F., Wagenbach, M., Wordeman, L., and Compton, D. A. (2007) The kinesin-13 proteins Kif2a, Kif2b, and Kif2c/MCAK have distinct roles during mitosis in human cells. *Mol Biol Cell* **18**, 2970-2979

139. Cimini, D., Howell, B., Maddox, P., Khodjakov, A., Degrassi, F., and Salmon, E. D. (2001) Merotelic kinetochore orientation is a major mechanism of aneuploidy in mitotic mammalian tissue cells. *J Cell Biol* **153**, 517-527

140. Gordon, D. J., Resio, B., and Pellman, D. (2012) Causes and consequences of aneuploidy in cancer. *Nat Rev Genet* **13**, 189-203

141. Boveri, T. (1914) *Zur frage der entstehung maligner tumoren*, G. Fischer, Jena,

142. Torres, E. M., Sokolsky, T., Tucker, C. M., Chan, L. Y., Boselli, M., Dunham, M. J., and Amon, A. (2007) Effects of aneuploidy on cellular physiology and cell division in haploid yeast. *Science* **317**, 916-924

143. Williams, B. R., Prabhu, V. R., Hunter, K. E., Glazier, C. M., Whittaker, C. A., Housman, D. E., and Amon, A. (2008) Aneuploidy affects proliferation and spontaneous immortalization in mammalian cells. *Science* **322**, 703-709

144. Nigg, E. A. (2002) Centrosome aberrations: cause or consequence of cancer progression? *Nat Rev Cancer* **2**, 815-825

145. Quintyne, N. J., Reing, J. E., Hoffelder, D. R., Gollin, S. M., and Saunders, W. S. (2005) Spindle multipolarity is prevented by centrosomal clustering. *Science* **307**, 127-129

146. Barber, T. D., McManus, K., Yuen, K. W., Reis, M., Parmigiani, G., Shen, D., Barrett, I., Nouhi, Y., Spencer, F., Markowitz, S., Velculescu, V. E., Kinzler, K. W., Vogelstein, B., Lengauer, C., and Hieter, P. (2008) Chromatid cohesion defects may underlie chromosome instability in human colorectal cancers. *Proc Natl Acad Sci U S A* **105**, 3443-3448

147. Cahill, D. P., Lengauer, C., Yu, J., Riggins, G. J., Willson, J. K., Markowitz, S. D., Kinzler, K. W., and Vogelstein, B. (1998) Mutations of mitotic checkpoint genes in human cancers. *Nature* **392**, 300-303

148. Kops, G. J., Weaver, B. A., and Cleveland, D. W. (2005) On the road to cancer: aneuploidy and the mitotic checkpoint. *Nat Rev Cancer* **5**, 773-785

149. Compton, D. A. (2011) Mechanisms of aneuploidy. *Curr Opin Cell Biol* **23**, 109-113

150. Toledo, C. M., Herman, J. A., Olsen, J. B., Ding, Y., Corrin, P., Girard, E. J., Olson, J. M., Emili, A., DeLuca, J. G., and Paddison, P. J. (2014) BuGZ is required for Bub3 stability, Bub1 kinetochore function, and chromosome alignment. *Dev Cell* **28**, 282-294

151. Ding, Y., Hubert, C. G., Herman, J., Corrin, P., Toledo, C. M., Skutt-Kakaria, K., Vazquez, J., Basom, R., Zhang, B., Risler, J. K., Pollard, S. M., Nam, D. H., Delrow, J. J., Zhu, J., Lee, J., DeLuca, J., Olson, J. M., and Paddison, P. J. (2013) Cancer-Specific requirement for BUB1B/BUBR1 in human brain tumor isolates and genetically transformed cells. *Cancer Discov* **3**, 198-211

152. Bakhoum, S. F., Genovese, G., and Compton, D. A. (2009) Deviant kinetochore microtubule dynamics underlie chromosomal instability. *Curr Biol* **19**, 1937-1942

153. Duensing, S., and Munger, K. (2002) The human papillomavirus type 16 E6 and E7 oncoproteins independently induce numerical and structural chromosome instability. *Cancer Res* **62**, 7075-7082

154. Scheffner, M., Huibregtse, J. M., Vierstra, R. D., and Howley, P. M. (1993) The HPV-16 E6 and E6-AP complex functions as a ubiquitin-protein ligase in the ubiquitination of p53. *Cell* **75**, 495-505

155. Thompson, D. A., Belinsky, G., Chang, T. H., Jones, D. L., Schlegel, R., and Munger, K. (1997) The human papillomavirus-16 E6 oncoprotein decreases the vigilance of mitotic checkpoints. *Oncogene* **15**, 3025-3035

156. Liu, X., Clements, A., Zhao, K., and Marmorstein, R. (2006) Structure of the human Papillomavirus E7 oncoprotein and its mechanism for inactivation of the retinoblastoma tumor suppressor. *J Biol Chem* **281**, 578-586

157. Musacchio, A., and Salmon, E. D. (2007) The spindle-assembly checkpoint in space and time. *Nat Rev Mol Cell Biol* **8**, 379-393

158. Lara-Gonzalez, P., Westhorpe, F. G., and Taylor, S. S. (2012) The spindle assembly checkpoint. *Curr Biol* **22**, R966-980

159. Knowlton, A. L., Lan, W., and Stukenberg, P. T. (2006) Aurora B is enriched at merotelic attachment sites, where it regulates MCAK. *Curr Biol* **16**, 1705-1710

160. Bakhoum, S. F., Thompson, S. L., Manning, A. L., and Compton, D. A. (2009) Genome stability is ensured by temporal control of kinetochore-microtubule dynamics. *Nat Cell Biol* **11**, 27-35

161. Halbert, C. L., Demers, G. W., and Galloway, D. A. (1991) The E7 gene of human papillomavirus type 16 is sufficient for immortalization of human epithelial cells. *J Virol* **65**, 473-478

162. Shin, S. I., Freedman, V. H., Risser, R., and Pollack, R. (1975) Tumorigenicity of virus-transformed cells in nude mice is correlated specifically with anchorage independent growth in vitro. *Proc Natl Acad Sci U S A* **72**, 4435-4439

163. Mori, S., Chang, J. T., Andrechek, E. R., Matsumura, N., Baba, T., Yao, G., Kim, J. W., Gatza, M., Murphy, S., and Nevins, J. R. (2009) Anchorage-independent cell growth signature identifies tumors with metastatic potential. *Oncogene* **28**, 2796-2805

164. Thomas, J. T., and Laimins, L. A. (1998) Human papillomavirus oncoproteins E6 and E7 independently abrogate the mitotic spindle checkpoint. *J Virol* **72**, 1131-1137

165. Kops, G. J., Foltz, D. R., and Cleveland, D. W. (2004) Lethality to human cancer cells through massive chromosome loss by inhibition of the mitotic checkpoint. *Proc Natl Acad Sci U S A* **101**, 8699-8704

166. Saeki, A., Tamura, S., Ito, N., Kiso, S., Matsuda, Y., Yabuuchi, I., Kawata, S., and Matsuzawa, Y. (2002) Frequent impairment of the spindle assembly checkpoint in hepatocellular carcinoma. *Cancer* **94**, 2047-2054

167. Yuan, B., Xu, Y., Woo, J. H., Wang, Y., Bae, Y. K., Yoon, D. S., Wersto, R. P., Tully, E., Wilsbach, K., and Gabrielson, E. (2006) Increased expression of mitotic checkpoint genes in breast cancer cells with chromosomal instability. *Clin Cancer Res* **12**, 405-410

168. Choi, J. W., Kim, Y., Lee, J. H., and Kim, Y. S. (2013) High expression of spindle assembly checkpoint proteins CDC20 and MAD2 is associated with poor prognosis in urothelial bladder cancer. *Virchows Arch* **463**, 681-687

169. Collin, P., Nashchekina, O., Walker, R., and Pines, J. (2013) The spindle assembly checkpoint works like a rheostat rather than a toggle switch. *Nat Cell Biol* **15**, 1378-1385

170. Takizawa, S., Nagasaka, K., Nakagawa, S., Yano, T., Nakagawa, K., Yasugi, T., Takeuchi, T., Kanda, T., Huibregtse, J. M., Akiyama, T., and Taketani, Y. (2006) Human scribble, a novel tumor suppressor identified as a target of high-risk HPV E6 for ubiquitin-mediated degradation, interacts with adenomatous polyposis coli. *Genes Cells* **11**, 453-464

171. Daum, J. R., Potapova, T. A., Sivakumar, S., Daniel, J. J., Flynn, J. N., Rankin, S., and Gorbsky, G. J. (2011) Cohesion fatigue induces chromatid separation in cells delayed at metaphase. *Curr Biol* **21**, 1018-1024

172. Cimini, D. (2008) Merotelic kinetochore orientation, aneuploidy, and cancer. *Biochim Biophys Acta* **1786**, 32-40

173. Green, R. A., Wollman, R., and Kaplan, K. B. (2005) APC and EB1 function together in mitosis to regulate spindle dynamics and chromosome alignment. *Mol Biol Cell* **16**, 4609-4622

174. Tanenbaum, M. E., Galjart, N., van Vugt, M. A., and Medema, R. H. (2006) CLIP-170 facilitates the formation of kinetochore-microtubule attachments. *EMBO J* **25**, 45-57

175. Wood, K. W., Lad, L., Luo, L., Qian, X., Knight, S. D., Nevins, N., Brejc, K., Sutton, D., Gilmartin, A. G., Chua, P. R., Desai, R., Schauer, S. P., McNulty, D. E., Annan, R. S., Belmont, L. D., Garcia, C., Lee, Y., Diamond, M. A., Faucette, L. F., Giardiniere, M., Zhang, S., Sun, C. M., Vidal, J. D., Lichtsteiner, S., Cornwell, W. D., Greshock, J. D., Wooster, R. F., Finer, J. T., Copeland, R. A., Huang, P. S., Morgans, D. J., Jr., Dhanak, D., Bergnes, G., Sakowicz, R., and Jackson, J. R. (2010) Antitumor activity of an allosteric inhibitor of centromere-associated protein-E. *Proc Natl Acad Sci U S A* **107**, 5839-5844

176. Kaplan, K. B., Burds, A. A., Swedlow, J. R., Bekir, S. S., Sorger, P. K., and Nathke, I. S. (2001) A role for the Adenomatous Polyposis Coli protein in chromosome segregation. *Nat Cell Biol* **3**, 429-432

177. Dikovskaya, D., Schiffmann, D., Newton, I. P., Oakley, A., Kroboth, K., Sansom, O., Jamieson, T. J., Meniel, V., Clarke, A., and Nathke, I. S. (2007) Loss of APC induces polyploidy as a result of a combination of defects in mitosis and apoptosis. *J Cell Biol* **176**, 183-195

178. Manning, A. L., Longworth, M. S., and Dyson, N. J. (2010) Loss of pRB causes centromere dysfunction and chromosomal instability. *Genes Dev* **24**, 1364-1376

179. Zheng, Z. M., Tao, M., Yamanegi, K., Bodaghi, S., and Xiao, W. (2004) Splicing of a cap-proximal human Papillomavirus 16 E6E7 intron promotes E7 expression, but can be restrained by distance of the intron from its RNA 5' cap. *J Mol Biol* **337**, 1091-1108

180. Etemad, B., and Kops, G. J. (2016) Attachment issues: kinetochore transformations and spindle checkpoint silencing. *Curr Opin Cell Biol* **39**, 101-108

181. Taylor, S. S., Ha, E., and McKeon, F. (1998) The human homologue of Bub3 is required for kinetochore localization of Bub1 and a Mad3/Bub1-related protein kinase. *J Cell Biol* **142**, 1-11

182. Zhang, G., Kruse, T., Lopez-Mendez, B., Sylvestersen, K. B., Garvanska, D. H., Schopper, S., Nielsen, M. L., and Nilsson, J. (2017) Bub1 positions Mad1 close to KNL1 MELT repeats to promote checkpoint signalling. *Nat Commun* **8**, 15822

183. Sironi, L., Mapelli, M., Knapp, S., De Antoni, A., Jeang, K. T., and Musacchio, A. (2002) Crystal structure of the tetrameric Mad1-Mad2 core complex: implications of a 'safety belt' binding mechanism for the spindle checkpoint. *EMBO J* **21**, 2496-2506

184. Bailer, S. M., Siniossoglou, S., Podtelejnikov, A., Hellwig, A., Mann, M., and Hurt, E. (1998) Nup116p and nup100p are interchangeable through a conserved motif which constitutes a docking site for the mRNA transport factor gle2p. *EMBO J* **17**, 1107-1119

185. Wang, X., Babu, J. R., Harden, J. M., Jablonski, S. A., Gazi, M. H., Lingle, W. L., de Groen, P. C., Yen, T. J., and van Deursen, J. M. (2001) The mitotic checkpoint protein hBUB3 and the mRNA export factor hRAE1 interact with GLE2p-binding sequence (GLEBS)-containing proteins. *J Biol Chem* **276**, 26559-26567

186. Gillett, E. S., Espelin, C. W., and Sorger, P. K. (2004) Spindle checkpoint proteins and chromosome-microtubule attachment in budding yeast. *J Cell Biol* **164**, 535-546

187. Harris, L., Davenport, J., Neale, G., and Goorha, R. (2005) The mitotic checkpoint gene BubR1 has two distinct functions in mitosis. *Exp Cell Res* **308**, 85-100

188. Malureanu, L. A., Jeganathan, K. B., Hamada, M., Wasilewski, L., Davenport, J., and van Deursen, J. M. (2009) BubR1 N terminus acts as a soluble inhibitor of cyclin B degradation by APC/C(Cdc20) in interphase. *Dev Cell* **16**, 118-131

189. Millband, D. N., and Hardwick, K. G. (2002) Fission yeast Mad3p is required for Mad2p to inhibit the anaphase-promoting complex and localizes to kinetochores in a Bub1p-, Bub3p-, and Mph1p-dependent manner. *Mol Cell Biol* **22**, 2728-2742

190. Jiang, H., He, X., Wang, S., Jia, J., Wan, Y., Wang, Y., Zeng, R., Yates, J., 3rd, Zhu, X., and Zheng, Y. (2014) A microtubule-associated zinc finger protein, BuGZ, regulates mitotic chromosome alignment by ensuring Bub3 stability and kinetochore targeting. *Dev Cell* **28**, 268-281

191. Huang, Y., Li, T., Ems-McClung, S. C., Walczak, C. E., Prigent, C., Zhu, X., Zhang, X., and Zheng, Y. (2018) Aurora A activation in mitosis promoted by BuGZ. *J Cell Biol* **217**, 107-116

192. Jiang, H., Wang, S., Huang, Y., He, X., Cui, H., Zhu, X., and Zheng, Y. (2015) Phase transition of spindle-associated protein regulate spindle apparatus assembly. *Cell* **163**, 108-122

193. Campbell, L., and Hardwick, K. G. (2003) Analysis of Bub3 spindle checkpoint function in Xenopus egg extracts. *J Cell Sci* **116**, 617-628

194. Fang, G. (2002) Checkpoint protein BubR1 acts synergistically with Mad2 to inhibit anaphase-promoting complex. *Mol Biol Cell* **13**, 755-766

195. Mansfeld, J., Collin, P., Collins, M. O., Choudhary, J. S., and Pines, J. (2011) APC15 drives the turnover of MCC-CDC20 to make the spindle assembly checkpoint responsive to kinetochore attachment. *Nat Cell Biol* **13**, 1234-1243

196. Nilsson, J., Yekezare, M., Minshull, J., and Pines, J. (2008) The APC/C maintains the spindle assembly checkpoint by targeting Cdc20 for destruction. *Nat Cell Biol* **10**, 1411-1420

197. Tanenbaum, M. E., Macurek, L., Galjart, N., and Medema, R. H. (2008) Dynein, Lis1 and CLIP-170 counteract Eg5-dependent centrosome separation during bipolar spindle assembly. *EMBO J* **27**, 3235-3245

198. Mattiuzzo, M., Vargiu, G., Totta, P., Fiore, M., Ciferri, C., Musacchio, A., and Degrassi, F. (2011) Abnormal kinetochore-generated pulling forces from expressing a N-terminally modified Hec1. *PLoS One* **6**, e16307

199. Peters, J. M., Tedeschi, A., and Schmitz, J. (2008) The cohesin complex and its roles in chromosome biology. *Genes Dev* **22**, 3089-3114

200. Sapkota, H., Wasiak, E., Daum, J. R., and Gorbsky, G. J. (2018) Multiple determinants and consequences of cohesion fatigue in mammalian cells. *Mol Biol Cell* **29**, 1811-1824

201. Vallardi, G., Allan, L. A., Crozier, L., and Saurin, A. T. (2019) Division of labour between PP2A-B56 isoforms at the centromere and kinetochore. *Elife* **8**

202. Smith, R. J., Cordeiro, M. H., Davey, N. E., Vallardi, G., Ciliberto, A., Gross, F., and Saurin, A. T. (2019) PP1 and PP2A Use Opposite Phospho-dependencies to Control Distinct Processes at the Kinetochore. *Cell Rep* **28**, 2206-2219 e2208

203. Nijenhuis, W., Vallardi, G., Teixeira, A., Kops, G. J., and Saurin, A. T. (2014) Negative feedback at kinetochores underlies a responsive spindle checkpoint signal. *Nat Cell Biol* **16**, 1257-1264

204. DeLuca, K. F., Meppelink, A., Broad, A. J., Mick, J. E., Peersen, O. B., Pektas, S., Lens, S. M. A., and DeLuca, J. G. (2018) Aurora A kinase phosphorylates Hec1 to regulate metaphase kinetochore-microtubule dynamics. *J Cell Biol* **217**, 163-177

205. Wimbish, R. T., and DeLuca, J. G. (2020) Hec1/Ndc80 Tail Domain Function at the Kinetochore-Microtubule Interface. *Front Cell Dev Biol* **8**, 43

206. Kendall, S. D., Linardic, C. M., Adam, S. J., and Counter, C. M. (2005) A network of genetic events sufficient to convert normal human cells to a tumorigenic state. *Cancer Res* **65**, 9824-9828

207. Hubert, C. G., Bradley, R. K., Ding, Y., Toledo, C. M., Herman, J., Skutt-Kakaria, K., Girard, E. J., Davison, J., Berndt, J., Corrin, P., Hardcastle, J., Basom, R., Delrow, J. J., Webb, T., Pollard, S. M., Lee, J., Olson, J. M., and Paddison, P. J. (2013) Genome-wide RNAi screens

in human brain tumor isolates reveal a novel viability requirement for PHF5A. *Genes Dev* **27**, 1032-1045

208. Huang, W., Kessler, D. S., and Erikson, R. L. (1995) Biochemical and biological analysis of Mek1 phosphorylation site mutants. *Mol Biol Cell* **6**, 237-245

209. Kohn, A. D., Takeuchi, F., and Roth, R. A. (1996) Akt, a pleckstrin homology domain containing kinase, is activated primarily by phosphorylation. *J Biol Chem* **271**, 21920-21926

210. Gradishar, W. J. (2012) Taxanes for the treatment of metastatic breast cancer. *Breast Cancer (Auckl)* **6**, 159-171

211. Moudi, M., Go, R., Yien, C. Y., and Nazre, M. (2013) Vinca alkaloids. *Int J Prev Med* **4**, 1231-1235